CATALYSTS FOR THE HYDROLYSIS OF THIOPHOSPHATE TRIESTERS

A Dissertation

by

ALEXANDRE PICOT

Submitted to the Office of Graduate Studies of
Texas A&M University
in partial fulfillment of the requirements for the degree of

DOCTOR OF PHILOSOPHY

December 2004

Major Subject: Chemistry

CATALYSTS FOR THE HYDROLYSIS OF THIOPHOSPHATE TRIESTERS

A Dissertation

by

ALEXANDRE PICOT

Submitted to Texas A&M University
in partial fulfillment of the requirements
for the degree of

DOCTOR OF PHILOSOPHY

Approved as to style and content by:

François P. Gabbaï (Chair of Committee)	Dragomir B. Bukur (Member)
Kevin Burgess (Member)	Victoria J. DeRose (Member)
	Emile A. Schweikert (Head of Department)

December 2004

Major Subject: Chemistry

ABSTRACT

Catalysts for the Hydrolysis of Thiophosphate Triesters.

(December 2004)

Alexandre Picot, B.S.; M.S., Université Paul Sabatier at Toulouse, France

Chair of Advisory Committee: Dr. François P. Gabbaï

The degradation of phosphate triesters is efficiently catalyzed by organophosphate hydrolases (OPH). While a number of recent studies have focused on optimizing the rate of hydrolysis observed with the native enzyme, no dinuclear complexes that mimic the function of OPH have been reported or investigated. Our present research focuses on the synthesis of dinuclear metal complexes and on the study of their catalytic abilities. An important aspect of this research concerns the investigation of the coordination chemistry of dinuclear ligands designed to hold two metal cations in well defined positions. The ability of the different complexes to catalyze the degradation of thiophosphate triester is presented. Out of several complexes studied, ortho-metallated Pd (II) complexes have been found to display the highest catalytic activity for the hydrolysis of parathion.

DEDICATION

To Aurore

ACKNOWLEDGEMENTS

First, I'm really grateful to Dr. François P. Gabbaï for allowing me to work on a new and challenging project with a great environment. Thank you François for your guidance and understanding.

I wish to also express my gratitude to my committee members, Professor Dragomir B. Bukur, Professor Kevin Burgess, Professor Victoria J DeRose, and Professor Donald J. Darensbourg for their insightful suggestions during my graduate career.

I would like to extend my thanks to the Gabbaï group: Charlotte N. Burress, Ching-Wen Chui, Samuel Cozzens, Mason R. Haneline, James D. Hoefelmeyer, Julie B. King, Mieock Kim, Mohand-Ameziane Melaimi, Stephane Sole, Thomas J. Taylor, and Huadong Wang. I have very much appreciated sharing help, support, suggestions, and laughs in the lab with all of them.

I would like to express my gratitude to Béatrice Martres and all my friends Basiou, Chris, Cieut, Coco, Delphine, Evelyne, Franky, George, Guillaume, Jacques, Jérome, Lolo, Nat, Pull up's, Queb, Sandrine, Seb, Solange, Sylvere, Tahar, Titac, Titus, Vanessa, le NO, *et j'en passe,* for their support through letters and during my stay back home.

I would like to thank mamoun's family, Alain, Alfred, Bernadette, Christian, Coye, Damien, Davidou, Geneu, Jean Claude, Louise, Martine, Maryse, Patrick, Pierrette, Roger, Yvonne, for taking good care of me and keeping me well hydrated during all family reunions.

I will surely not forget Primal, and all my friends from }i{nstagiber, even you Dr. Speth, who did a wonderful job keeping me amused at all times.

I would like to particularly thank my best friend and roommate Aurore Loudet. I'm really grateful for her standing up to me during all these years.

Finally, I would like to thank my parents, Bernadette and Daniel Picot, my sister Bérengère Charrier, my grandmothers Jacqueline Durrieu, and Jeanne Picot, for all their amazing support, and endless love.

TABLE OF CONTENTS

Page

ABSTRACT..... iii

DEDICATION..... iv

ACKNOWLEDGEMENTS..... v

TABLE OF CONTENTS..... vii

LIST OF FIGURES..... ix

LIST OF TABLES..... xv

CHAPTER

I INTRODUCTION AND RESEARCH OBJECTIVES……..... 1

1.1 Acetylcholine esterase inhibitors: Pesticides and chemical warfare agents..... 1
1.2 General decontamination procedures…..... 3
1.3 *o*-Iodocarboxylates..... 6
1.4 Related nucleophiles..... 11
1.4.1 α effect nucleophiles..... 11
1.4.2 Alkoxydes..... 12
1.5 Enzymes catalysed hydrolysis and mechanisms..... 13
1.6 Organometallic catalysis and mechanisms..... 18
1.7 Objectives…..... 24

II EXPERIMENTAL PROCEDURES..... 27

2.1 General considerations..... 27
2.2 Spectroscopy..... 28

III LIGAND DESIGN..... 30

3.1 Introduction..... 30
3.2 Dinuclear pyridazine based ligands..... 34
3.2.1 Ligands derived from 3,6-dihydroxymethylpyridazine..... 34
3.2.2 Dinuclear bis Schiff base ligands..... 43
3.3 Dinuclear (iminomethyl)benzene ligands..... 50
3.4 Summary…..... 56
3.5 Experimental..... 57

CHAPTER Page

IV COORDINATION CHEMISTRY..... 72

4.1 Introduction..... 72
4.2 Investigation of the coordination chemistry of the bis-Schiff base ligands..... 72
4.3 Coordination chemistry of the ligands derived from 3,6-bis-(hydroxymethyl)-pyridazine..... 80
4.3.1 NMR studies..... 80
4.3.2 Synthesis of dinuclear copper complexes..... 83
4.4 Summary..... 90
4.5 Experimental..... 91

V ORTHOMETALATED PD (II) COMPLEXES..... 92

5.1 Introduction..... 92
5.2 Mononuclear palladium (II) complexes..... 94
5.3 Dinuclear palladium (II) complexes..... 103
5.4 Summary..... 108
5.5 Experimental..... 108

VI METAL CATALYSED ORGANOPHOSPHATE ESTER HYDROLYSIS..... 115

6.1 Introduction..... 115
6.2 Dinuclear Cu (II) complexes catalysis..... 116
6.3 Metal ion screening..... 118
6.4 Dinuclear Pd (II) complexes catalysis..... 120
6.5 Mononuclear Pd (II) complexes catalysis..... 124
6.6 Summary…..... 139
6.7 Experimental..... 140

VII GENERAL CONCLUSIONS..... 142

REFERENCES..... 146

APPENDIX..... 158

VITA..... 160

LIST OF FIGURES

FIGURE		Page
1	Structure of GA, VX, GB, and GD	2
2	Detoxification of G- agents and VX with Bleach	4
3	Detoxification of G- agents with DS2	5
4	Structure and reactivity of various Heterocyclic iodanes with PNPDPP	7
5	Structure of INA and various analogues	8
6	Cleavage of 10^{-5} M parathion by 10^{-4} M IBA (■) or INA (○) as a function of cetyltrimethylammonium chloride (CTACl) (M) at pH 8.0 and 25°C	9
7	Structure of duplex-IBA and silica-bound IBA	10
8	Structure of various oximes	12
9	Structure of 18-22	13
10	Representation of the binuclear Zn^{2+}/Zn^{2+} metal center at the active site of OPH	15
11	Cartoon of the possible enzymatic hydrolysis mechanisms	16
12	Proposed mechanisms for the hydrolysis of warfare agents at the active site of OPH	18
13	Structure of diisopropyl phosphorofluoridate and 2,4-dinitrophenyl diethyl phosphate	19
14	Structure of related lanthanides and Cu (II) diamine complexes	20
15	Structure of related Zinc (II) and Cu (II) complexes	21
16	Structure of related Pd (II) and Pt(II) orthometalated aryl oximes	23
17	Proposed mechanisms for the hydrolysis of parathion with Pd (II) and Pt (II) complexes	24

FIGURE Page

18 Maruoka, and Hawthorne's catalysts..... 31

19 Shibasaki, Trost, and Jacobsen's catalysts..... 33

20 Pfaltz's binuclear ligand design..... 34

21 Synthesis of 3,6-di(hydroxymethyl)pyridazine..... 35

22 ORTEP view of 3,6-distyrylpyridazine and **41** (50% ellipsoids)..... 36

23 Synthesis of 3,6-di(hydroxymethyl)pyridazine di-*p*-tosylate..... 37

24 3,6-di[-N-(1*R,*2*R,*3*R,*5*S*)-(-)-isopinocampheylaminomethyl]-pyridazine..... 38

25 Synthesis of 3,6-di[N-(1R-2S)-norephedrinylmethyl]pyridazine and 3,6-di[-N-(1R-2S)-1-amino-2-indanolylmethyl]pyridazine..... 39

26 ORTEP view of **48** in the crystal (50% ellipsoids)..... 40

27 Reaction of 3,6-di(hydroxymethyl)pyridazine di-*p*-tosylate with various amino-alcohols in MeCN/Na_2CO_3..... 42

28 ORTEP view of **55** in the crystal (50% ellipsoids)..... 42

29 Reaction of 3,6-di(hydroxymethyl)Pyridazine di-*p*-tosylate with 2-[N-(1*R,*2*R,*3*R,*5*S*)-(-)-isopinocampheylaminomethyl]pyridine..... 43

30 Synthesis of ((1*R,*2*S*)-(2-hydroxy-1-methyl-2-phenylethyl)-amino-methylene)pyridazine..... 44

31 ORTEP view of **60** in the crystal (50% ellipsoids)..... 45

32 ((1*R,*2*S*)-(2-hydroxy-1-methyl-2-phenylethyl)-aminomethylene)-pyridazine isomer equilibrium..... 45

33 Synthesis of **62**..... 46

34 ORTEP view of **62** in the crystal (50% ellipsoids)..... 47

35 Synthesis of ((1*R,*2*S*)-(2-*O*-benzylhydroxy-1-methyl-2-phenylethyl)-aminomethylene)pyridazine..... 48

FIGURE Page

36 ORTEP view of **65** in the crystal (50% ellipsoids)..... 48

37 Synthesis of ((1*R,*2*S*)-(2-*O*-^{t}butyldimethylsilylhydroxy-1-methyl-2-phenylethyl)-aminometylene)pyridazine..... 49

38 Dinuclear organometallic design..... 50

39 Synthesis of 2,3-dimethoxy-benzene-1,4-dicarbaldehyse..... 51

40 Synthesis of 3,6-di[-N-(1R,2R,3R,5S)-(-)isopinocampheylamino-methyl]-1,2-dimethoxy-benzene..... 52

41 Synthesis of 3,6-di[-N-(2,4,6-trimethylphenyliminomethyl)]-1,2-dimethoxy-benzene..... 53

42 ORTEP view of **71** in the crystal (50% ellipsoids)..... 53

43 Synthesis of 3,6-di[-N-(2,6-diisopropylphenyliminomethyl)]-1,2-dimethoxy-benzene..... 54

44 ORTEP view of **73** in the crystal (50% ellipsoids)..... 55

45 Synthesis of 3,6-di[-N-*t*-butyliminomethyl]-1,2-dimethoxy-benzene.... 56

46 NMR spectra of **66** in the presence of increasing amount of $BiCl_3$..... 73

47 Coordination reaction of **66** with $BiCl_3$..... 74

48 Coordination chemistry of $BiCl_3$..... 75

49 Coordination reaction of **66** with uranyl nitrate..... 76

50 NMR spectra of **66** in the presence of increasing amount of UO_2^{2+}..... 76

51 Coordination chemistry of UO_2 (II)..... 77

52 Coordination reaction of **66** with Sc^3..... 78

53 NMR spectra of **66** in the presence of increasing amount of Sc^{3+}..... 78

54 Coordination reaction of **66** with Y^{3+}..... 79

FIGURE Page

55 NMR spectra of **66** in the presence of increasing amount of Y^{3+}..... 79

56 Coordination reaction of **44** with $AlMe_3$..... 80

57 NMR resolution of **82** from C_6D_6 to pyridine-d_5..... 81

58 Coordination reaction of **46** with Y and Sc triflate..... 82

59 NMR spectra of **46** in the presence of increasing amount of Sc^{3+}..... 83

60 Spectrometric titration of **46** (10^{-4} M) with $CuCl_2$ in EtOH..... 84

61 Spectrometric titration of **48** (10^{-4} M) with $CuCl_2$ in EtOH..... 85

62 Coordination reaction of **46** and with Cu^{2+}..... 86

63 Coordination reaction of **48** and with Cu^{2+}..... 86

64 ESI mass spectrometry of **48** and with Cu^{2+}..... 87

65 Spectrometric titration of **86** (10^{-2} M) with $CuCl_2$ in EtOH..... 88

66 Coordination reaction of **86** and with Cu^{2+}..... 89

67 Spectrometric titration of **87** ($8x10^{-3}$ M) with $CuCl_2$ in EtOH..... 89

68 Coordination reaction of **87** and with Cu^{2+}..... 90

69 Ryabov's cyclopalladated Complex, catalytic process..... 93

70 Coordination reaction of [2-(2-pyridyl)-phenyl-*C,N*]palladium(II) with methylparathion..... 94

71 ^{31}P $\{^1H\}$ NMR spectra of a solution of methylparathion (5 mg) in the presence of **90** (1 mg) in THF..... 95

72 Proposed structure of **92**..... 96

73 Structure of complex **91** in the crystal (50% ellipsoid)..... 97

74 Solid state $^{31}P\{^1H\}$ NMR spectra of **91**..... 99

FIGURE Page

75 Regio-isomers **93-94** equilibrium..... 100

76 Coordination reaction of di-μ-(dimethylthiophosphate-*S,*S)-bis[2-(2-pyridyl)phenyl-*C,N*]dipalladium(II) with triphenylphosphine..... 101

77 Structure of complex **95** in the crystal (50% ellipsoid)..... 102

78 Reaction of **71** with $Pd(OAc)_2$..... 103

79 Reaction of **71** with Na_2PdCl_4..... 105

80 ORTEP view of **97** in the crystal (50% ellipsoids)..... 106

81 Reaction of **69** with Na_2PdCl_4..... 107

82 Reaction of **73** with Na_2PdCl_4..... 107

83 Hydrolysis of methylparathion, primary tests..... 117

84 Hydrolysis of methylparathion by **85**, and **89** at 60^{o}C and pH 8..... 116

85 Hydrolysis of methylparathion by metal ions at 60^{o}C and pH 8..... 119

86 Hydrolysis of methylparathion by **97**, **98**, and **99** at RT at pH 9..... 121

87 Pseudo first order kinetic resolution of the hydrolysis of **20** ($3.5\ 10^{-5}$ M) by **97** at pH 9..... 123

88 Pseudo first order kinetic resolution of the hydrolysis of **20** by **97** ($1.75\ 10^{-6}$ M) at pH 9..... 124

89 Hydrolysis reaction of methylparathion by **91** at RT..... 125

90 Pseudo first order kinetic resolution of the hydrolysis of methylparathion ($3.5\ 10^{-5}$ M) by **91** at pH 7..... 126

91 Pseudo first order kinetic resolution of the hydrolysis of methylparathion by **91** ($1.75\ 10^{-6}$ M) at pH 7..... 127

92 ^{1}H PGSE analysis of **91** (1 mg) in DMSO-d_6..... 128

FIGURE Page

93 Proposed mechanism for the hydrolysis of **20** by **91** at neutral pH..... 129

94 Pseudo first order kinetic resolution of the hydrolysis of methylparathion by **91** ($1.75\ 10^{-6}$ M) at pH 9..... 131

95 Pseudo half order kinetic resolution of the hydrolysis of **20** ($3.5\ 10^{-5}$ M) by **91** at pH 9..... 132

96 Equilibrium constant K_{eq} = [monomer]^2 /[Dimer])..... 132

97 Expression of the Kobs vs pH for the hydrolysis of methylparathion by **91** ([methylparathion] = $3.5\ 10^{-5}$ M; [**91**] = $1.75\ 10^{-6}$ M)..... 133

98 UV recording of **91** (35 μmol) in aqueous buffer with 16% dioxane from pH 7 to pH 9.5..... 134

99 Complex **91** equilibrium between neutral and basic pH..... 134

100 ^{1}H PGSE analysis of **91** (1 mg) in a 50% DMSO/D2O mixture..... 135

101 Formation of the dimeric hydroxide bridged complex..... 137

102 Proposed mechanism for the hydrolysis of **20** by **91** at basic pH..... 138

LIST OF TABLES

TABLE		Page
1	Crystal data for 3,6-distyrylpyridazine and **41**	67
2	Crystal data for complexes **48** and **55**	68
3	Crystal data for complexes **60** and **62**	69
4	Crystal data for complexes **65** and **71**	70
5	Crystal data for complex **73**	71
6	Crystal data for complexes **91** and **95**	113
7	Crystal data for complex **97**	114

CHAPTER I

INTRODUCTION AND RESEARCH OBJECTIVES

1.1 Acetylcholine esterase inhibitors: Pesticides and chemical warfare agents.

Organophosphorus pesticides are acetylcholinesterase inhibitors. These species, which typically consist of phosphate or thiophosphate triester derivatives, were introduced to replace organochlorine pesticides, and have become widely used in the agricultural industry around the world.[1] While most of these pesticides have been designed to decompose rapidly, their solubility in water facilitates their transport into rivers[2]. As a result, these pesticides are often detected in streams and ground waters across the U.S. with diazinon, malathion, and chloropyrifos as the most abundant.[3] According to a recent survey, these pesticides have also been detected in ground water used for drinking water as well as in air, and rain.[4] Other important concerns come from the fact that several water treatment facilities in the U.S. have failed toxicity tests as a result of organophosphorus pesticides contamination.[5] With an increasing need for agricultural products, it can be expected that the amount of organophosphorus pesticides present in the environment will keep on growing.

World War II witnessed the appearance of organophosphorus nerve agents. These agents are also acetylcholinesterase inhibitors which have been designed to exhibit a

---

This dissertation follows the style and format of the *Journal of the American Chemical Society*.

higher toxicity toward humans. Some of the most common examples of such agents include tabun (GA) (**1**, figure 1), VX (**2**, figure 1), Sarin (GB) (**3**, figure 1), soman (GD) (**4**, figure 1), which were all mass produced by several countries around the globe. These agents are phosphonates derivatives,[6] and their chemistry present important parallels. [6,7]

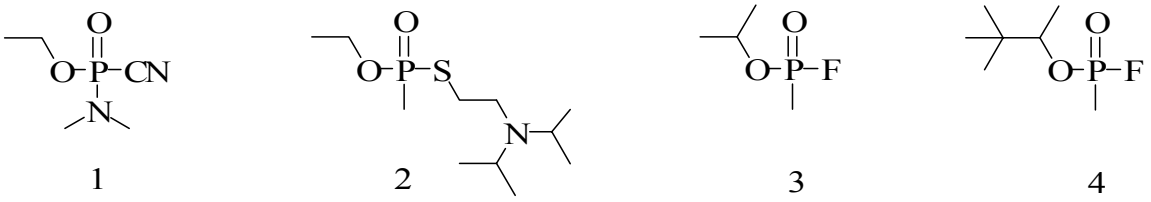

Figure 1. Structure of GA, VX, GB, and GD.

In particular, the toxicity of these agents stems from their ability to phosphorylate the serine residue at the active site of the acetylcholinesterase enzyme (AChE).[8 9] This phosphorylation is accompanied by a deactivation of the enzyme which is no longer able to hydrolyze acetylcholine, a neurotransmitter. As a result of these chemical events, regulation of the acetylcholine concentration is greatly affected and increased amount of

this neurotransmitter are present in the synapses. This triggers motor responses including spasms which, depending on the nature of the organ affected, can have lethal consequences. Following the decree of the chemical weapons convention treaty in 1997, The United States has started to destroy stockpiles of these agents. Despite intense research during the second half of the last century, the decontamination and demilitarization of organophosphorus nerve agents is still, unfortunately a critical problem.[10] Moreover, these chemical agents have been used by terrorist groups and continue to pose a threat to civilian populations. Hence efforts toward the development of decontamination techniques are fully justified and have become the prime objective of diverse research groups.[11]

1.2 General decontamination procedures

Hyprochlorite solution can be used to decontaminate V- and G-agents (figure 2).[12] At low pH, the use of hypochloric acid is efficient for the neutralization reaction of VX, while under basic pH, 10 moles of active chlorines are actually needed to oxidize 1 mole of VX. In both mechanisms the hypochlorite anion functions as a nucleophilic catalyst. In fact, super chlorinated bleach solutions remained the most common general purpose decontaminants during and after World War II. However, the active chlorines would rapidly decompose upon storage and large excesses of bleach were needed for the oxidation of the agents. As these solutions were also corrosive to most surfaces and ineffective under cold weather, alternative decontamination techniques were developed.

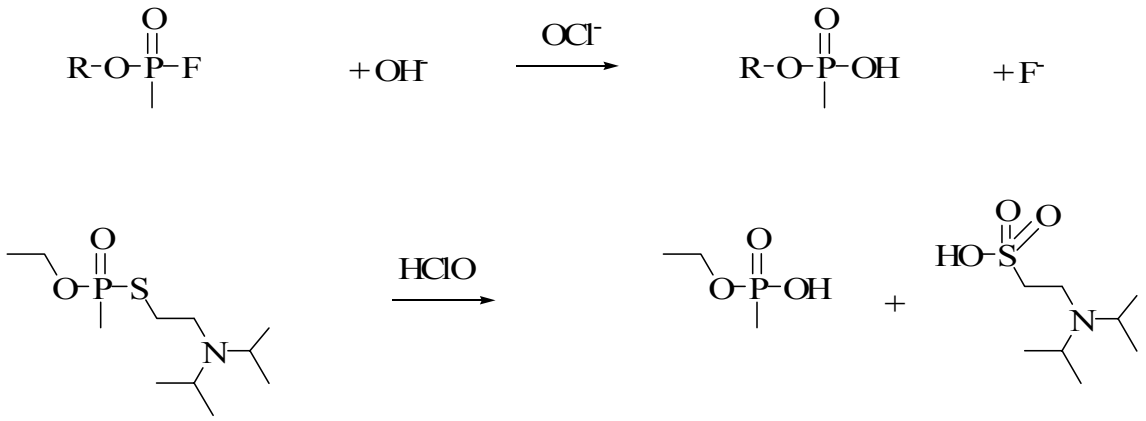

Figure 2. Detoxification of G- agents and VX with Bleach.

These efforts led to the formulation of a new decontamination solution, namely DS2, which was developed in 1960.[13] DS2 is a polar non aqueous solution able to dissolve any warfare agents. It is a noncorrosive solution, stable upon storage and active from -26 ^{o}C to 52 ^{o}C. This solution in composed of 70% of diethylenetriamine, 28% of ethylene glycol monomethyl ether and 2% of sodium hydroxide. The reactive compound in this solution is in fact the conjugated base of ethylene glycol monomethyl which vigorously reacts with organophosphonate chemical warfare agents (figure 3). This reaction leads to the formation of a non-toxic phosphonate diester bearing a monomethyl ethylene glycoxy group and which further reacts with hydroxide ions to form the corresponding phosphonate monoesters.[14] While DS2 has shown to be a

powerful decontaminant agent, it remains armful toward paints, plastic, rubber and leather materials, and more importantly it is corrosive to skin.

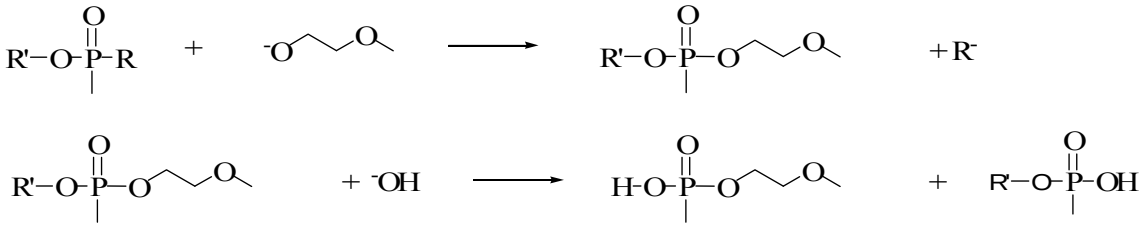

Figure 3. Detoxification of G- agents with DS2.

Earliest decontaminant used on skin remained bleach on dry form for half a century. During the 60s, the soviet army discovered a new personal decontamination kit which was believed to be very efficient against both VX and G- agents. This kit contained a solution of chloramines-B ($PhS(O)_2$)NClNa and was effective against VX agent.

1.3 *o*-Iodocarboxylates

Heterocyclic iodanes, such as *o*-iodosylcarboxylates (**5**, figure 4) and *o*-iodylcarboxylates (**6**, figure 4), contain hypervalent iodine and oxygen incorporated in a five membered ring fused to a phenylene ring. These molecules, as well as their chemical reactivity, have been the subject of several reviews.[15] In 1983, the respective conjugate bases of **5** and **6**, IBA (**7**, figure 4) and IBX (**8**, figure 4) were discovered to be an effective nucleophiles for the cleavage of chemical warfare simulants such as *p*-nitrophenyl diphenyl phosphate (PNPDPP) in aqueous micellar media (figure 4).[16] These compounds are in fact supernucleophiles. Owing to the presence of a lone pair in α from the nucleophilic center, these derivtiaves display an enhanced reactivity when compared with other nucleophile of similar basicity and are often referred to as supernucleophiles. Because of their relatively low pKa, these species exist in their deprotonated nucleophilic form even at low pH's.

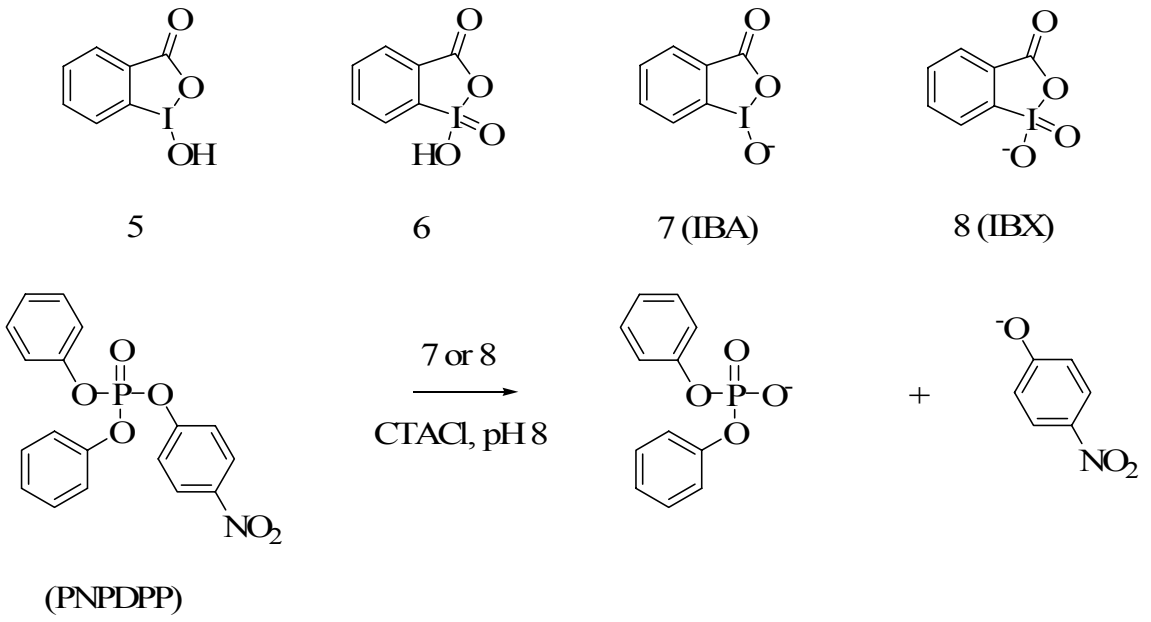

Figure 4. Structure and reactivity of various Heterocyclic iodanes with PNPDPP.

Following this discovery, a large variety of iodine carboxylates were synthesized and tested.[17] Data derived from X-ray structurural studies and computational studies show a highly distorted five-membered ring with approximately T-shaped geometry at iodine. It appeared that IBA, the most reactive nucleophile toward PNPDPP, had the shortest endocyclic I-O bond and the largest electron density on its exocyclic oxygen.[18] In the same way, the stability of these iodosyl derivatives in aqueous solution is directly linked to the stability of the endocyclic I-O bond. Thus, IBA is one of the most stable and reactive oxygen nucleophile. Various analogues of IBA, such as INA (**9**, figure 5) and other compounds (**10**, **11**, figure 5) have also been synthesized.[19] It appeared also

that **9** is 4 times more reactive than IBA. As the typical reaction is done in presence of surfactants, the significant rate enhancement was explained by the additional aromatic ring which increases the hydrophobicity and binding to micellar system where the reaction occurs. **10** and **11** show an even greater nucleophilic reactivity. This was suggested by the additional steric interaction between the 8-*peri*-H atoms and the adjacent oxygen (**10**) and carbonyl (**11**) which where relieved by a shortened endocyclic I-O bond leading to an enhanced negative charge and nucleophilicity at the O^-.

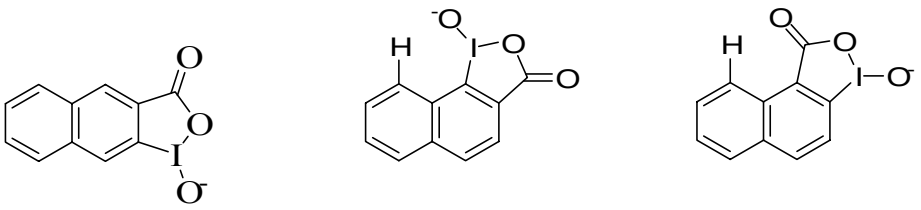

Figure 5. Structure of INA and various analogues.

Reactivity in association with surfactants has been thoroughly studied during the past decades.[20] It is now widely accepted that the rate enhancements observed in such media are largely the result of increased concentrations of reactants in the small

interfacial volumes in which the reactions are believed to occur. This theory can be fully revealed if the concentration of the reactants is kept constant, and the surfactant concentration gradually increased (figure 6).[21]

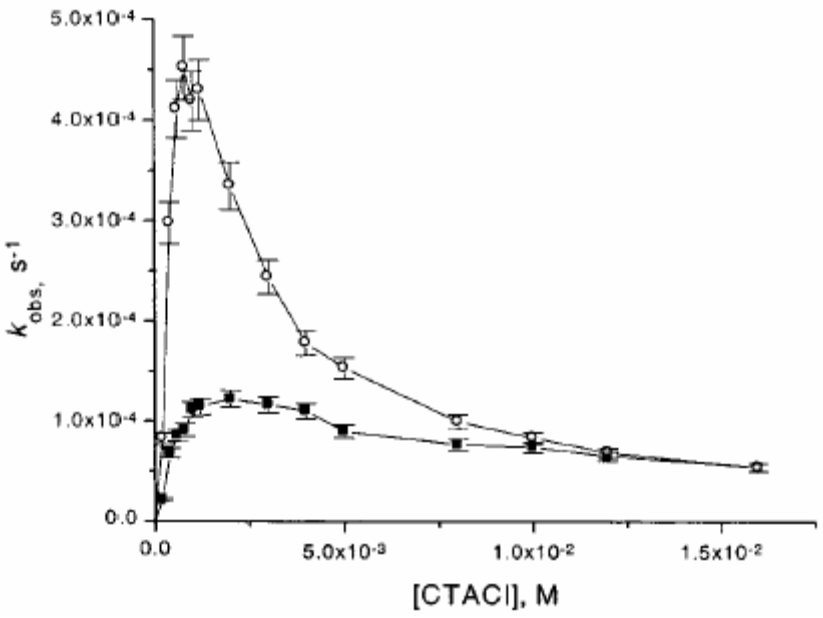

Figure 6. Cleavage of 10^{-5} M parathion by 10^{-4} M IBA (■) or INA (○) as a function of cetyltrimethylammonium chloride (CTACl) (M) at pH 8.0 and 25°C.

The rate constant versus cationic surfactant goes through a maximum which is the balance point between the positive addition of reactive interfacial volumes and the negative dilution of the nucleophile.

Finally, the incorporation of heterocyclic iodanes in cationic surfactants, such as the duplex-IBA catalyst (**12**, figure 7), and solid supports, such as the silica-bound IBA (**13**, figure 7),[22] permitted another catalytic enhancement of the nucleophilic cleavage of PNPDPP by a further increase of the local concentration of the nucleophilic iodane moities at the micellar interface where the reaction occurs.

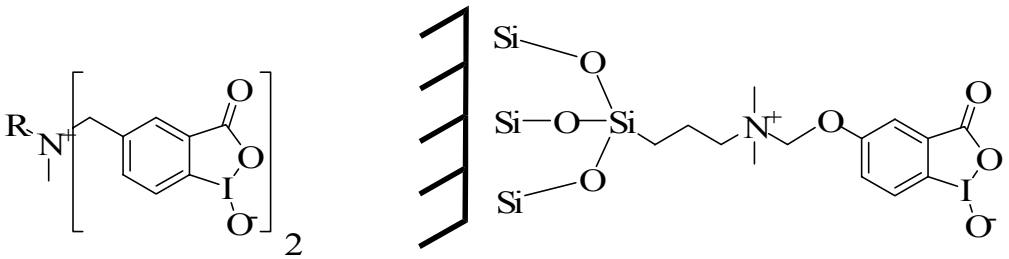

12 13

Figure 7. Structure of duplex-IBA and silica-bound IBA.

1.4 Related nucleophiles

1.4.1 α effect nucleophiles

Other supernucleophiles have also been successfully used as nucleophilic catalysts for the hydrolysis of organophosphorus esters. Just like iodine carboxylates, PNPDPP hydrolysis is also largely enhanced by the addition of oximate anions such as benzaldoximes (**14**, figure 8) and pyridinealdoxime (**15**, figure 8) in presence of the cationic surfactants (CTACL).[23] These oximes posses a rather high p*K*a (9-12) which leads to a poor catalytic activity at neutral or slightly basic pH. However, pyridinium-oxime derivatives, such as 2-PAM (**16**, figure 8) show an effective enhancement of their catalytic activities at a lower p*K*a.[24] The incorporation of amphiphilic oximes in cationic surfactants (**17**, figure 8) also lead to the efficient phosphorylic cleavage of PNPDPP with high turnover.[25]

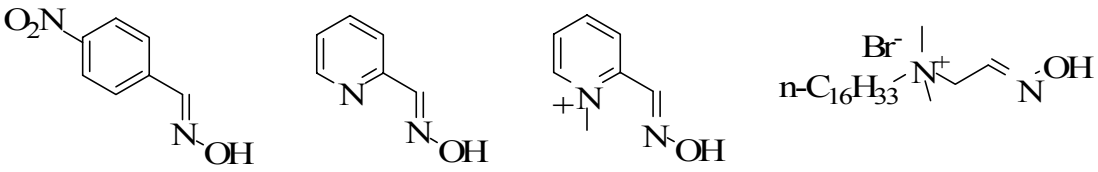

14 15 16 17

Figure 8. Structure of various oximes.

Peroxyanions such as monoperoxyphthalate (**18**, figure 9) and hydroperoxide also display an enhanced nucleophilic reactivity compared to other nucleophiles with the same basicity due to α effect (increase nucleophilicity provoked by the proximity of an unshared pair of electrons on an atom adjacent to the nucleophilic site). The dephosphorylation of PNPDPP,[26] and more importantly of VX,[27] with HO_2^- in cationic micelles displayed a very good reactivity. As the p*K*a of H_2O_2 is greater than 11, the use of this nucleophile requires extreme conditions. Monoperoxyphthalate (p*K*a ≈ 8), however, has shown a slower reactivity in cationic micelles for the hydrolysis of PNPDPP as well as paraoxon (**19**, figure 9) and parathion (**20**, figure 9).[28]

1.4.2 Alkoxydes

Nucleophilic cleavage of PNPDPP by simple nucleophiles such as alkoxides is also effective.[29] The larger problem to overcome is the use of strongly basic non aqueous solvents as the p*K*a of these alcohols are usually as high as 15. However, surfactants with long alkyl chain terminated by hydroxyethylammonium (**21**, **22**, figure 9) with polyols as cosolvents were shown to efficiently cleave PNPDPP under mild conditions.[30]

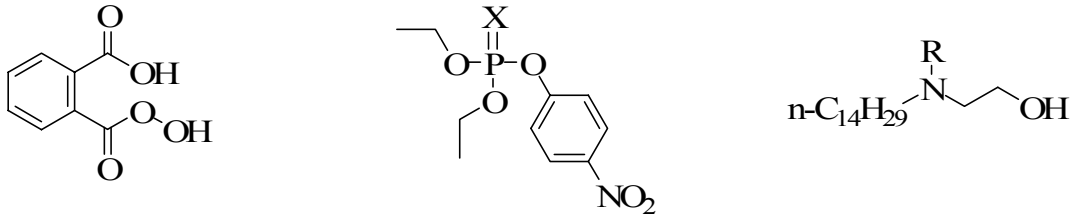

18

19 (X=O Paraoxon)
20 (X=S Parathion)

21 (R=H)
22 (R=CH_3)

Figure 9. Structure of 18-22.

1.5 Enzyme catalyzed hydrolysis and mechanisms

Approximately 30 years ago, two types of enzymes were found to be capable of the catalytic hydrolysis of organophosphotriesters. These bacterial phosphotriesterases (PTE) isolated from, *Pseudomonas diminuta* and *Flavobacterium* have the ability to hydrolyse a broad range of organophosphate pesticides and warfare agents with extremely high turnover.[31] In fact, organophosphorus warfare agent tolerance is directly correlated to the concentration levels of PTE that can be found in various organisms. For example, mammals, with high level of PTE, are more tolerant to organophosphorus acetylcholine inhibitors than birds and insect lacking PTE.[32]

During the past decade the organophosphorus hydrolase (OPH), from *Pseudomonas diminuta*, has received much attention.[33] More specifically, it is able to hydrolyse most warfare agents including **2**, **3**, **4**, **19**, and **20**. OPH is also the only known enzyme able to hydrolyse thiophosphorus esters at a significant rate.[34] The native enzyme is known to be composed of a zinc subunit. X-ray analyses of OPH were initiated in 1994 with the first unintentional crystal structure of the Cd (II) substituted enzyme.[35] Indeed, it was immediately obvious, contrary to previous reports,[36] that the active site was a dinuclear Cd (II) moiety containing a bridging hydroxide. With the molecular model of the Cd (II) substituted OPH, the next achievement was the growth of crystals of the active Zn (II)/Zn (II) enzyme (figure 10).[37] As shown by a crystal structure, this enzyme possesses a deeply buried and unsymmetrical dinuclear active site in which the two metals are bridged by a carbamylated lysine as well as a hydroxide. One of the zinc centers coordinates to two histidines as well as an aspartic acid and features a more hindered coordination sphere, while the other coordinates to the two other histidines and a solvated hydroxide. The metal centers are separated by 3.3 Å and the metal ligand bond distances range from 1.9 to 2.3 Å.

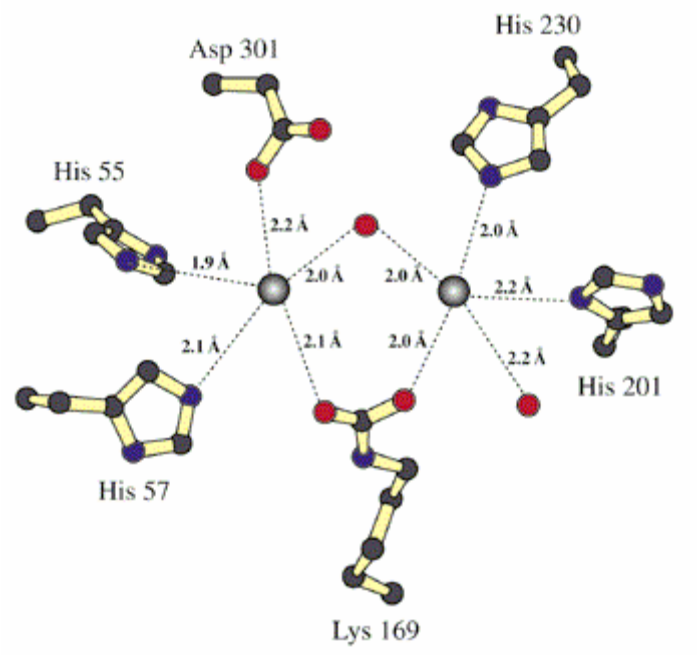

Figure 10. Representation of the binuclear Zn^{2+}/Zn^{2+} metal center at the active site of OPH.

The native enzyme remains highly active in the hydrolysis of **19** after substitution of one or both Zn (II) by Cd (II), Mn (II), Ni (II), or Co (II). Interestingly, the dicobalt (II) substituted enzyme revealed to be the most efficient.[38] The mechanism of action of OPH is not fully understood and the precise role of the two divalent cations in the catalytic process has been investigated.[39] The mechanism for the enzymatic hydrolysis of **19** can be viewed as proceeding by three possible routes (figure 11). In the first mechanism, a nucleophilic attack occurs at the C-1 of the aromatic ring (**A**, figure 11).

Eventhough this mechanism appears to be less likely to happen, the removal of the intermediate stabilizing NO_2 substituent diminished the overall reactivity by 5 orders of magnitude.

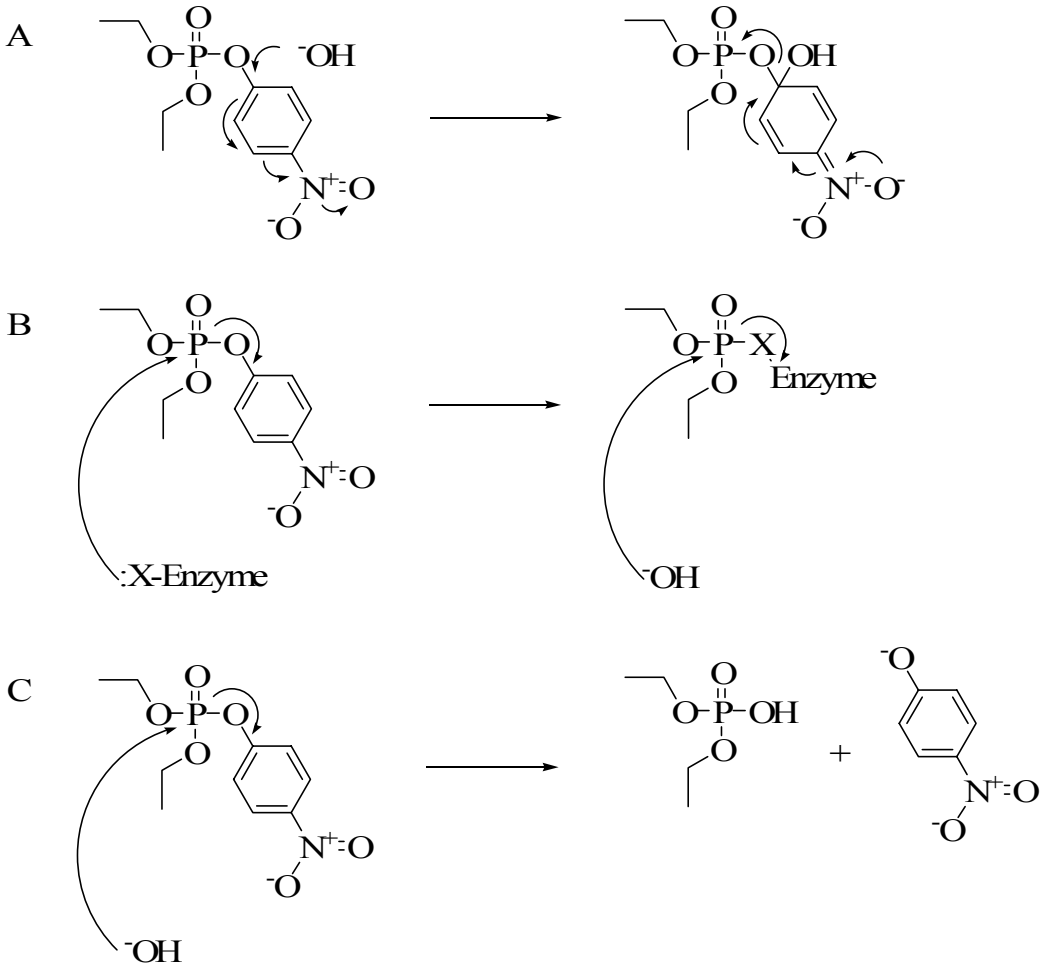

Figure 11. Cartoon of the possible enzymatic hydrolysis mechanisms.

The other two mechanisms can be described by a S_n2 mechanism in which the water molecule attacks the phosphoryl center and displaces the leaving group. The second mechanism proposes the attack of a side chain of the protein, followed by another S_n2 by water at the phosphorus regenerating the free enzyme (**B**, figure 11). This overall mechanism results in a retention of configuration at the phosphorus.

The third mechanism involves a single displacement by a hydroxide molecule at the phosphorus yielding the phosphoric acid product in a single step with an inversion of configuration at the phosphorus center (**C**, figure 11). As OPH hydrolytically cleaves the insecticides (*S*)-EPN (23) to produce (*S*)-*O*-ethyl phenylphosphonothioic acid (24) with inversion of configuration, the later single S_n2 mechanism **C** was strongly suggested.[39]

The replacement of any of the donating histidines leads to a dramatic 400-5000 fold drop in organophosphorus triester hydrolysis, showing the importance of the use of both metal center in the catalytic cycle.[40] On the basis of these studies, two mechanisms have been proposed involving either an intramolecular nucleophilic attack of the bridged hydroxide onto the phosphorus center (**D**, figure 12), or the nucleophilic attack of a solvated hydroxide to the organophosphorus bridging adduct (**E**, figure 12).

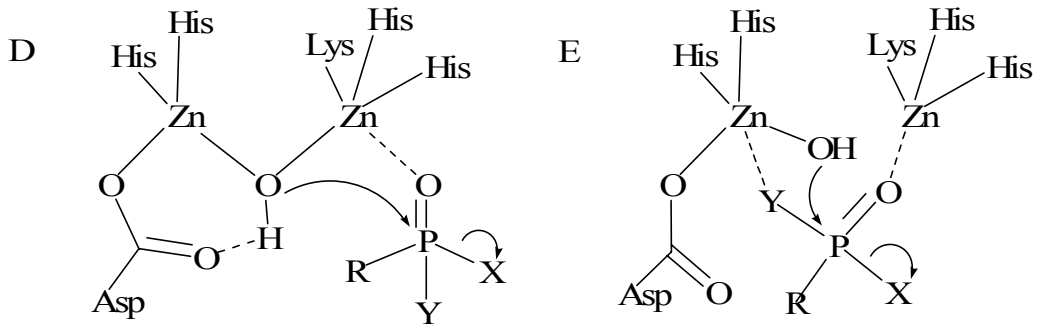

Figure 12. Proposed mechanisms for the hydrolysis of warfare agents at the active site of OPH.

At this time, there is only few example of bidentate coordination of organophosphorus triester to metal centers,[41,42] while there are numerous example of η^1-coordinated phosphate triester. Diisopropylmethyl-phosphonate was found to coordinate to a single Zn metal center of OPH.[43]

1.6 Organometallic catalysis and mechanisms

Hydrolysis of organophosphorus triesters has also been achieved using "green" catalysts such as transition metal cations and their complexes.[44] Much of the interest was generated by the efficient use of Cu (II) cation for the degradation of the G- agent stimulant diisopropyl phosphorofluoridate (**23**, figure 13) and the hydrolysis of

thiophosphoester such as **19**.[45] Other early available examples indicated that the divalent Hg (II) cation constituted as well a rather potent candidate accelerating the hydrolysis rate of **19** by a magnitude of 2 to 3.[46] The use of lanthanide metal cation Ln (III) has also been investigated. As the stability of highly charged metal cations in aqueous media is always a concern, macrocyclic (**25**, figure 14)[47] and cryptate (**26**, figure 14)[48] lanthanides were prepared and tested with effective turnover for the hydrolytic decomposition of 2,4-dinitrophenyl diethyl phosphate (**24**, figure 13) and PNPDPP respectively.

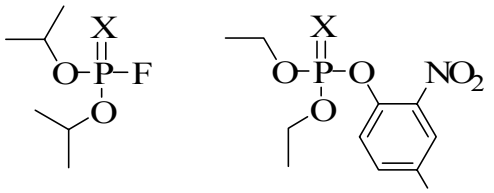

23 24

Figure 13. Structure of diisopropyl phosphorofluoridate and 2,4-dinitrophenyl diethyl phosphate.

Coordination complexes have also proved to be active. Early reports of Martell and others revealed that Cu (II) diamine complexes (**27**, figure 14) catalyzed the hydrolysis of Sarin (**3**) and the isopropyl derivative **23**.[12,49]

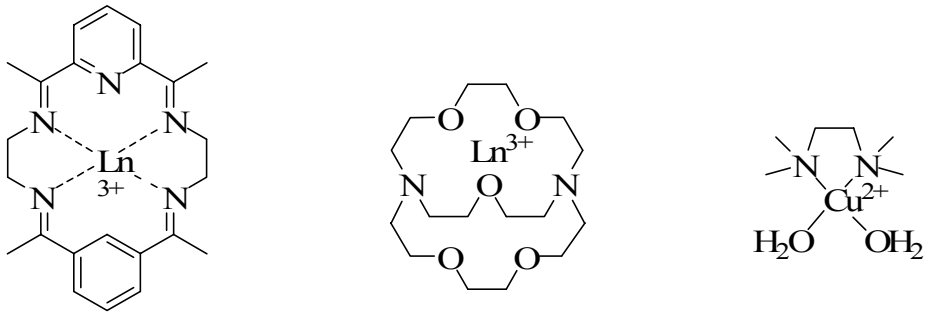

Figure 14. Structure of related lanthanides and Cu (II) diamine complexes.

Reactivity of transition metal complexes in micelles has also been thoroughly studied in the past two decades. The earliest work was done by Breslow with the synthesis of a zinc complex of a tetraaza macrocycle (**28**, figure 15) with a pendant long alkyl chain.[50] The metallomicelle was able to catalyse the hydrolysis of PNPDPP. Another significant advance was achieved with the introduction of a Cu (II) metallomicelle (**29**, figure 15).[51] This molecule derives from the earlier work done by

Martell in the early 60s. It appeared that this long chain Cu (II) complex displayed an even greater reactivity for the cleavage of PNPDPP. Other examples of Cu (II) metallomicellar systems (**30**, figure 15) were also studied and compared to non micellar analogues.[52] For instance, the analysis of the rate of cleavage of PNPDPP and paraoxon by **30** revealed an increase in reactivity for the metallomicellar complex.

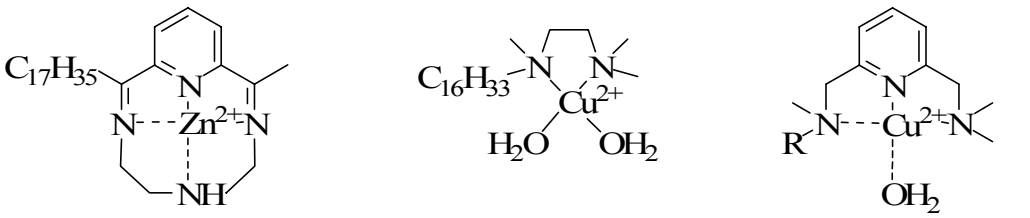

28 29 30 (R = CH_3, $C_{16}H_{33}$)

Figure 15. Structure of related Zinc (II) and Cu (II) complexes.

New classes of coordination complexes have also been investigated. Complexes of Rh (III), Ir (III),and Mo (IV) also demonstrate a good reactivity.[44,53] Interestingly, the use of the water soluble molybdenum metallocene catalyst provided the first example of a nucleophilic attack at the C-1 of the aromatic ring (mechanism **A**, figure 11). Furthermore, labelling studies using **20** proved that the nucleophilic attack occurs at the

α-carbon of the organothiophosphate and not at the phosphorus center. It is also important to note that several minerals including alumina, titania, goethite and clays can surface catalyse the hydrolysis of thiophosphate triesters.

Another interesting nonmicellar approach to nucleophilic decomposition of organophosphorus triesters employs the group 8 metal complexes (**31**, **32**, figure 16). Recently, Ryabov et all introduced Pd (II) and Pt (II) orthometalated aryl oxime complexes ([MCl{*C*,*N*-($C_6H_4C(CH_3)$=NOH)-2}(L)], M = Pd or Pt, L = DMSO or pyridine) for the cleavage of thiophosphate triesters.[54] It could be argued that palladium and platinum are too soft Lewis acids, and that the square-planar configuration of the metal centers which has never been reported in the enzymatic system is less likely to demonstrate any decent catalytic activity. Nevertheless, Pd and Pt electrophilicity coupled to the nucleophilicity of the coordinated oximate anion, provided an outstanding reactivity toward thiophosphate triester hydrolysis such as **20** at pH 8.5. Although no reaction intermediates have been isolated, it has been proposed that the activity of such catalysts results from the coordination of parathion at the metal center followed by an intramolecular nucleophilic attack by the neighboring oximate (figure 17).

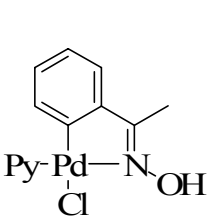

31

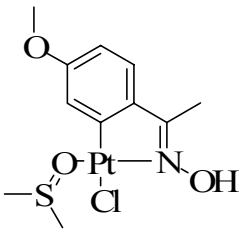

32

Figure 16. Structure of related Pd (II) and Pt(II) orthometalated aryl oximes.

With a catalytic amount of the Pt (II) complex, first-order kinetic hydrolysis of **20** follows. The k_2 were also measured for all of the above catalysts and compared to the hydroxide catalyzed hydrolysis. It appeared that the catalytic activity of the Pd (II) and Pt (II) complexes at a concentration as low as 10^{-4} M revealed an activity 10^6-10^7 times higher than the hydroxide, representing by far the most efficient biomimetic system ever encountered.

The proposed mechanism of the hydrolysis is depicted in **F** (figure 17). Initial coordination to the metal activates the thioester toward intramolecular nucleophilic attack of the oximate to the phosphorus center, providing rate enhancement of 10^9 fold over the hydroxide catalyzed reaction at pH 8. Moreover, rapid decomposition of the phosphorylated oxime intermediate must account for the observed turnover. In such mechanism the role of Pd (II) and Pt (II) is double. Not only they increase the positive

charge on the phosphorus, but the added coordination to the oxime lowers its pK_a enhancing their nucleophilicity at neutral pH.

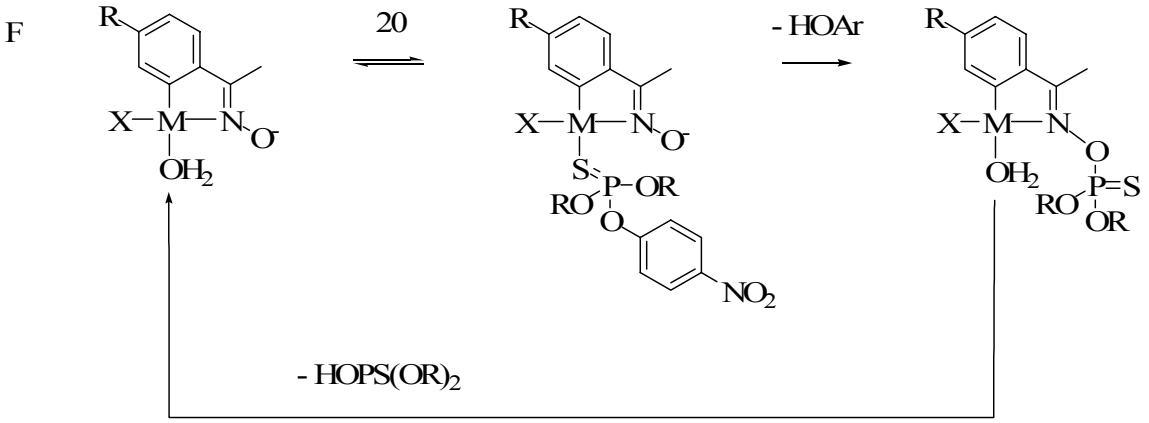

Figure 17. Proposed mechanisms for the hydrolysis of parathion with Pd (II) and Pt (II) complexes.

1.7 Objectives

As the lack of current "green" decontamination process still remains, recent researches have been focused on the study of a large variety of methods for the degradation of these compounds. Significant advances have been made with the use of

organic nucleophiles. Many iodosylcarboxylate derivatives have been prepared and shown interesting catalytic properties for the hydrolysis of G- type agents. However, these compounds are not active in the hydrolysis of V type agents as well as thiophosphorus esters.

As of today, OPH remains the most active catalyst for the hydrolysis of organophosphorus triesters remain the most efficient catalysts. Although, a large variety of G- type warfare agents as well as V-types are efficiently decomposed by OPH, the mass production of the enzyme remains a struggling problem. The active site has been shown to consist of a unique binuclear metal center delivering a hydroxide for a S_n2 attack onto the phosphorus center.

Many research groups have also investigated a broad range of mononuclear coordination and organometallics complexes as catalysts. These catalysts have been shown to be highly efficient for the hydrolysis of the G- type agents. Furthermore, as the molecular weight of these synthetic catalysts is very low compared to OPH, their production remains very competitive even if used at higher loading. However, these complexes have shown a lesser affinity for the cleavage of harder oxygen donor pesticides compared to the thiono derivatives. Also, no synthetic complexes have been proven suitable for the catalytic decontamination of the V- type nerve agents. Finally, it is important to note that so far, very few dinuclear complexes that would mimic the OPH active site have been investigated. [55]

Based on the above, it has become the objective of this work to attempt the preparation of dinuclear complexes that mimic the active site of PTE. In order to progress toward this goal, the following tasks have been identified:

To synthesize chiral dinucleating ligands with pyridazine as a central core.

To synthesize dinucleating ligands with 1,4-(iminomethyl)benzene as central core.

To study the ligative behavior of the ligands toward various metal cations.

To study the interaction of the dinuclear metal complexes with phosphorus triesters.

To test the catalytic activity of the complexes in organophosphate ester hydrolysis.

CHAPTER II

EXPERIMENTAL PROCEDURES

2.1 General considerations

Methylparathion is highly toxic and should be handled in a well-ventilated fume hood. All glassware exposed to methylparathion should be decontaminated with bleach. All anhydrous reactions were carried out under nitrogen atmosphere in oven-dried (130 °C) glassware by using Schlenk and glovebox techniques unless noted otherwise. The nitrogen source was passed over P_2O_5 immediately prior to entering any glassware. For the handling and the use or synthesis of air-sensitive compounds, solvents and deuterated solvents were freshly distilled prior to use. Tetrahydrofuran (THF) was freshly distilled over NA/K amalgam. Acetonitrile (MeCN), chlorophorm ($CHCl_3$) dichloromethane (CH_2Cl_2), diethylether (Et_2O), hexane, pentane, pyridine, and triethylamine (TEA) were distilled from calcium hydride (CaH_2) prior to use. Benzene (PhH), and toluene (PhMe) over K. Methanol, Ethanol, and Ethyl acetate were used without purification. The methylparathion solution was provided by A/S CHEMINOVA, LEMVIG, DK-7620, Denmark as a gift. 2 were freshly prepared using literature protocols. 3,6-distyrylpyridazine, *O*-TBDMS-(1*R*,2*S*)-(-)-norephedrine, *O*-TBDMS-(1*R*,2*S*)-(-)-norephedrine, 3,6-pyridazinedicarboxaldehyde, *O*-benzyl-(1*R*,2*S*)-(-)-norephedrine, 2,3-dimethoxy-benzene-1,4-dicarbaldehyse derivatives, (1*R*,2*S*) (-)-2-(N-norephedrinyl-methyl)pyridine, (1S-2R)-1-[(pyridin-2-ylmethyl)-amino]-indan-2-ol, [2-(2-pyridyl)-

phenyl-*C,N*]palladium(II) acetate was prepared following the published synthesis.[56] Other chemicals were commercially available and were purchased from Aldrich, or VWR and used without purification.

2.2 Spectroscopy

Reactions were followed by thin layer chromatography (TLC) on EMD chemicals silica gel 60 and aluminum oxide 60 F_{254} (250 μm thick). TLC's were visualized with a UV lamp and stained using vanillin. Purifications of compounds were carried out by flash chromatography using Natland silica gel (100-230 mesh). All NMR studies were carried out on an Inova 300 and 500 MHz NMR spectrometer (300 and 500 MHz for ^{1}H, 100.5 and 125.7 MHz for ^{13}C, 121.4 MHz for ^{31}P NMR). 85% H_3PO_4 was used as an external standard for the solution ^{31}P NMR spectra. The proton and carbon signals of the deuterated solvent were used as internal standard for the ^{1}H and ^{13}C NMR spectra, respectively. Solvents are indicated for each compound. ^{1}H NMR coupling constants (J) are reported on Hertz (Hz) and multiplicity is abbreviated as follows: *app* = apparent, s = singlet, d = doublet, dd = doublet of doublets, t = triplet, q = quartet, m = multiplet, *br* = broad signal. IR spectra were acquired using an ATI Mattson genesis series spectrometer in the solvent indicated. Vibration frequencies are expressed in cm^{-1}. Elemental analyses were performed by Atlantic Microlab Inc. at Norcross, GA 30091. Melting points were measured on a Laboratory Devices Mel-Temp apparatus and were not corrected. All UV/Vis absorption spectra and spectrophotometric measurements

were recorded on a JASCO V530 UV/Vis spectrometer equipped with an automatic cell changer. Single-crystal X-ray analysis for 2 was collected on a bruker SMART-CCD diffractometer using graphite-monochromated Mo Kα radiation (=0.710 73 Å). Specimen of suitable size and quality was selected and mounted onto a glass fiber with Apiezon grease. The structure was solved by direct methods, which successfully located most of the non-hydrogen atoms. Subsequent refinement on F^2 using the SHELXTL/PC package (version 5.1) allowed location of the remaining non-hydrogen atoms.

CHAPTER III

LIGAND DESIGN

3.1 Introduction

Inspired by the role of dinuclear metalloenzymes in several biological processes, recent developments in the area of Lewis acid catalysis have been concerned with the study of bifunctional catalysts that mimic the functions of these enzymes.[57] An impressive collection of dinuclear complexes has been prepared and their catalytic properties tested.[58],[59],[60],[61],[62],[63],[64],[65] While dinuclear metalloenzymes fulfill diverse functions,[66] a large proportion of the biomimetic studies focus on hydrolase catalysts similar to those encountered in phosphoesterase.[67] Structural analyses supported by kinetic studies indicate that the catalytic properties of these complexes result from synergistic effects that occur at the proximal metal centers of these derivatives.

The knowledge gathered from these studies has served to fuel a growing number of investigations in the field of organic reaction catalysis. A large majority of the complexes investigated so far utilize main group elements or early transition metals at the active site of the catalyst. The group of Maruoka has been especially industrious in this area and has described a series of achiral complexes that utilize 1,8-biphenylenedioxy and 1,8-anthraquinonedioxy ligands in combination with hard metal cations such as aluminum (III) and titanium (IV) (**33**, **34**, figure 18).[68] These complexes are effective catalysts in a number of reactions that involve carbonyl substrates such as

the Mukayama aldol condensation. Supported by NMR studies, the activity of these catalysts has been proposed to result from the double coordination of the carbonyl oxygen atom of the substrate to the two juxtaposed metallic centers.[69] This proposal, which remains largely unsupported and lends itself to some debate, has been advanced to rationalize the higher reaction rate observed when bifunctional rather than monofunctional catalysts are used. Parallel studies carried out on thiocarbonyl derivatives by Hawthorne suggest that analogous phenomena occur with mercury-based polyfunctional Lewis acid catalysts (**35**, figure 18).[61] While these studies are likely to shine some light on the mechanisms that are at play in bifunctional Lewis acid catalysis, the absence of chirality in the complexes will undoubtedly limit the scope of their use. It is therefore logical that a number of chiral dinuclear complexes have now been investigated for the asymmetric inductions of organic reactions.

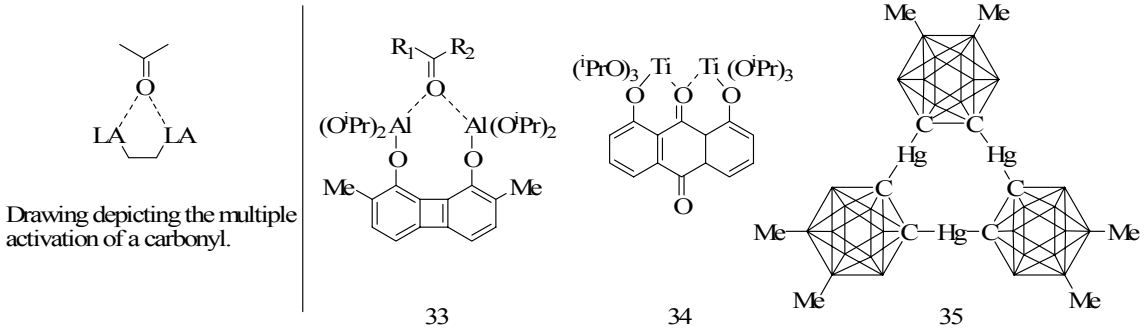

Figure 18: Maruoka, and Hawthorne's catalysts.

A series of catalysts that utilize the 1,1'-(*S*)-binaphthol ligands to bridge two metal centers (**36**, **37**, figure 19) have been described by the group of Shibasaki who observed unusually high enantiomeric excesses in various reactions including Michael addition and nitro-aldol condensation.[70] The results have been rationalized in terms of a mechanism that involves the activation of the electrophilic substrate at one metal center while the remaining metal center coordinates and transfers the nucleophile. Such phenomena present direct analogies with mechanisms independently proposed by Corey and Noyori earlier on.[58,71] More recently, catalysts that function on the basis of the same principles have been reported by Trost who demonstrated the use of chiral dinuclear zinc catalysts of type **38** for enantioselective aldol reactions (figure 19).[72] One of the clearest examples for the occurrence of two-center catalysis has been obtained by the group of Jacobsen who carry out a study on flexible dinculear Schiff base Cr(III) complexes **39** as catalysts for the ring opening reactions of epoxides (figure 19).[73] In particular, compelling kinetic evidence has been obtained for the cooperation of the two metal centers in the reaction of oxiranes with various nucleophiles including water and azide.

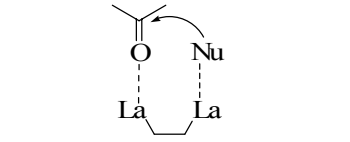

Drawing depicting the activation of a carbonyl and cooordination of the nucleophile at neighboring site.

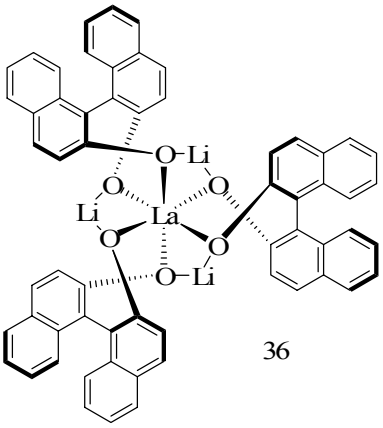

36

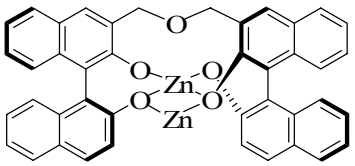

37

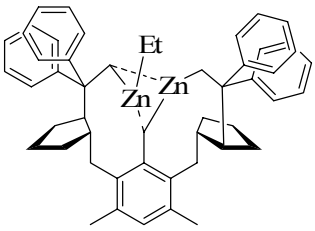

38

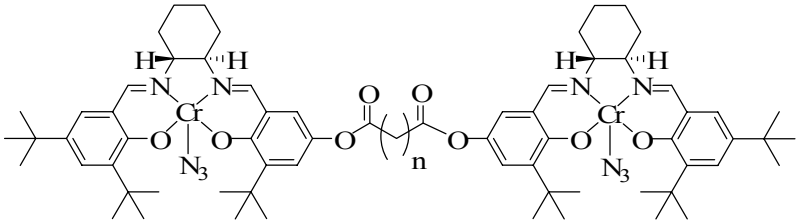

39

Figure 19: Shibasaki, Trost, and Jacobsen's catalysts.

It occurred to us that, while fairly elaborated structures had been considered, chiral versions of well studied dinuclear complexes have not been systematically investigated. For example, despite the widespread use of 3,6-substituted pyridazine ligands in the chemistry of dinuclear metal complexes,[74] only on one occasion has the preparation of a

chiral example of such a ligand been reported (**40**, figure 20).[75] Thus, it became the objective of this work to prepare chiral dinucleating ligands derived from structurally simple motifs and investigate the scope of their utility in phosphonate triester hydrolysis.

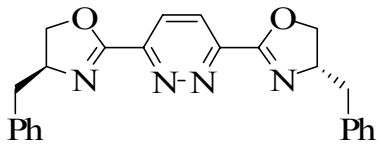

40

Figure 20: Pfaltz's binuclear ligand design.

3.2 Dinuclear pyridazine based ligands

3.2.1 Ligands derived from 3,6-dihydroxymethylpyridazine

In order to insure the monomeric nature of the transition metal complexes, the preparation of ligands able to present at least three basic sites to each metal center should be prepared. For this reason, the introduction of aminoalcohol pendant arms at the methyl positions of a 3,6-dimethylpyridazine was selected as a synthetic target. As part

of this work, we revisited the synthesis of 3,6-bis(hydroxymethyl)pyridazine (**41**, figure 21) which had been previously prepared in less than 25% yield starting from 2,5-bis(hydroxymethyl)furan.[76] Ozone was bubbled through a solution of 3,6-distyrylpyridazine at -78ºC in methanol until the blue color of ozone appeared. Excess of ozone was then removed by degassing, and an excess of sodium borohydride (3 equivalents) was added. The reaction mixture was warmed to ambient temperature allowing the isolation of **41** as a white powder in 75% yield after chromatography.

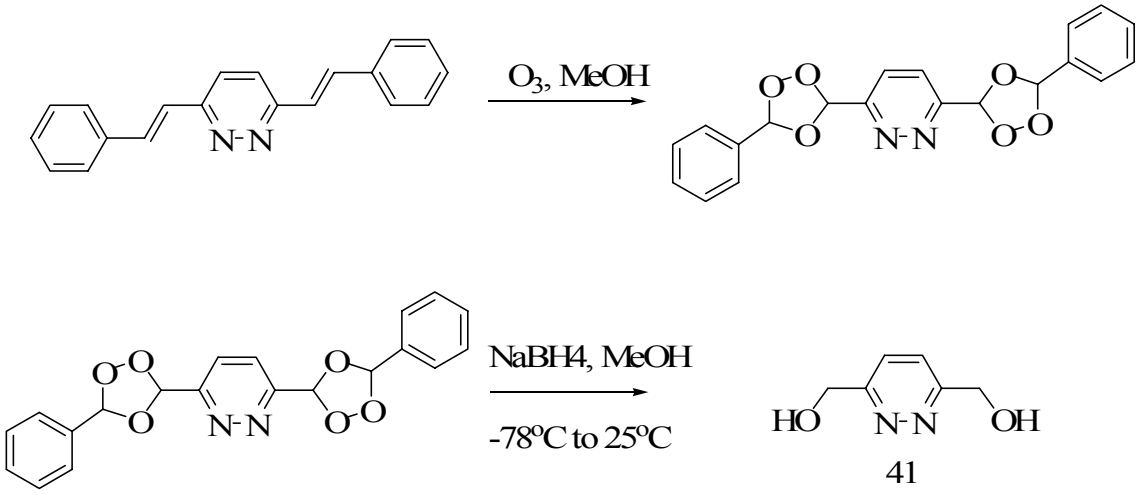

Figure 21. Synthesis of 3,6-di(hydroxymethyl)pyridazine.

In the course of this work, single crystals of distyrylpyridazine and **41** were isolated and subjected to X-ray crystallographic measurements (figure 22). Molecules of distyrylpyridazine crystallize in the triclinic space group $P2_{(1)}/c$ with one molecule per unit cell (table on page 67). The bond angles and bond lengths observed in the structure of the pyridazine core resemble those previously reported for related molecules such as the 3,6-dicarboxylic-pyridazine acid.[77] There are no unusual bond lengths and angles in the styryl pendant arms that flank each side of the pyridazine ring. Compound **4**1 crystallizes in the orthorhombic space group $Pca2_{(1)}$ with one molecule per unit cell (table on page 67). The bond angles and bond lengths observed in the structure of the pyridazine core resemble those previously reported for related molecules such as the 3,6-dicarboxylic-pyridazine acid.[78]

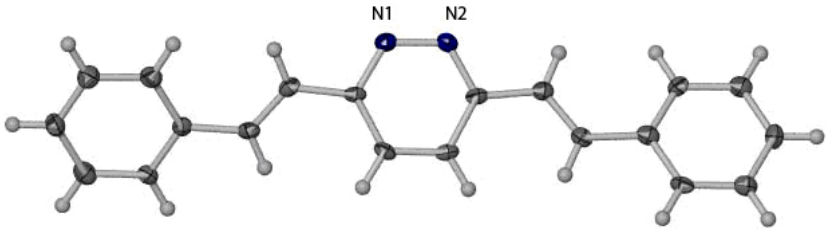

Figure 22. ORTEP view of 3,6-distyrylpyridazine and **41** (50% ellipsoids).

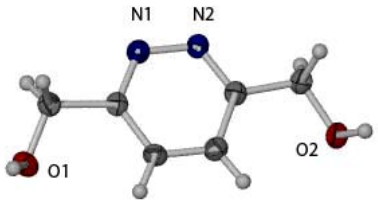

Figure 22. Continued.

Compound **41** was treated with *p*-toluenesulfonyl chloride in a THF/H_2O/NaOH mixture to afford the bistosylate 3,6-di(hydroxymethyl)pyridine di-*p*-tosylate (**42**, figure 23). Following flash chromatography purification and rapid evaporation of the solvent, **42** was isolated as white needles in 85 % yield. Compound **42** is stable when stored as a solid at -20ºC but slowly decompose at room temperature.

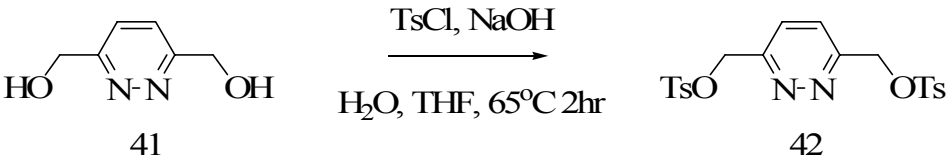

Figure 23. Synthesis of 3,6-di(hydroxymethyl)pyridazine di-*p*-tosylate.

In order to test the potential of compound **42** to serve as a starting material for the synthesis of dinucleating ligands, its reaction with (1R, 2R, 3R, 5S)-(-)-isopinocampheylamine (**43**, figure 24) in MeCN in presence of Na_2CO_3 was first investigated. After refluxing for two hours, this reaction afforded 3,6-di[-N-(1*R,*2*R,*3*R,*5*S*)-(-)-isopinocampheylaminomethyl]pyridazine (**44**, figure 24) which was purified by flash chromatography using CH_2Cl_2/10% MeOH as the eluent.

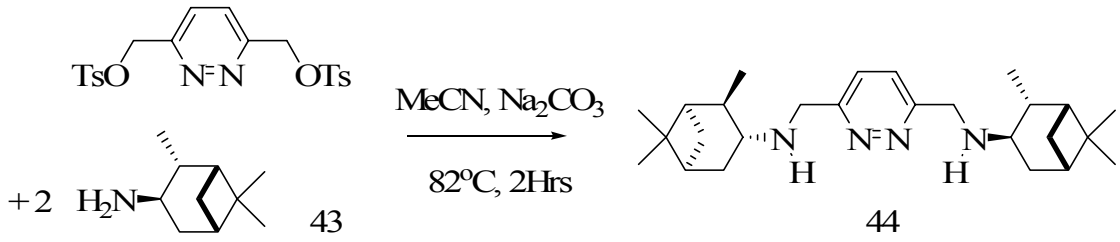

Figure 24. 3,6-di[-N-(1*R,*2*R,*3*R,*5*S*)-(-)-isopinocampheylaminomethyl]-pyridazine.

Compound **42** reacts also with two equivalent of (1R-2S)-norephedrine (**45**, figure 25) in the presence of Na_2CO_3 to afford 3,6-di[N-(1R-2S)-norephedrinylmethyl]pyridazine (**46**, figure 25) in 88 % yield after recrystallization from acetonitrile. It is important to note that this substitution reaction is regioselective and

that no O-substituted products or oligomers could be observed in the reaction mixture. In a similar fashion, **42** reacts with (1S-2R)-1-amino-2-indanol (**47**, figure 25) to afford 3,6-di[-N-(1R-2S)-1-amino-2-indanolylmethyl]-pyridazine (**48**, figure 25) in 76 % yield. As in the case of **44** and **46**, the identity of **48** has been characterized by EA, ^{1}H NMR, ^{13}C NMR and FAB mass spectrometry.

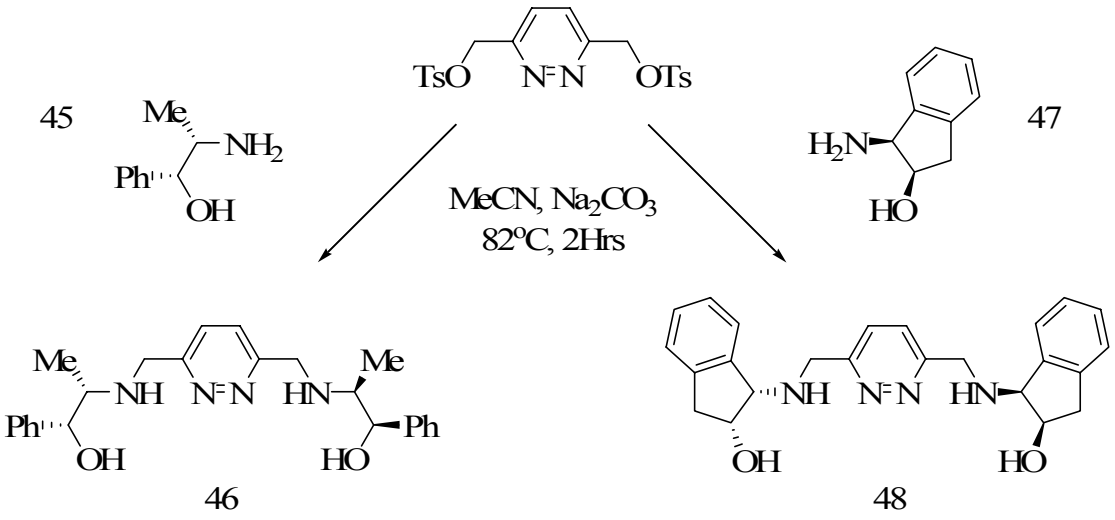

Figure 25. Synthesis of 3,6-di[N-(1R-2S)-norephedrinylmethyl]pyridazine and 3,6-di[-N-(1R-2S)-1-amino-2-indanolylmethyl]pyridazine.

Slow cooling of an ethanol solution of **48** leads to the formation of single crystals that were subjected to X-ray analysis. Compound **48** crystallizes in the orthorhombic space group $P2_{(1)}2_{(1)}2$ (table on page 68) with two molecules per unit cells (figure 26). Examination of the structure confirms the proposed connectivity and in particular, the N-attachment of the 1-amino-2-indanolyl group. Molecules of **48** have a crystallographically imposed C_2 symmetry. The bond angles and bond lengths observed in the structure of the pyridazine core of **48** resemble those previously reported for related molecules such as **41**[78] or 3,6-dicarboxylic-pyridazine acid.[78] There are no unusual bond lengths and angles in the amino-indanol moieties that flank each side of the pyridazine ring.

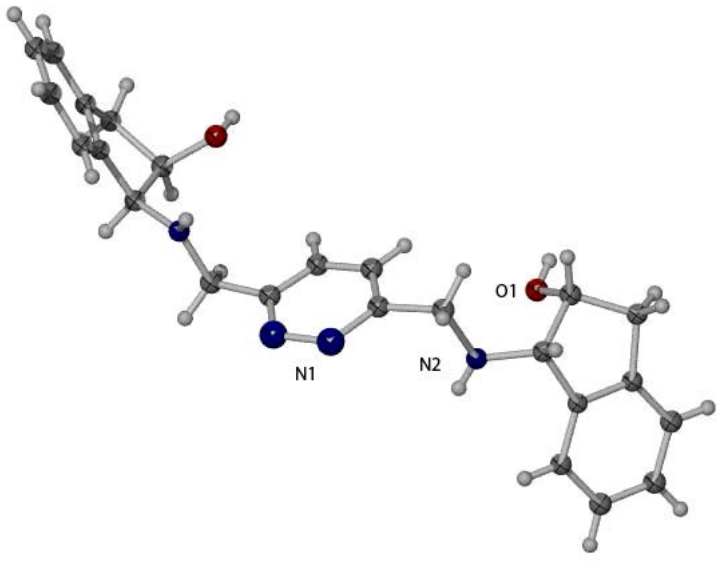

Figure 26. ORTEP view of **48** in the crystal (50% ellipsoids).

In order to generalize the synthesis of such dinucleating ligands, the reactions of **42** with various aminoalcohol reagents were investigated. These investigations lead to the observation that **42** reacts smoothly with *O*-TBDMS-(1*R*,2*S*)-(-)-norephedrine (**49**, figure 27), *O*-TBDMS-(1*R*,2*S*)-(-)-norephedrine (**50**, figure 27), (1*R*,2*S*)-(-)-ephedrine (**51**, figure 27), and L-alanine methyl ester (**52**, figure 27), respectively, to afford a variety of C_2 symmetrical dinucleating ligands in high yield (**53-56**, figure 27). All of these derivatives have been characterized by EA, ^{1}H NMR, ^{13}C NMR and FAB mass spectrometry. Furthermore, molecules of **55** have a crystallographically imposed C_2 symmetry (figure 28) (table on page 68). The bond angles and bond lengths observed in the structure of the pyridazine core resemble the bis(hydroxymethyl)pyridazine and those previously reported for related molecules such as 3,6-dicarboxylic-pyridazine acid.[78] Finally, there are no unusual bond lengths and angles in the ephedrine moieties that flank each side of the pyridazine ring.

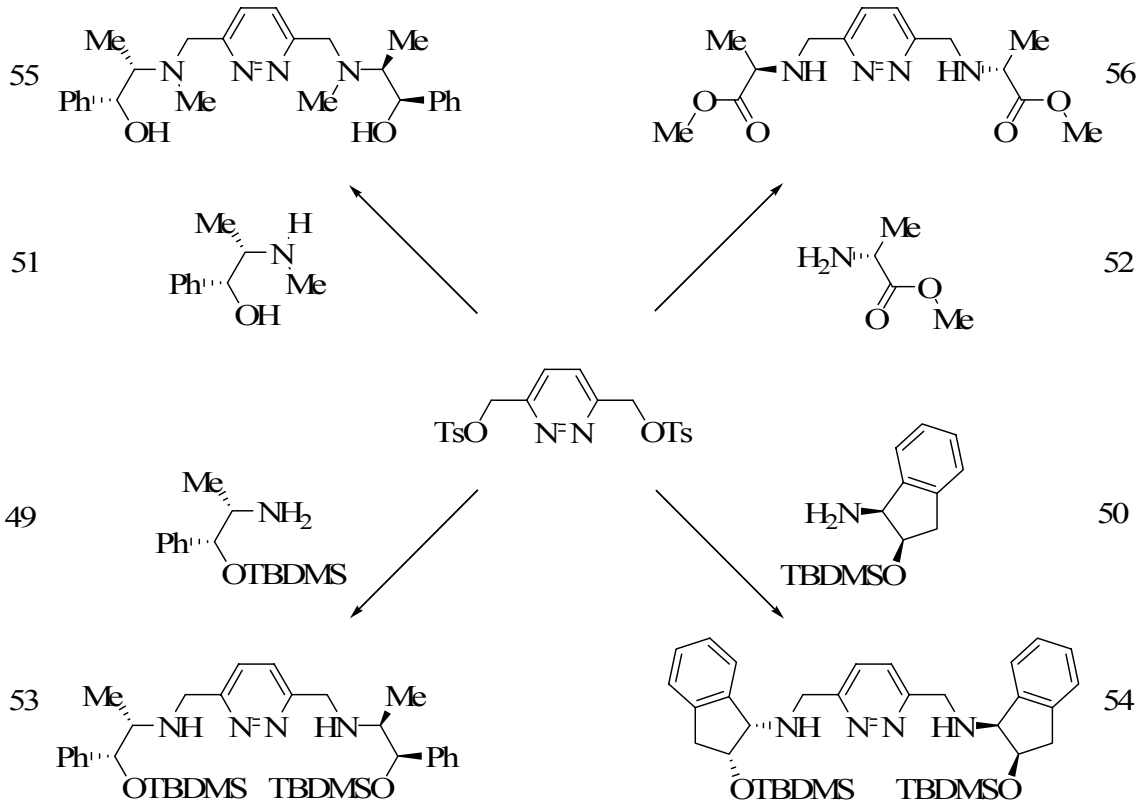

Figure 27. Reaction of 3,6-di(hydroxymethyl)pyridazine di-*p*-tosylate with various amino-alcohols in $MeCN/Na_2CO_3$

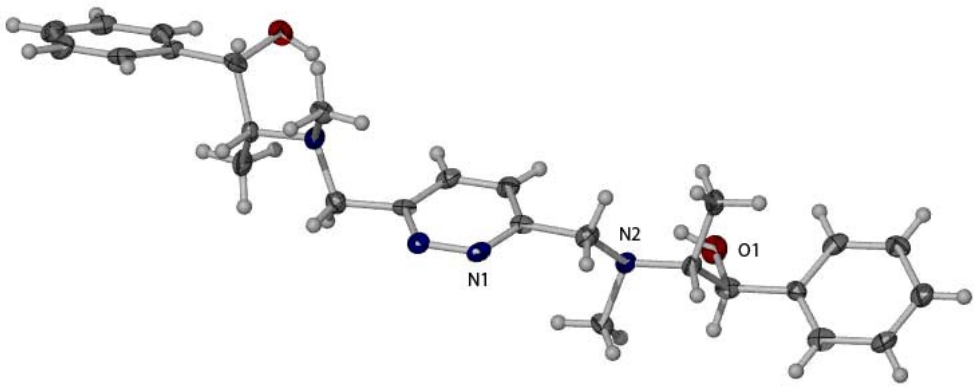

Figure 28. ORTEP view of **55** in the crystal (50% ellipsoids).

Compound **42** reacts also with bulky secondary amines such as 2-[N-(1*R*,2*R*,3*R*,5*S*)-(-)-isopinocampheylaminomethyl]pyridine (**57**, figure 29) leading to the formation of **58** (figure 29) also in high yield.

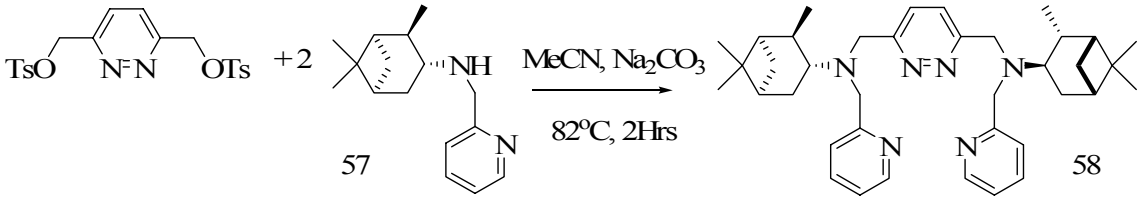

Figure 29. Reaction of 3,6-di(hydroxymethyl)pyridazine di-*p*-tosylate with 2-[N-(1*R*,2*R*,3*R*,5*S*)-(-)-isopinocampheylaminomethyl]pyridine.

3.2.2 Dinuclear bis Schiff base ligands

In parallel to the investigations described in the above section, the preparation of Schiff base ligands by condensation reactions of various aminoalcohols with 3,6-pyridazinedicarboxaldehyde[79] (**59**, figure 30) has also been investigated. The reaction of **59** with **45** proceeded at 65ºC in methanol to afford after work-up a low yield of the C_2 symmetrical dinucleating ligand ((1*R*,2*S*)-(2-hydroxy-1-methyl-2-phenylethyl)-

aminomethylene)-pyridazine (**60**, figure 30) which could be recrystallized from acetone as colorless crystals suitable for X-ray analysis (figure 31). Molecules of **60** crystallizes in the orthorhombic space group $P2_{(1)}2_{(1)}2_{(1)}$ with one molecule per unit cell (table on page 69). The bond angles and bond lengths observed in the structure of the pyridazine core resemble those previously reported for related molecules such as **41**[79] or 3,6-dicarboxylic-pyridazine acid.[78] Compound **60** has also been characterized by ^{1}H, ^{13}C NMR and FAB mass spectrometry. Efforts to use **60** as a ligand for metal cations were frustrated by the sensitive nature of the compound,[80] as compound **60** is in equilibrium and rapidly isomerize leading to the formation of **61** (figure 32).

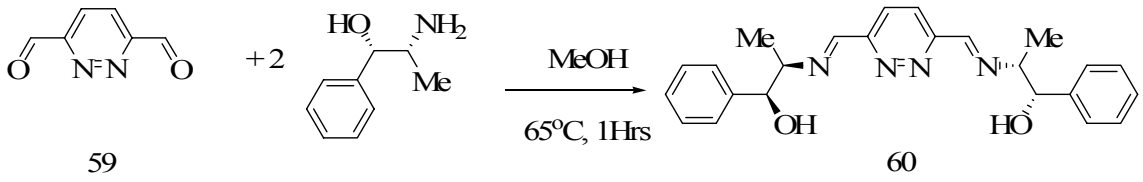

59 60

Figure 30. Synthesis of ((1*R*,2*S*)-(2-hydroxy-1-methyl-2-phenylethyl)-aminomethylene)pyridazine.

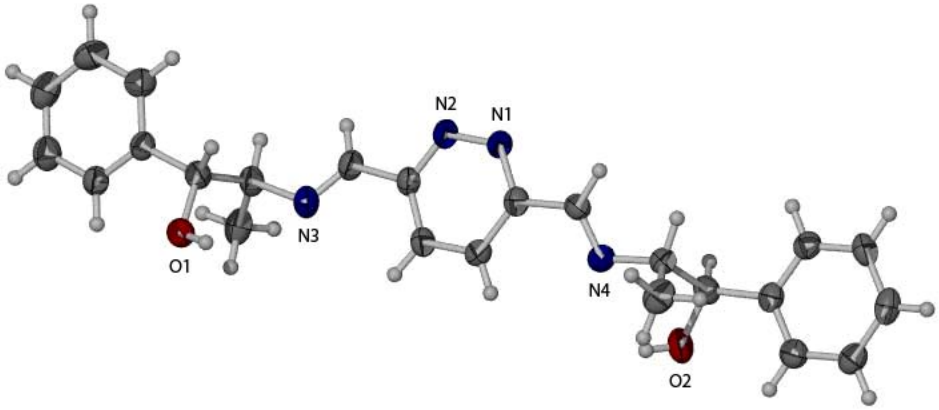

Figure 31. ORTEP view of **60** in the crystal (50% ellipsoids).

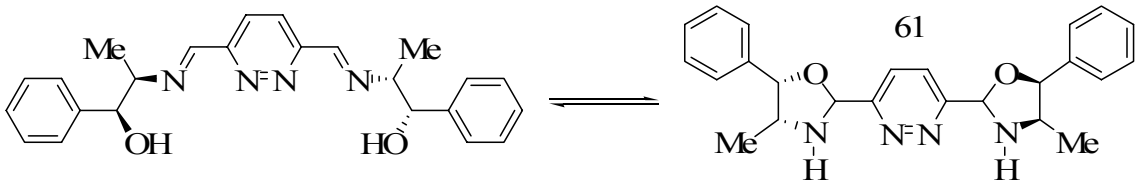

Figure 32. ((1*R*,2*S*)-(2-hydroxy-1-methyl-2-phenylethyl)-aminomethylene)pyridazine isomer equilibrium.

A similar reaction with **59** and (1S-2R)-1-amino-2-indanol (**47**) was attempted to afford after chromatography high yield of the bis(oxazolidine) derivative **62** (figure 33)

which is a structural isomer of the desired product **63** (figure 33). **62** was recrystallized from acetone as colorless crystals suitable for X-ray analysis (figure 34). Molecules of **62** crystallizes in the triclinic space group *P1* (table on page 69). The bond angles and bond lengths observed in the structure of the pyridazine core resemble those previously reported for related molecules such as **41**[79] or 3,6-dicarboxylic-pyridazine acid.[78] After completion of the X-ray, compound **62** was not characterized further.

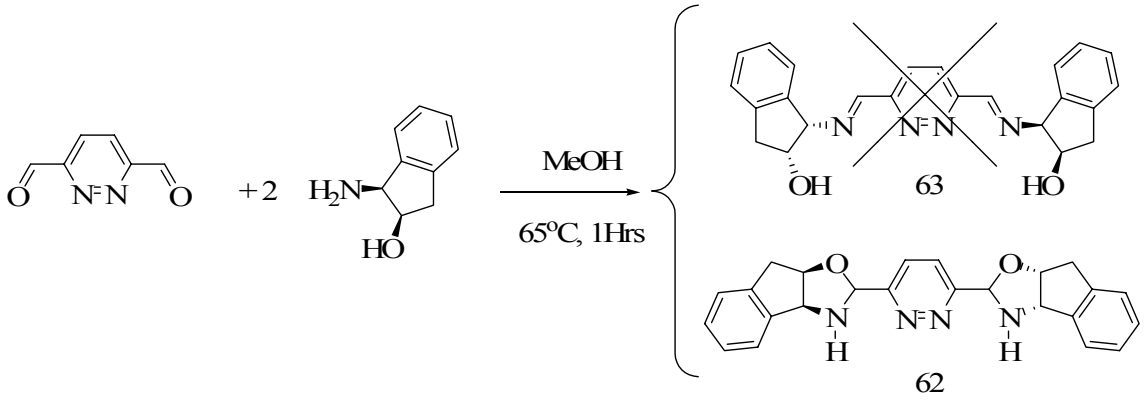

Figure 33. Synthesis of **62**.

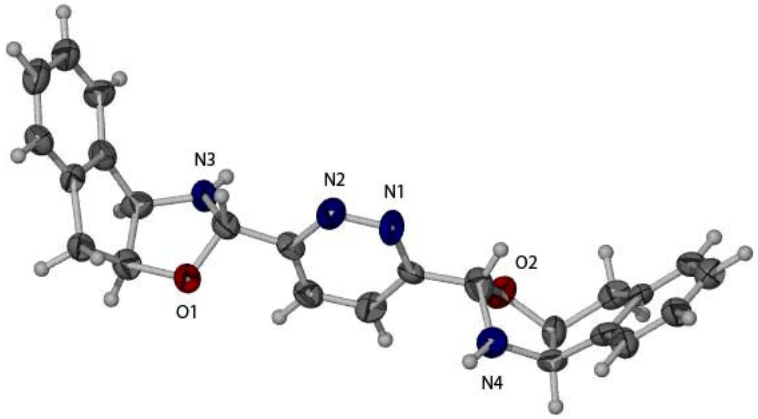

Figure 34. ORTEP view of **62** in the crystal (50% ellipsoids).

In order to avoid the formation of oxazolidine derivatives, protection of the alcohol functionality was investigated. Following typical literature procedure,[81,82] the *O*-benzyl-(1*R*,2*S*)-(-)-norephedrine (**64**, figure 35) was obtained. Treatment of two equivalents of **64** with **59** in methanol at 65ºC afforded a new C_2 symmetrical dinucleating ligand, namely ((1*R,*2*S*)-(2-*O*-benzylhydroxy-1-methyl-2-phenylethyl)-aminomethylene)-pyridazine (**65**, figure 35) in 70% yield. Compound **65** was purified by chromatography and fully characterized. Single crystals suitable for an X-ray analysis were obtained from methanol (figure 36). Compound **65** crystallizes in the orthorhombic space group $P2_{(1)}$ with two molecules per unit cell (table on page 70). The bond angles and bond lengths observed in the structure of the pyridazine core of **65** resemble the bis(hydroxymethyl)pyridazine and those previously reported for related molecules such

as 3,6-dicarboxylic-pyridazine acid.[78] There are no unusual bond lengths and angles in the benzylated norephedrine moieties that flank each side of the pyridazine ring.

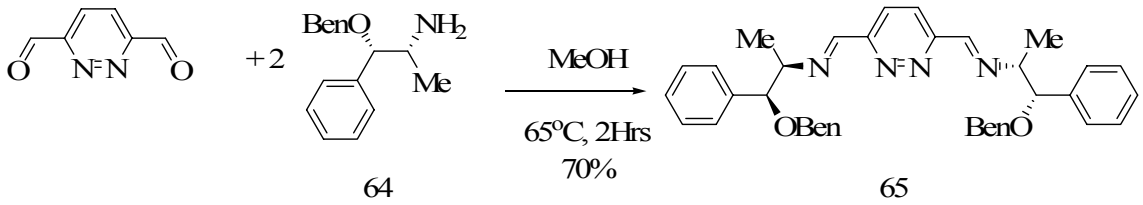

Figure 35. Synthesis of ((1*R*,2*S*)-(2-*O*-benzylhydroxy-1-methyl-2-phenylethyl)-aminomethylene)pyridazine.

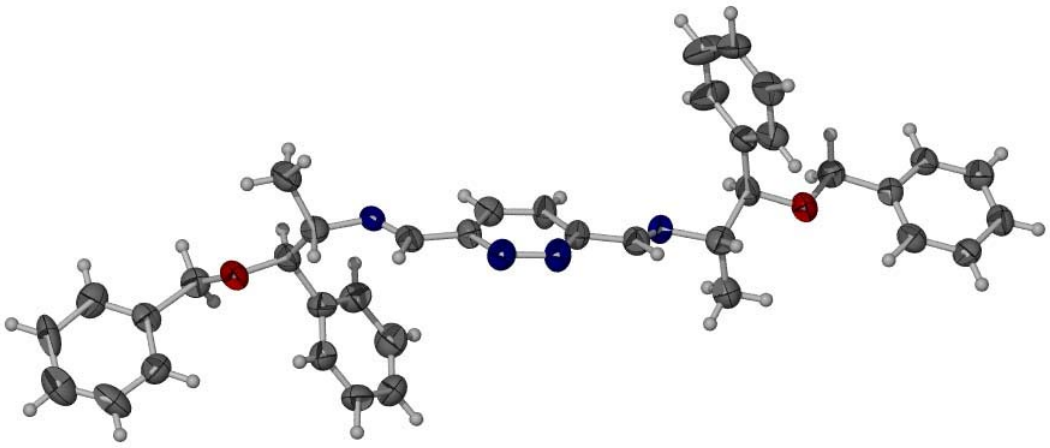

Figure 36. ORTEP view of 65 in the crystal (50% ellipsoids).

Similarly, **59** reacts with **49** to afford a 77% yield ((1*R*,2*S*)-(2-*O*-^{t}butyldimethylsilylhydroxy-1-methyl-2-phenylethyl)-aminometylene)-pyridazine (**66**, figure 37) which has been fully characterized. While compound **65** and **66** form dinuclear complexes with various metal cations, preparation of these ligands is complicated by the rather tedious synthesis and isolation of **59** which is hygroscopic and readily polymerizes. In order to provide a more convenient access to this type of ligand, we explored alternative directions and considered the preparation of analogs of these bis(imine) ligands featuring a phenylene rather than a pyridazine core.

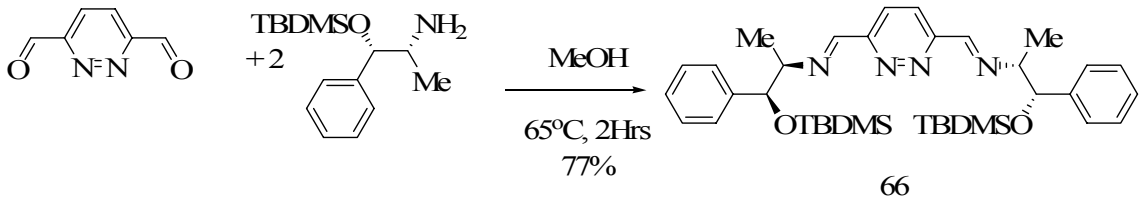

Figure 37. Synthesis of ((1*R*,2*S*)-(2-*O*-^{t}butyldimethylsilylhydroxy-1-methyl-2-phenylethyl)-aminometylene)pyridazine.

3.3 Dinuclear (iminomethyl)benzene ligands.

The ligands described in the above sections are well adapted to the formation of dinuclear coordination complexes. In order to broaden the scope of our investigations, we decided to investigate dinucleating ligands specifically designed for the preparation of dinuclear organometallic complexes (Figure 38).

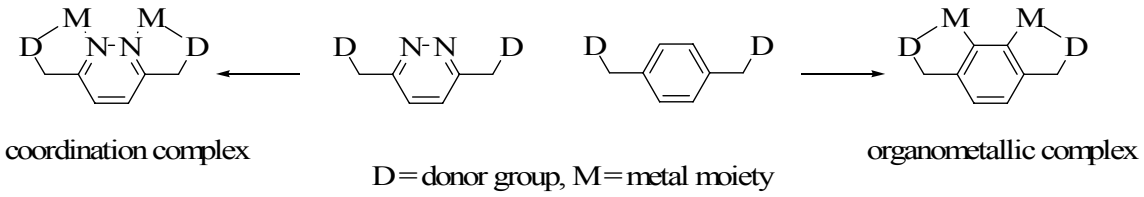

Figure 38: Dinuclear organometallic design.

2,3-dimethoxy-benzene-1,4-dicarbaldehyde derivative (**67**) was chosen as a starting material. This choice was guided by the fact that this derivative should smoothly react with secondary amines to afford a new type of dinucleating bis(Schiff base) ligands. Secondly, the presence of two adjacent methoxy groups should only allow for the 1,2-

rather than 1,4-metallation of the aromatic core of the ligand.[83] To this end, catechol (**68**, figure 39) was converted into **67** (figure 39) following the published procedures.[84]

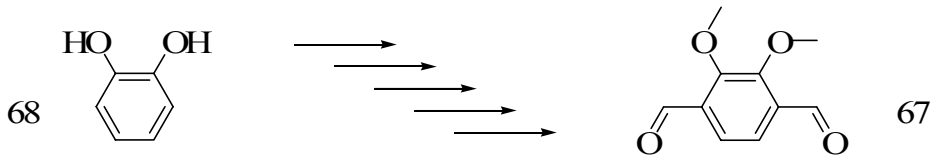

1) MeOH/NaOH 2) CO_2 200°C 3) MeOH/HCl 4) $CsCO_3$, MeI
5) $NaAlH_2(OCH_2CH_2OMe)_2$, N-methylpiperazine.

Figure 39. Synthesis of 2,3-dimethoxy-benzene-1,4-dicarbaldehyse.

Since the reaction of **59** with aminoalcohols leads to the formation of the undesired isomers, new dinucleating side arms were investigated. Just like we synthesized compound **44**, **67** was added to a colorless solution of **43** in acetone at room temperature for 20 hours. After evaporation of the solvents, flash chromatography in CH_2Cl_2 with 5% MeOH afforded 3,6-di[-N-(1R,2R,3R,5S)-(-)isopinocampheylaminomethyl]-1,2-dimethoxy-benzene (**69**, figure 40) as a white powder with 70% yield. Compound **69** was characterized by ^1H and ^{13}C NMR spectroscopy, melting point, elemental analysis, and FAB mass spectrometry.

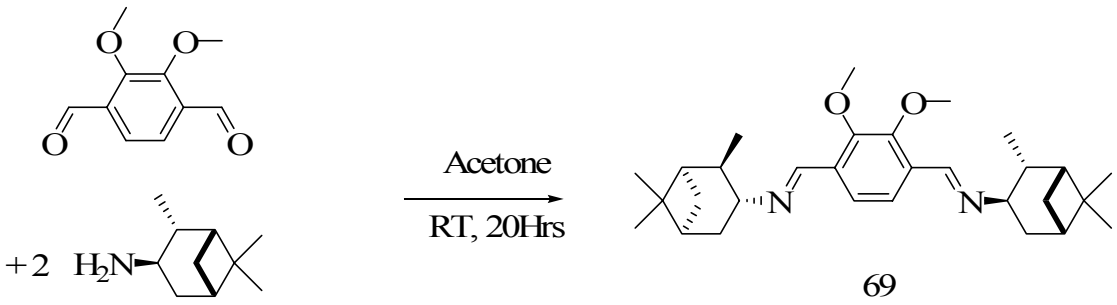

Figure 40. Synthesis of 3,6-di[-N-(1R,2R,3R,5S)-(-)isopinocampheylaminomethyl]-1,2-dimethoxy-benzene.

In a similar fashion, compound **67** can react easily with two equivalents of 2,4,6-trimethylaniline (**70**, figure 41) in acetone to afford colorless crystals of 3,6-di[-N-(2,4,6-trimethylphenyliminomethyl)]-1,2-dimethoxy-benzene (**71**, figure 41). This compound was purified by recrystallization from pentane at -20^{o}C in 85% yield. **71** has been characterized by ^{1}H and ^{13}C NMR spectroscopy, melting point, elemental analysis, and FAB mass spectrometry. In addition, its crystal structure has been determined. Compound **71** crystallizes in the monoclinic space group $P2_{(1)}/n$ (table on page 70) with one molecule per unit cell (figure 42). Examination of the structure confirms the proposed connectivity as well as the presence of two imine functionalities. All bond lengths and angles fall in the normal range and do not deserve further comments. We can also notice that compared to the structure of the distyrylpyridazine, the mesityl

groups are not coplanar with the rest of the molecule due to steric constrains (C11-C6-N1-C5 = 91.9^{o}).

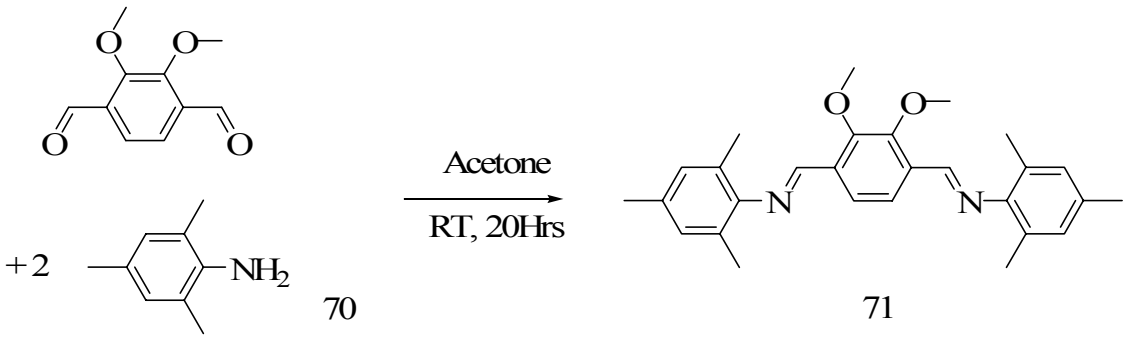

Figure 41. Synthesis of 3,6-di[-N-(2,4,6-trimethylphenyliminomethyl)]-1,2-dimethoxy-benzene.

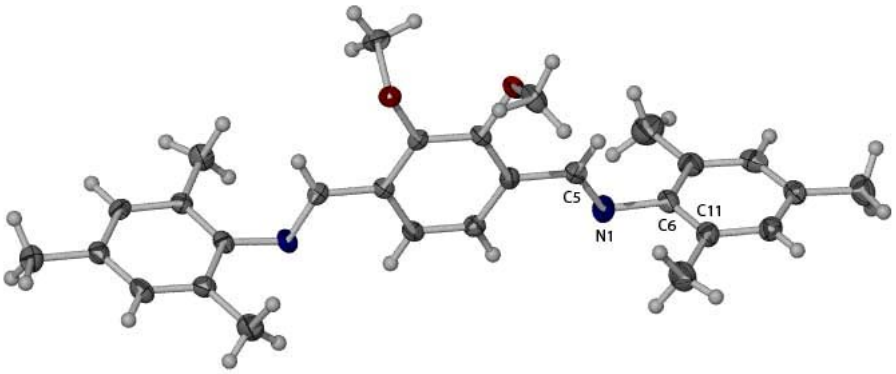

Figure 42. ORTEP view of **71** in the crystal (50% ellipsoids).

In the same way, reaction of compound **67** with 2,6-diisopropylaniline (**72**, figure 43) afforded colorless crystals of 3,6-di[-N-(2,6-diisopropylphenyliminomethyl)]-1,2-dimethoxy-benzene after recrystallisation from pentane (**73**, 82% yield, figure 43) Compound **73** has been characterized by ^{1}H, ^{13}C NMR spectroscopy, melting point, elemental analysis, FAB mass spectrometry, and its crystal structure determined. Compound **73** (table on page 71) crystallizes in the triclinic space group *P-1* with one molecule per unit cell (figure 44). Its structure is similar to that of **63**. Once again, the increased bulk of the isopropyl group leads to the same type of dihedral angle with the pyridazine central core of the molecule (C11-C6-N1-C5 = 84.7°).

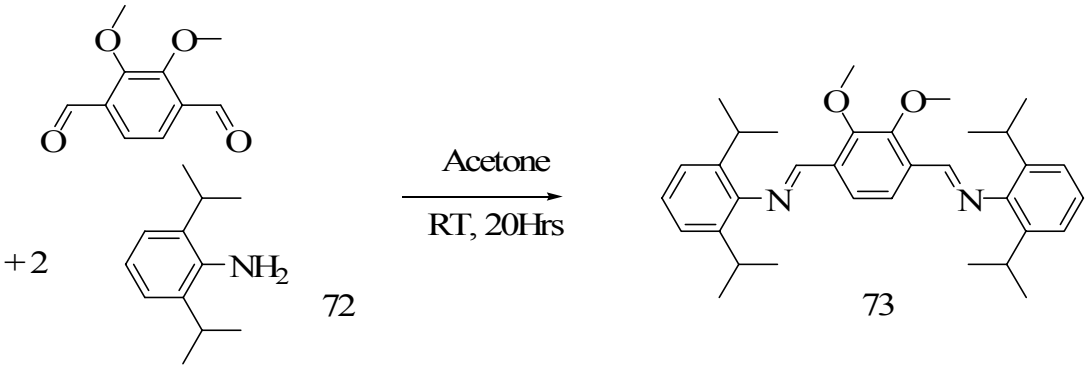

Figure 43. Synthesis of 3,6-di[-N-(2,6-diisopropylphenyliminomethyl)]-1,2-dimethoxy-benzene.

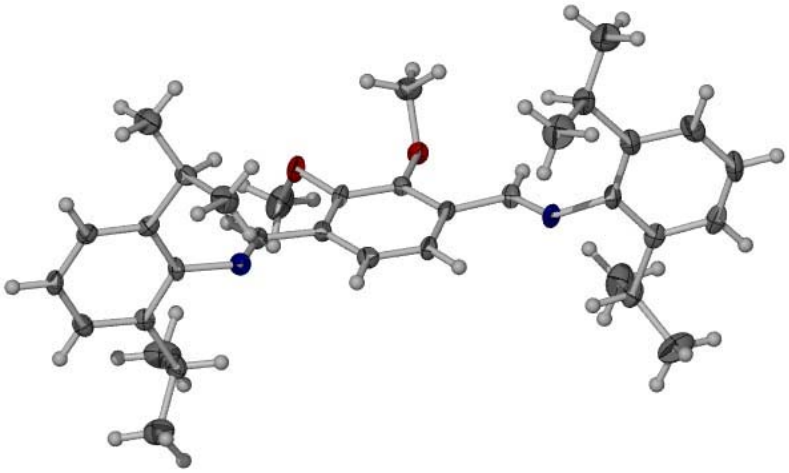

Figure 44. ORTEP view of **73** in the crystal (50% ellipsoids).

The *t*-butyl derivative **74** (figure 45) was prepared by reaction of **59** with *t*-butylamine in methanol (**75**, figure 45). It was obtained in a 95% yield and did not necessitate further purifications. Its identity has been confirmed by ^{1}H and ^{13}C NMR spectroscopy, elemental analysis, and FAB mass spectrometry.

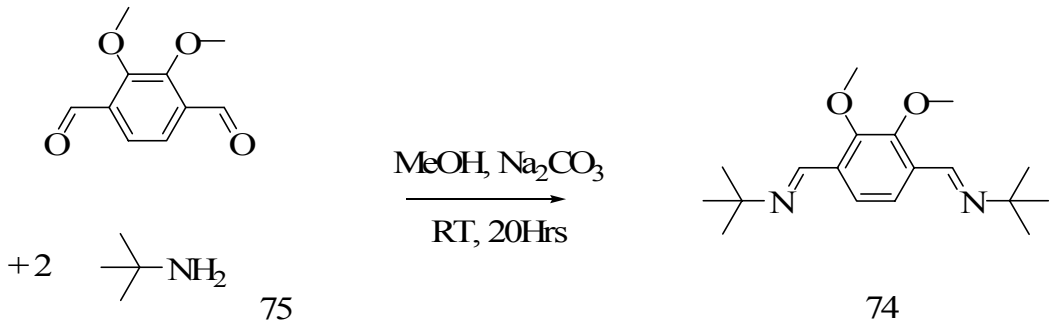

Figure 45. Synthesis of 3,6-di[-N-*t*-butyliminomethyl]-1,2-dimethoxy-benzene

3.4 Summary

New symmetric and asymmetric dinucleating ligands, revealed itself to be a success as 15 new ligands have been successfully prepared by condensation reaction of primary, secondary amines, as well as amino-alcohols to 3,6-Di(hydroxymethyl)Pyridazine di-*p*-tosylate, 2,3-dimethoxy-benzene-1,4-dicarbaldehyde, and 3,6-pyridazinedicarboxaldehyde. These methods allowed the rapid generation of a library of enantiomerically pure dinucleating ligands.

3.5 Experimental

Synthesis of 3,6-bis(hydroxymethyl)pyridazine (**41**): Ozone was bubbled through a suspension of 3,6-distyrylpyridazine (10g, 35.2 mmol) at -78ºC in methanol (250ml) until all 3,6-distyrylpyridazine dissolves resulting by the formation of a blue color of the solution indicating the end of the reaction. Excess of ozone was then removed by degassing the solution with nitrogen, and an excess of sodium borohydride (4g, 106 mmol, 3 equivalents) was added. The reaction mixture was then warmed to ambient temperature and the methanol evaporated under vacuum. The crude product was purified by flash chromatography (silica, 3:1/CH_2Cl_2/MeOH) allowing the isolation of **41** as a white powder in 75% yield. The identity of **41** was confirmed by comparing ^{1}H and ^{13}C NMR and Mass spectroscopy to the literature.[77]

Synthesis of 3,6-Di(hydroxymethyl)Pyridazine di-*p*-tosylate (**42**): A solution of *p*-toluenesulfonyl chloride (13.7 g, 72 mmol) in THF (30 mL) was added to a solution of **41** (5 g, 36 mmol) and NaOH (4 g, 0.1 mol) in a mixture of water (20 mL) and THF (20 mL). After stirring at room temperature for 3 h and precipitation of the white product, the THF was evaporated and the mixture filtrated. The crude product was purified by flash chromatography (washed with dichloromethane and purified with ethylacetate) to give 1,4-Pyridazinedimethanol di-*p*-tosylate (13.7 g, 85% yield) as a white solid. M.p.: 118-120°C. [MH^+] 449. ^{1}H NMR (CDCl3, 300 MHz): δ 2.46 (s, 6H), 5.36 (s, 4H), 7.36 (d, $^{3}J_{HH}$ = 8.4 Hz ,4H), 7.65 (s, 2H), 7.83 (d, $^{3}J_{HH}$ = 8.4 Hz ,4H). ^{13}C NMR (CDCl3, 300

MHz): δ 21.8, 69.8, 126.2, 128.3, 130.3, 132.7, 145.7, 157.1. Elemental analysis calc. (%) for $C_{20}H_{20}N_2O_6S_2$: C 53.56, H 4.49, N 6.25; found: C 53.56, H 4.79, N 6.32.

Synthesis of 3,6-di[-N-(1*R,2R,3R,5S*)-(-)-isopinocampheylaminomethyl]-pyridazine (**44**): A solution of **43** (1.1 g, 7.2 mmol) in acetonitrile was added to a solution of **42** (1.6 g, 3.6 mmol) and Na_2CO_3 (2.65g, 25 mmol) in acetonitrile. After reflux at 82°C for 2 h, the residue was filtrated and the solvent evaporated. The final product was purified by flash chromatography (silica, 9:1/CH_2Cl_2/MeOH) as light brown oil (1.08 g, 73 % yield). ^{1}H NMR ($CDCl_3$, 300 MHz): δ 0.94 (s, 6H), 1.11 (d, $^3J_{HH}$ = 7.5 Hz, 6H), 1.22 (s, 6H), 1.70 (m, 2H), 1.74 (m, 2H) 1.86 (m, 4H), 2.39 (m, 4H), 2.96 (m, 2H), 4.10 (d, $^2J_{HH}$ = 15 Hz, 2H), 4.17 (d, $^2J_{HH}$ = 15 Hz, 2H), 7.57 (s, 2H) . ^{13}C NMR ($CDCl_3$, 300 MHz): δ 21.7, 28.0, 33.0, 36.6, 41.9, 45.3, 48.1, 51.5, 56.7, 126.8, 161.0. Elemental analysis calc. (%) for $C_{26}H_{42}N_4$: C 76.05, H 10.31, N 13.64; found: C 76.2, H 9.9, N 13.4.

Synthesis of 3,6-Di[-N-(1R-2S)-norephedrinylmethyl]pyridazine (**46**): A solution of **45** (3.7 g, 25 mmol) in acetonitrile was added to a solution of **42** (5.6 g, 12.5mmol) and Na_2CO_3 (5g, 50 mmol) in acetonitrile. After stirring at room temperature for 3 h, the residue was filtrated and the solvent evaporated. The final product was purified by recrystallization from CH_3CN as a white solid (4.5 g, 88 % yield). M.p. 152-154°C. [MH^+] 407. ^{1}H NMR (CDCl3, 300 MHz): δ 0.93 (d, $^3J_{HH}$ = 6.6 Hz, 6H), 3.03 (qd, $^3J_{HH}$ = 6.6 Hz $^3J_{HH}$ = 3.6 Hz, 2H), 4.17 (d, $^2J_{HH}$ = 14.7 Hz, 2H), 4.25 (d, $^2J_{HH}$ = 14.7 Hz, 2H), 4.81 (d, $^3J_{HH}$ = 3.6 Hz, 2H), 7.31 (m, 12H), 7.50 (s, 2H) . ^{13}C NMR (CDCl3, 300 MHz):

δ 14.8, 51.0, 58.7, 73.8, 126.3, 126.7, 127.4, 128.3, 140.8, 160.7. Elemental analysis calc. (%) for $C_{24}H_{30}N_4O_2$: C 70.91, H 7.44, N 13.78; found: C 70.5, H 7.7, N 13.4.

Synthesis of 3,6-Di[-N-(1R-2S)-1-amino-2-indanolylmethyl]pyridazine (**48**): The same procedure as described for the preparation of ligand **46** was followed except that **47** (3.7 g, 25 mmol) was used. The final product was purified by recrystallization from CH_3CN as a white solid (3.8 g, 76 % yield). Colorless crystals suitable for X-ray analysis were grown by recrystallization in ethanol at room temperature. M.p. 164-166°C. [MH^+] 403. ^{1}H NMR (CDCl3, 300 MHz): δ 2.99 (dd, $^3J_{HH}$ = 3 Hz $^2J_{HH}$ = 13.5 Hz, 2H), 3.07 (dd, $^3J_{HH}$ = 4.8 Hz $^2J_{HH}$ = 13.5 Hz, 2H), 4.16 (d, $^3J_{HH}$ = 5.1 Hz, 2H), 4.30 (d, $^2J_{HH}$ = 15 Hz, 2H), 4.37 (d, $^2J_{HH}$ = 15 Hz, 2H), 4.45 (m, 2H), 7.27 (m, 6H), 7.38 (m, 2H), 7.58 (s, 2H). ^{13}C NMR (pyridine-d6, 300 MHz): δ 40.5, 52.0, 66.6, 72.0, 125.4, 125.5, 126.6, 126.7, 127.8, 141.7, 144.6, 162.0. Elemental analysis calc. (%) for $C_{24}H_{26}N_4O_2$: C 71.62, H 6.51, N 13.92; found: C 71.18, H 6.53, N 13.79.

Synthesis of 3,6-Di[-N-(1R-2S)-O-(tert-butyldimethylsilyl)-1-amino-2-indanolylmethyl]pyridazine (**53**): A solution of **49** (2.23 g, 8.5 mmol) in acetonitrile was added to a solution of **42** (1.88 g, 4.2 mmol) and Na_2CO_3 (2.65g, 25 mmol) in acetonitrile. After reflux at 82^{o}C for 2 h, the residue was filtrated and the solvent evaporated. The final product was purified by flash chromatography (silica, 9:1/CH_2Cl_2/MeOH) as light brown oil (1.94 g, 74 % yield). ^{1}H NMR ($CDCl_3$, 300 MHz) δ -0.17 (s, 6H), 0.05 (s, 6H), 0.90 (s, 18H), 1.05 (d, $^3J_{HH}$ = 3.9 Hz, 6H), 2.77 (m, 4H),

4.03 (d, $^{2}J_{HH}$ = 6.9 Hz, 2H), 4.01 (d, $^{2}J_{HH}$ = 6.9 Hz, 2H), 4.68 (d, $^{3}J_{HH}$ = 3 Hz, 2H), 7.28 (m, 10H), 7.35 (s, 2H) . ^{13}C NMR ($CDCl_3$, 300 MHz) δ -4.4, -4.2, 18.3, 27.1, 50.2, 57.8, 74.9, 126.1, 126.3, 127.2, 128.5, 160.3. Elemental analysis calc. (%) for $C_{36}H_{58}N_4O_2Si_2$: C 68.09, H 9.21, N 8.82; found: C 68.0, H 9.1, N 8.9.

Synthesis of 3,6-Di[-N-(1R-2S)-O-(tert-butyldimethylsilyl)norephedrinyl-methyl]-pyridazine (**54**): A solution of **50** (1.81 g, 6.9 mmol) in acetonitrile was added to a solution of **42** (1.52 g, 3.4 mmol) and Na_2CO_3 (2.65g, 25 mmol) in acetonitrile. After reflux at 82^{o}C for 2 h, the residue was filtrated and the solvent evaporated. The final product was purified by flash chromatography (silica, 9:1/CH_2Cl_2/MeOH) as light brown oil (1.75 g, 82 % yield). ^{1}H NMR ($CDCl_3$, 300 MHz): δ -0.18 (s, 6H), 0.05 (s, 6H), 0.90 (s, 18H), 1.05 (d, $^{3}J_{HH}$ = 6 Hz, 6H), 2.99 (m, 4H), 3.96 (d, $^{2}J_{HH}$ = 5.4 Hz, 2H), 4.22 (d, $^{2}J_{HH}$ = 14.7 Hz, 2H), 4.30 (d, $^{2}J_{HH}$ = 14.7 Hz, 2H), 4.65 (m, 2H), 7.22 (m, 8H), 7.68 (s, 2H). ^{13}C NMR ($CDCl_3$, 300 MHz): δ -4.5, -4.3, 18.3, 26.1, 40.0, 50.9, 65.1, 75.7, 125.1, 125.3, 126.5, 126.6, 127.9, 140.7, 143.0, 161.5. Elemental analysis calc. (%) for $C_{36}H_{54}N_4O_2Si_2$: C 68.52, H 8.63, N 8.88; found: C 68.7, H 8.5, N 8.7.

Synthesis of 3,6-Di[(2S)-ephedrinyl] pyridazine (**55**): A solution of **51** hydrochloride (1.3 g, 6.5 mmol) in acetonitrile was added to a solution of **42** (1.4 g, 3.2 mmol) and Na_2CO_3 (2.65g, 25 mmol) in acetonitrile. After reflux at 82^{o}C for 3 h, the residue was filtrated and the solvent evaporated. The final product was purified by flash chromatography (silica, 9:1/CH_2Cl_2/MeOH) as a brown semi-solid (1.08 g, 78 % yield).

M.p. 72-75°C. ^{1}H NMR ($CDCl_3$, 300 MHz): δ 1.09 (d, $^{3}J_{HH}$ = 6.6 Hz, 6H), 2.24 (s, 6H), 2.94 (m, 2H), 3.88 (d, $^{2}J_{HH}$ = 8.7 Hz, 2H), 3.93 (d, $^{2}J_{HH}$ = 8.7 Hz, 2H), 4.82 (d, $^{3}J_{HH}$ = 3.3 Hz, 2H), 7.02 (s, 2H) 7.3 (m, 10H),. ^{13}C NMR ($CDCl_3$, 300 MHz): δ 10.0, 39.0, 58.5, 64.2, 74.8, 126.5, 126.9, 127.4, 128.3, 143.2, 161.1. Elemental analysis calc. (%) for $C_{26}H_{34}N_4O_2$: C 71.86, H 7.89, N 12.89; found: C 71.8, H 7.3, N 12.4.

Synthesis of 3,6-Di[l-Alaninemethylester]pyridazine (**56**): A solution of **52** hydrochloride (0.91 g, 6.5 mmol) in acetonitrile was added to a solution of **42** (1.55 g, 3.2 mmol) and Na_2CO_3 (2.65g, 25 mmol) in acetonitrile. After reflux at 82^{o}C for 3 h, the residue was filtrated and the solvent evaporated. The final product was purified by flash chromatography (silica, 9:1/CH_2Cl_2/MeOH) as dark brown oil (0.81g, 82 % yield). ^{1}H NMR ($CDCl_3$, 300 MHz): δ 1.36 (d, $^{3}J_{HH}$ = 7.2 Hz, 6H), 3.45 (q, $^{3}J_{HH}$ = 7.2 Hz, 2H), 3.74 (s, 6H), 4.02 (d, $^{2}J_{HH}$ = 14.4 Hz, 2H), 4.17 (d, $^{2}J_{HH}$ = 14.4 Hz, 2H), 7.56 (s, 2H) . ^{13}C NMR ($CDCl_3$, 300 MHz): δ 19.2, 51.4, 52.2, 56.3, 126.7, 160.5, 175.8. Elemental analysis calc. (%) for $C_{14}H_{22}N_4O_4$: C 54.18, H 7.15, N 18.05; found: C 53.9, H 7.9, N 17.6.

Synthesis of 3,6-Di[l-Alanine]pyridazine (**56'**): To a solution of **56** (0.6 g, 2.0 mmol) in methanol was added a 1N solution of NaOH (4ml, 4.0 mmol). After stirring at 25^{o}C for 4h the solvent was evaporated. The final product was purified by flash chromatography (silica, MeOH) as light brown oil (0.52 g, 92 % yield). ^{1}H NMR (D_2O, 300 MHz): δ 1.26 (d, $^{3}J_{HH}$ = 3.9 Hz, 6H), 3.23 (q, $^{3}J_{HH}$ = 3.9 Hz, 2H), 3.93 (d, $^{2}J_{HH}$ = 8.4

Hz, 2H), 4.08 (d, $^{2}J_{HH}$ = 8.4 Hz, 2H), 7.80 (s, 2H) . ^{13}C NMR (D_2O, 500 MHz): δ 18.5, 50.4, 58.7, 129.0 (quaternary carbons not detected). Elemental analysis calc. (%) for $C_{12}H_{18}N_4O_2$: C 51.06, H 6.43, N 19.85; found: C 50.7, H 6.5, N 19.5.

Synthesis of 2-[(1*R,*2*R,*3*R,*5*S*)-(-)-isopinocampheylaminomethyl]-Pyridine (**57**): To a solution of **43** (0.8 g, 5.2 mmol) in methanol was added the 2-picolyl chloride (8.5 g, 5.2 mmol). After maintained at Ph 9 by addition of concentrated NaOH solution at 65^{o}C for 20h, the solvents were evaporated. The final product was purified by flash chromatography (silica, 19:1/CH_2Cl_2/MeOH) as light brown oil (1.0 g, 78 % yield). ^{1}H NMR ($CDCl_3$, 300 MHz): δ 0.95 (s, 3H), 1.07 (d, $^{3}J_{HH}$ = 8.9 Hz, 3H), 1.18 (s, 3H), 1.89 (m, 1H), 2.05 (m, 4H), 2.36 (m, 2H), 3.26 (m, 1H), 4.09 (s, 2H), 7.11 (m, 1H), 7.47 (m, 1H), 7.60 (s, 1H), 8.46 (m, 1H). ^{13}C NMR ($CDCl_3$, 300 MHz): δ 21.7, 23.6, 28.0, 33.0, 36.8, 38.8, 41.9, 45.3, 48.1, 51.5, 56.7, 126.8, 160.9. Elemental analysis calc. (%) for $C_{16}H_{24}N_2$: C 78.64, H 9.90, N 11.46; found: C 78.4, H 9.4, N 11.6.

Synthesis of 3,6-Di(hydroxymethyl)Pyridazine di-*p*-tosylate with 2-[N-(1*R,*2*R,*3*R,*5*S*)-(-)-isopinocampheylaminomethyl]pyridine (**58**): A solution of **57** (1.46 g, 6.0 mmol) in acetonitrile was added to a solution of **42** (1.34 g, 3.0 mmol) and Na_2CO_3 (2.65g, 25 mmol) in acetonitrile. After reflux at 82^{o}C for 2 h, the residue was filtrated and the solvent evaporated. The final product was purified by flash chromatography (silica, 19:1/CH_2Cl_2/MeOH) as light brown oil (1.75 g, 65 % yield). ^{1}H NMR ($CDCl_3$, 300 MHz): δ 0.80 (s, 6H), 0.93 (d, $^{3}J_{HH}$ = 9.6 Hz, 6H), 1.16 (s, 6H), 1.78

(m, 2H), 1.97 (m, 8H), 2.26 (m, 4H), 3.12 (m, 2H), 3.81 (d, $^2J_{HH}$ = 14 Hz, 2H), 3.96 (d, $^2J_{HH}$ = 14 Hz, 2H), 4.05 (s, 2H), 7.11 (m, 2H), 7.47 (m, 2H), 7.60 (s, 2H), 7.61 (m, 2H), 8.46 (m, 2H). ^{13}C NMR ($CDCl_3$, 300 MHz): δ 21.1, 23.4, 27.5, 28.3, 33.8, 39.4, 41.2, 41.8, 48.2, 55.1, 57.2, 59.2, 122.1, 123.1, 127.0, 136.5, 149.1, 160.8, 161.5. Elemental analysis calc. (%) for $C_{38}H_{52}N_6$: C 76.98 H 8.84, N 14.18; found: C 77.1, H 8.9, N 14.1.

Synthesis of ((1*R,*2*S*)-(2-hydroxy-1-methyl-2-phenylethyl)-aminomethylene)-pyridazine (**60**): A solution of **45** (0.76 g, 5 mmol) in MeOH was added to a light yellow solution of **59** (0.35 g, 2.5 mmol) also in MeOH. After stirring for 6 hours at 65^{o}C, the solution was evaporated. The remaining yellow crude product was washed with ET_2O and the final product recrystallized in Acetone leading to the formation of colorless crystal suitable for X-ray analysis. $[MH]^+$ 403. ^{1}H NMR ($CDCl_3$, 300 MHz): δ 1.14 (d, $^3J_{HH}$ = 6Hz, 6H), 3.56 (dq, $^3J_{HH}$ = 6Hz, $^3J_{HH}$ = 3.3Hz, 2H), 5.04 (d, $^3J_{HH}$ = 3.3Hz, 2H), 7.23-7.32 (m, 6H) 8.04 (s, 2H). ^{13}C NMR ($CDCl_3$, 300 MHz): δ 17.1, 72.7, 78.9, 126.0, 126.8, 127.8, 128.4, 158,5 (Cq non detected). Elemental analysis calc. (%) for $C_{24}H_{26}N_4O_2$: C 71.62 H 6.51, N 13.92; found: C 77.76, H 6.89, N 13.71.

Synthesis of ((1*R,*2*S*)-(2-*O*-benzylhydroxy-1-methyl-2-phenylethyl)-amino-methylene)pyridazine (**65**): A solution of **64** (0.76 g, 5 mmol) in MeOH was added to a light yellow solution of **59** (0.35 g, 2.5 mmol) in H_2O. After stirring for 2 hours at 65^{o}C, the solution was stored in the fridge at -20^{o}C for 10 Hours until white crystal of **55** precipitated. The remaining yellow solution was filtered off, and the final product

washed with ethanol. Few colorless crystals were suitable for X-ray analysis. $[MH]^+$ 583. ^{1}H NMR ($CDCl_3$, 300 MHz) δ 1.35 (d, $^3J_{HH}$ = 6.6Hz, 6H), 3.60 (dq, $^3J_{HH}$ = 6.6Hz, $^3J_{HH}$ = 6.6Hz, 2H), 4.17 (d, $^2J_{HH}$ = 12Hz, 2H) , 4.36 (d, $^3J_{HH}$ = 6.6Hz, 2H), 4.44 (d, $^2J_{HH}$ = 12Hz, 2H) 6.97-7.25 (m, 20H), 7.7 (s, 2H), 8.32 (s, 2H). Elemental analysis calc. (%) for $C_{38}H_{38}N_4O_2$: C 78.32, H 6.57, N 9.61; found: C 77.96, H 6.46, N 9.44.

Synthesis of ((1*R*,2*S*)-(2-*O*-^{t}butyldimethylsilylhydroxy-1-methyl-2-phenylethyl)aminometylene)-pyridazine (**66**): A solution of **49** (1.09 g, 4.1 mmol) in methanol (75ml) was added to a solution of **59** (0.28 g, 2 mmol) in water (15ml). After reflux at 65^{o}C for 2 h, the methanol was evaporated and the oily residue extracted with CH_2Cl_2 (3x50 ml). The organic layer was then drying with $MgSO_4$ et evaporated. The final product was purified by flash chromatography (silica, 9:1/hexane/ethylacetate) as light brown oil (0.97 g, 77 % yield). ^{1}H NMR ($CDCl_3$, 300 MHz): δ -0.15 (s, 6H), -0.11 (s, 6H), 0.91 (s, 18H), 1.31 (d, $^3J_{HH}$ = 6.3 Hz, 6H), 3.78 (m, 2H), 4.86 (d, $^3J_{HH}$ = 5.2 Hz, 2H), 7.28 (m, 10H), 8.18 (s, 2H), 8.44 (m, 2H). ^{13}C NMR ($CDCl_3$, 300 MHz): δ -4.9, -4.7, 17.7, 18.2, 25.8, 73.0, 78.5, 124.4, 126.9, 127.2, 127.7, 142.5, 157.5, 158.5. Elemental analysis calc. (%) for $C_{36}H_{54}N_4O_2Si_2$: C 68.52, H 8.63, N 8.88; found: C 68.3, H 8.7, N 8.6.

Synthesis of 3,6-di[-N-(1R,2R,3R,5S)-(-)isopinocampheylaminomethyl]-1,2-dimethoxy-benzene (**69**): A solution of **67** (0.97 g, 5 mmol) in acetone was added to a solution of **43** (1.5 g, 10 mmol) in acetone. After stirring at room temperature for 20

hours, the solvent was evaporated. The final product was purified by flash chromatography (silica, 19:1/CH_2Cl_2/MeOH) as a white powder (1.62 g, 70 % yield). M.p. 121-123°C. $[MH]^+$ 465. ^{1}H NMR ($CDCl_3$, 300 MHz): δ 1.05 (d, $^3J_{HH}$ = 7.5Hz, 6H), 1.13 (s, 6H), 1.29 (s, 6H), 1.91 (m, 4H), 2.03 (m, 4H), 2.14 (m, 2H), 2.37 (m, 2H), 2.42 (m, 2H), 3.64 (m, 2H), 3.94 (s, 6H), 7.91 (s, 2H), 8.57 (s, 2H). ^{13}C NMR ($CDCl_3$, 300 MHz): δ 19.8, 23.6, 28.0, 33.9, 35.8, 38.9, 41.7, 43.3, 47.5, 61.6, 70.8, 122.5, 132.2, 152.8, 153.1. Elemental analysis calc. (%) for $C_{30}H_{44}N_2O_2$: C 77.54, H 9.54, N 6.03; found: C 77.21, H 9.09, N 5.66.

Synthesis of 3,6-di[-N-(2,4,6-trimethylphenyliminomethyl)]-1,2-dimethoxy-benzene (**71**): A solution of **67** (1.36 g, 7 mmol) in acetone was added to a solution of **70** (1.90 g, 14 mmol) in acetone. After stirring at room temperature for 20 hours, the solvent was evaporated. The final product was purified by recrystallization in pentane at -20^{o}C (2-3 times) as colorless crystals (2.55 g, 85 % yield). M.p. 161-164°C. $[MH]^+$ 429. ^{1}H NMR ($CDCl_3$, 300 MHz): δ 2.15 (s, 12H), 2.31 (s, 6H), 3.93 (s, 6H), 6.92 (s, 4H), 8.08 (s, 2H), 8.60 (s, 2H). ^{13}C NMR ($CDCl_3$, 300 MHz): δ 18.3, 20.7, 62.0, 122.2, 127.0, 128.7 132.7, 133.2, 149.1, 154.0, 158.4. Elemental analysis calc. (%) for $C_{28}H_{32}N_2O_2$: C 78.47, H 7.53, N 6.54; found: C 78.38, H 7.66, N 6.15.

Synthesis of 3,6-di[-N-(2,6-diisopropylphenyliminomethyl)]-1,2-dimethoxy-benzene (**73**): A solution of **67** (1 g, 10 mmol) in acetone was added to a solution of **72** (1.8 g, 10 mmol) in acetone. After stirring at room temperature for 20 hours, the

solvents were evaporated. After dissolving the remaining yellow precipitate in CH_2Cl_2, the starting material **72** was separated by washing thoroughly with 1m HCl solution (4 times). The remaining organic layer was then dried over anhydrous $MgSO_4$, filtrated, and evaporated. The final product was purified by recrystallization in pentane at room temperature (2.1 g, 82 % yield). M.p. 175-178°C. $[MH]^+$ 513. ^1H NMR ($CDCl_3$, 300 MHz): δ 1.18 (d, $^3J_{HH}$ = 6.9Hz, 24H), 2.99 (septuplet, $^3J_{HH}$ = 6.9Hz, 4H), 4.01 (s, 6H), 7.18 (m, 6H), 8.08 (s, 2H), 8.61 (s, 2H). ^{13}C NMR ($CDCl_3$, 300 MHz): δ 23.5, 28.0, 61.8, 122.4, 123.1, 124.3, 132.6, 137.6, 149.4, 154.2, 157.8. Elemental analysis calc. (%) for $C_{34}H_{44}N_2O_2$: C 79.65, H 8.65, N 5.46; found: C 79.14, H 8.74, N 5.44.

Synthesis of 3,6-di[-N-*t*-Butyliminomethyl]-1,2-dimethoxy-benzene (**74**): A solution of **67** (1.95 g, 10 mmol) in MeOH was added to a solution of **75** (1.5 g, 20 mmol) and Na_2CO_3 (3.2 g, 30 mmol) in MeOH. After stirring at room temperature for 20 hours, the residue was filtrated and the solvent evaporated. The final product was isolated as a white powder with no further purifications (2.89 g, 95 % yield). M.p. 133-135°C. $[MH]^+$ 305. ^1H NMR ($CDCl_3$, 300 MHz) δ 1.28 (s, 18H), 3.88 (s, 6H), 7.66 (s, 2H), 8.59 (s, 2H). ^{13}C NMR ($CDCl_3$, 300 MHz) δ 29.7, 57.8, 61.6, 122.0, 132.7, 150.9, 152.9. Elemental analysis calc. (%) for $C_{18}H_{28}N_2O_2$: C 71.02, H 9.27, N 9.20; found: C 70.7, H 8.6, N 8.9.

Table 1: Crystal data for 3,6-distyrylpyridazine and **41**.

Crystal data	3,6-distyrylpyridazine	**41**
Formula	C20 H16 N2	C6 H8 N2 O2
M_r	284.35	140.14
Crystal size (mm^3)	0.25x0.20x0.12	0.3x0.15*0.15
Crystal system	Triclinic	Orthorhombic
Space group	P2(1)/c	Pca2(1)
a (Å)	5.726(2)	13.0247(15)
b (Å)	18.449(7)	4.2030(5)
c (Å)	13.645(5)	11.9215(13)
α (°)	90	90
β (°)	96.637(7)	90
γ (°)	90	90
V ($Å^3$)	1431.7(9)	652.62(13)
Z	4	4
ρ_{calc} (Mg/m^3)	1.319	1.426
μ(Mo K_α)(mm^{-1})	0.078	0.109
F(000) (e)	600	296
Data Collection		
T/K	273	383(2)
Scan mode	ω	ω
hkl range	-6<=h<=6	-17<=h<=12
	-19<=k<=21	-4<=k<=5
	-14<=l<=16	-15<=l<=15
Measured refl.	7250	3720
Unique refl., [R_{int}]	2509 [R(int) = 0.1226]	1459 [R(int) = 0.0295]
Refl. used for refinement	2509	1459
Absorption correction	none	none
T_{min}/T_{max}	none	none
Refinement		
Refined parameters	199	99
R1, wR2 [I>2σ(I)]	R1 = 0.1191, wR2 = 0.2741	R1 = 0.0507, wR2 = 0.1283
ρ_{fin} (max/min) ($eÅ^{-3}$)	0.767 and -0.456	0.460 and -0.185

[a] $R1 = (F_o - F_c)/F_o$. [b] $wR2 = \{[w(F_o^2 - F_c^2)^2]/[w(F_o^2)^2]\}^{1/2}$; $w = 1/[\square^2(F_o^2) + (ap)^2 + bp]$; $p = (F_o^2 + 2F_c^2)/3$ with: a = 0.19 and b = 0 for 3,6-distyryl.; a = 0.0916 and b = 0 for **41.**

Table 2: Crystal data for complexes **48** and **55**.

Crystal data	**48**	**55**
Formula	C12 H13 N2 O	C26 H34 N4 O2
M_r	201.24	434.57
Crystal size (mm^3)	0.37x0.19x0.11	0.42x0.20x0.18
Crystal system	Orthorhombic	Monoclinic
Space group	P2(1)2(1)2	C2
a (Å)	37.790(9)	13.829(4)
b (Å)	4.6788(11)	5.8709(19)
c (Å)	5.6130(13)	14.814(5)
α (°)	90	90
β (°)	90	106.715(5)
γ (°)	90	90
V ($Å^3$)	992.4(4)	1151.9(7)
Z	4	2
ρ_{calc} (Mg/m^3)	1.347	1.253
μ(Mo K_α)(mm^{-1})	0.088	0.080
F(000) (e)	428	468
Data Collection		
T/K	383(2)	273(2)
Scan mode	ω	ω
hkl range	-50<=h<=47 -6<=k<=5 -6<=l<=7	-15<=h<=4 -5<=k<=6 -13<=l<=16
Measured refl.	5906	1621
Unique refl., [R_{int}]	2258 [R(int) = 0.0579]	1240 [R(int) = 0.0319]
Refl. used for refinement	2258	1240
Absorption correction	none	none
T_{min}/T_{max}	none	none
Refinement		
Refined parameters	61	149
R1, wR2 [I>2σ(I)]	R1 = 0.1046, wR2 = 0.2706	R1 = 0.0499, wR2 = 0.1380
ρ_{fin} (max/min) ($eÅ^{-3}$)	0.620 and -0.493	0.199 and -0.203

[a] $R1 = (F_o - F_c)/F_o$. [b] $wR2 = \{[w(F_o^2 - F_c^2)^2]/[w(F_o^2)^2]\}^{1/2}$; $w = 1/[\sigma^2(F_o^2) + (ap)^2 + bp]$; $p = (F_o^2 + 2F_c^2)/3$ with: a = 0.1305 and b = 2.2654 for **48**; a = 0.055 and b = 2.0994 for **55**.

Table 3: Crystal data for complexes **60** and **62**.

Crystal data	**60**	**62**
Formula	C24 H28 N4 O2.5	C24 H22 N4 O2
M_r	412.50	398.46
Crystal size (mm^3)	0.27x0.30x0.30	0.06x0.07x0.04
Crystal system	Orthorhombic	Triclinic
Space group	P2(1)2(1)2(1)	P1
a (Å)	9.2103(7)	5.5582(17)
b (Å)	11.0209(8)	9.698(3)
c (Å)	21.4829(17)	11.646(4)
α (°)	90	75.915(5)
β (°)	90	90.000(6)
γ (°)	90	73.348(5)
V ($Å^3$)	2180.6(3)	581.7(3)
Z	4	1
ρ_{calc} (Mg/m^3)	1.256	1.137
μ(Mo K_α)(mm^{-1})	0.083	0.074
F(000) (e)	880	210
Data Collection		
T/K	173(2)	173(2)
Scan mode	ω	ω
hkl range	-10<=h<=9 -12<=k<=12 -18<=l<=23	-6<=h<=7 -9<=k<=13 -15<=l<=15
Measured refl.	9795	3925
Unique refl., [R_{int}]	3132 [R(int) = 0.0392]	3331 [R(int) = 0.0685]
Refl. used for refinement	3132	3331
Absorption correction	none	none
T_{min}/T_{max}	none	none
Refinement		
Refined parameters	275	307
R1, wR2 [I>2σ(I)]	R1 = 0.0554, wR2 = 0.1344	R1 = 0.0750, wR2 = 0.1751
ρ_{fin} (max/min) ($eÅ^{-3}$)	0.345 and -0.233	0.362 and -0.248

[a] R1 = $(F_o - F_c)/F_o$. [b] wR2 = $\{[w(F_o^2 - F_c^2)^2]/[w(F_o^2)^2]\}^{1/2}$; $w = 1/[\square^2(F_o^2) + (ap)^2 + bp]$; $p = (F_o^2 + 2F_c^2)/3$ with: a = 0.0983 and b = 0 for **60**; a = 0.0921 and b = 0 for **62.**

Table 4: Crystal data for complexes **65** and **71**.

Crystal data	**65**	**71**
Formula	C38 H40 N4 O3	C28 H32 N2 O2
M_r	600.74	428.56
Crystal size (mm^3)	0.24x0.24x0.16	0.34x0.20x0.31
Crystal system	Monoclinic	Monoclinic
Space group	P2(1)	P2(1)/n
a (Å)	16.005(5)	15.437(4)
b (Å)	5.5989(17)	8.255(2)
c (Å)	19.655(6)	19.116(5)
α (°)	90	90
β (°)	91.467(6)	90.566(5)
γ (°)	90	90
V ($Å^3$)	1760.7(9)	2435.8(11)
Z	2	4
ρ_{calc} (Mg/m^3)	1.133	1.169
μ(Mo K_α)(mm^{-1})	0.072	0.073
F(000) (e)	640	920
Data Collection		
T/K	173(2)	273(2)
Scan mode	ω	ω
hkl range	-21<=h<=20 -7<=k<=6 -23<=l<=26	-17<=h<=17 -9<=k<=9 -21<=l<=11
Measured refl.	11066	10665
Unique refl., [R_{int}]	6840 [R(int) = 0.0937]	3515 [R(int) = 0.0536]
Refl. used for refinement	6840	3515
Absorption correction	none	none
T_{min}/T_{max}	none	none
Refinement		
Refined parameters	406	297
R1, wR2 [I>2σ(I)]	R1 = 0.0714, wR2 = 0.1881	R1 = 0.0408, wR2 = 0.0905
ρ_{fin} (max/min) ($eÅ^{-3}$)	0.487 and -0.243	0.210 and -0.163

[a] R1 = $(F_o - F_c)/F_o$. [b] wR2 = $\{[w(F_o^2 - F_c^2)^2]/[w(F_o^2)^2]\}^{1/2}$; $w = 1/[\square^2(F_o^2) + (ap)^2 + bp]$; $p = (F_o^2 + 2F_c^2)/3$ with: a = 0.1033 and b = 0 for **65**; a = 0.0603 and b = 0 for **71.**

Table 5: Crystal data for complex **73**.

Crystal data	**73**
Formula	C34 H40 N2 O2
M_r	508.68
Crystal size (mm^3)	0.50x0.40x0.35
Crystal system	Triclinic
Space group	P-1
a (Å)	9.871(8)
b (Å)	12.755(11)
c (Å)	13.245(11)
α (°)	113.951(17)
β (°)	93.809(19)
γ (°)	91.971(17)
V ($Å^3$)	1517(2)
Z	2
ρ_{calc} (Mg/m^3)	1.113
μ(Mo K_α)(mm^{-1})	0.069
F(000) (e)	548
Data Collection	
T/K	173(2)
Scan mode	ω
hkl range	-11<=h<=10 -14<=k<=14 -9<=l<=14
Measured refl.	7062
Unique refl., [R_{int}]	4425 [R(int) = 0.0836]
Refl. used for refinement	4425
Absorption correction	none
T_{min}/T_{max}	none
Refinement	
Refined parameters	353
R1, wR2 [I>2σ(I)]	R1 = 0.0565, wR2 = 0.1192
ρ_{fin} (max/min) ($eÅ^{-3}$)	0.235 and -0.208

[a] R1 = $(F_o - F_c)/F_o$. [b] wR2 = $\{[w(F_o^2 - F_c^2)^2]/[w(F_o^2)^2]\}^{1/2}$; $w = 1/[\square^2(F_o^2) + (ap)^2 + bp]$; $p = (F_o^2 + 2F_c^2)/3$ with: a = 0.0602 and b = 0.

CHAPTER IV

COORDINATION CHEMISTRY

4.1 Introduction

Organophosphorus pesticides are for the most part thiophosphate triesters and undergo oxidation to yield the more toxic oxon derivatives. As a result, their destruction is typically achieved by hydrolysis which leads to the formation of the corresponding thiophosphate diesters. The hydrolysis reaction takes up to several months in water under neutral pH condition[85] but is greatly accelerated in the presence of the dinuclear metalloenzyme phosphotriesterase (PTE).[86] So far, all of the coordination complexes that have been investigated as hydrolysis catalysts are monofunctional.[87] As these complexes typically display only marginal activity, our main goal has become to synthesize a series of dinuclear complexes in order to test their catalytic properties in the hydrolysis reaction of phosphotriester. In this work, we report the coordination chemistry of the dinucleating ligands defined in chapter III.

4.2 Investigation of the coordination chemistry of the bis-Schiff base ligands

With the preparation of dinuclear complexes as a goal, it became important to investigate the ligative behavior of the different ligands toward metal cation moieties. In a titration experiment monitored by ^{1}H NMR, portions of 0.5 mol-equivalent of bismuth

trichloride were added to a CD_3CN solution of the dinucleating ligand **66** (Figure 46). At 0.5 equivalents of cations, the appearance of a new set of sharp ^1H NMR signals indicates the formation of a new species which most likely correspond to a bismuth complex of **66**. Further addition of $BiCl_3$ to the solution leads to an increase in the intensity of the signal corresponding to the new complex. At two equivalents of added $BiCl_3$, the signals corresponding to the free ligand have completely disappeared and further addition of $BiCl_3$ does not lead to further changes of the spectrum.

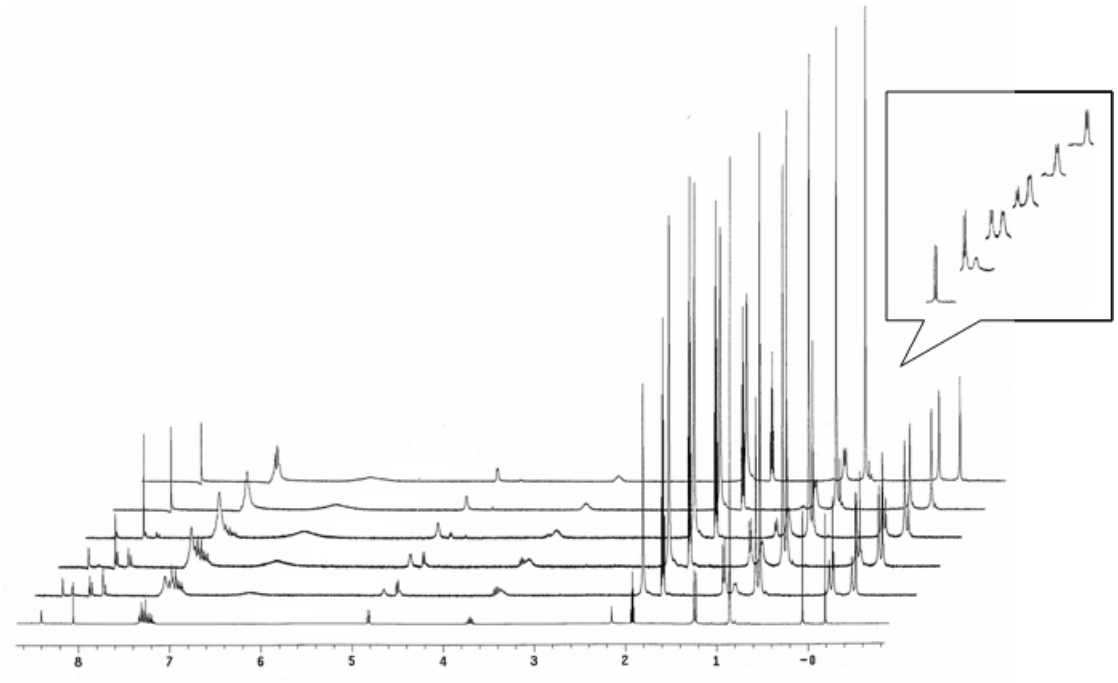

Figure 46. NMR spectra of **66** in the presence of increasing amount of $BiCl_3$.

These observations are in agreement with the formation of a dinuclear bismuth complex of **66**. The detection of a single signal for the aromatic protons suggests that the new complex (**76**, figure 47) retains C_2 symmetry. The proposed structure **76** is in agreement with studies by Keppler who synthesized and characterized this new type of binuclear Bi (III) compounds (**77**, figure 48).[88]

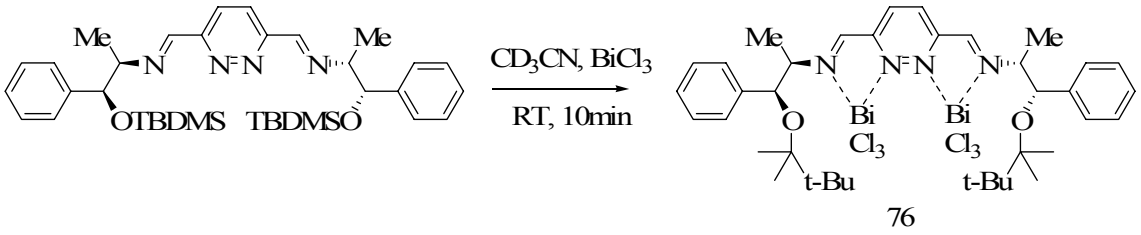

76

Figure 47. Coordination reaction of **66** with $BiCl_3$.

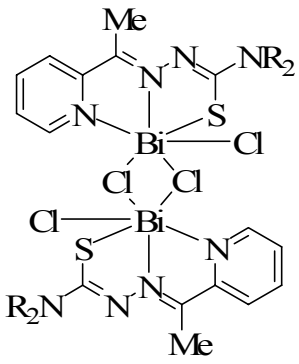

77

Figure 48. Coordination chemistry of $BiCl_3$.

The formation of a dinuclear complex is also observed by NMR when uranyl nitrate is added to the dinucleating ligand **66** (figure 49). From 0 equivalent to 2 equivalents of added uranyl nitrate, a new set of lines appears while the original peaks corresponding to the free ligand decrease. After addition of 2 equivalents, a well-resolved spectrum of the pure complex is observed (**78**, figure 50) which does not changes after further additions of uranyl nitrate. The proposed structure **78** is in agreement with the studies by Indrasenan and his work on uranyl coordination chemistry (**79**, figure 51). [89]

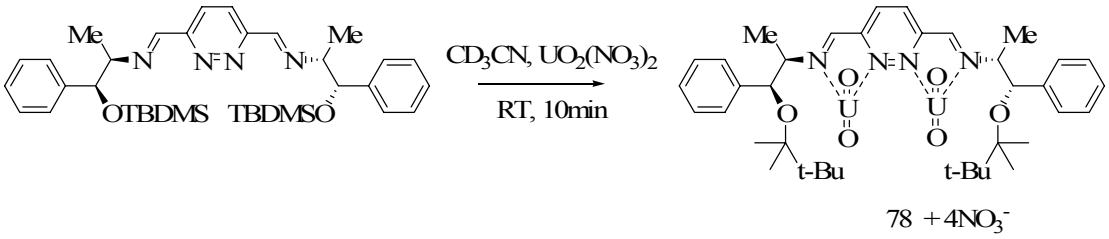

Figure 49. Coordination reaction of **66** with uranyl nitrate.

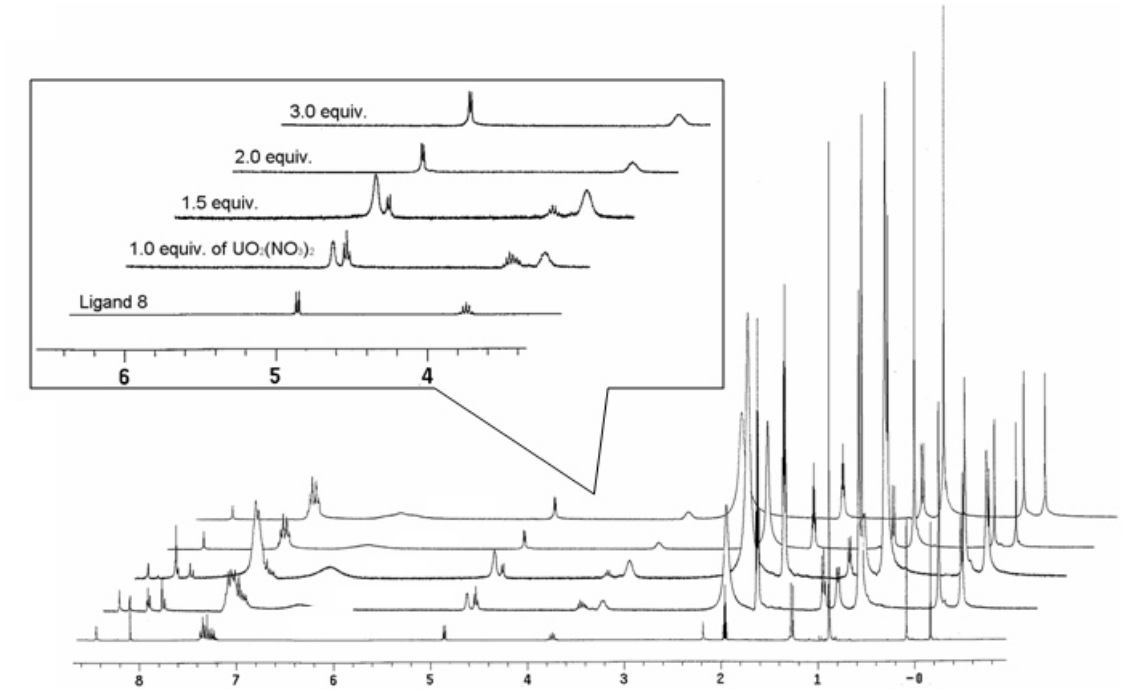

Figure 50. NMR spectra of **66** in the presence of increasing amount of UO_2^{2+}.

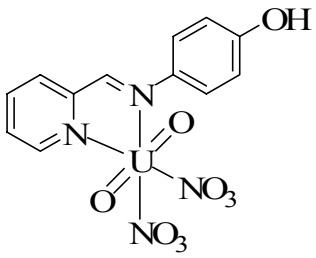

79

Figure 51. Coordination chemistry of UO_2 (II).

While ambiguous results were obtained with Zn^{2+}, titration of ligand **66** in CD_3CN with scandium (III) and yttrium (III) triflates monitored by ^{1}H-NMR suggested the formation of 2:2 complexes (**80**, **81**, figure 52, and 54 respectively). Indeed, when portions of 0.5 mol equivalents of the triflate salts were added to the solution containing the ligand, extensive broadenings and consequent shifts of the resonance are observed. At 1 mol equivalent of cations, well-resolved spectra, which do not change upon further additions, are observed suggesting the formation the symmetrical complexes (figures 53 and 55. Also, the signal of the aromatic protons indicated that the C_2 symmetry of the ligands was retained which reinforce the proposed structures of 2/2 complexes.

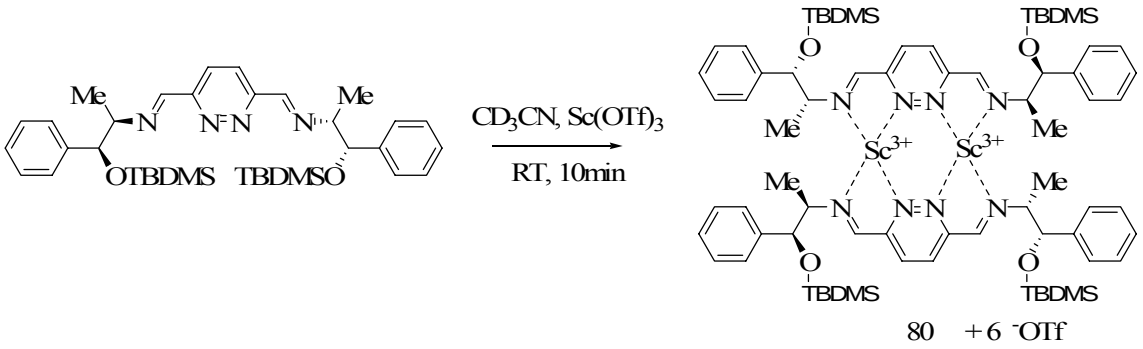

Figure 52. Coordination reaction of **66** with Sc^{3+}.

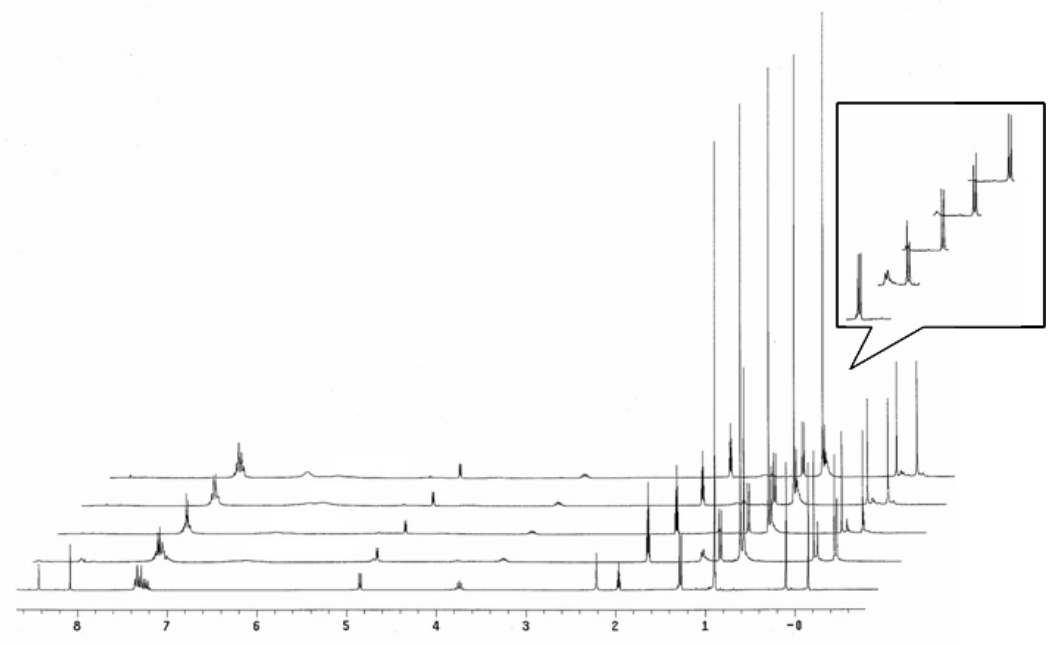

Figure 53. NMR spectra of **66** in the presence of increasing amount of Sc^{3+}.

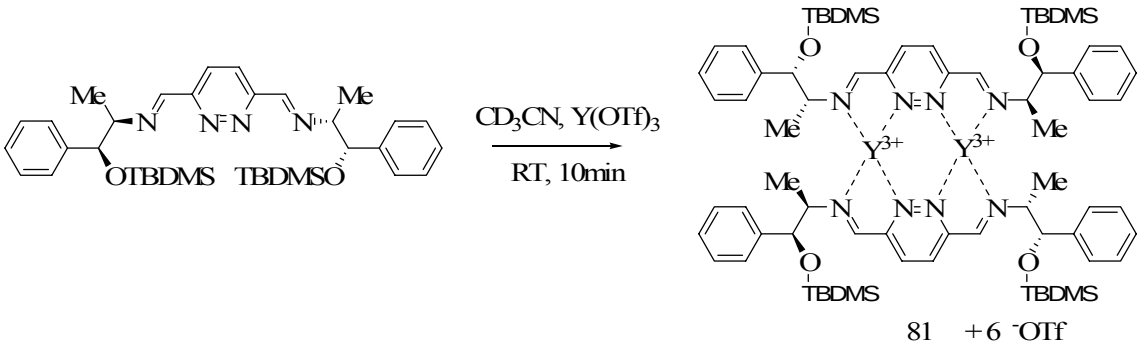

Figure 54. Coordination reaction of **66** with Y^{3+}.

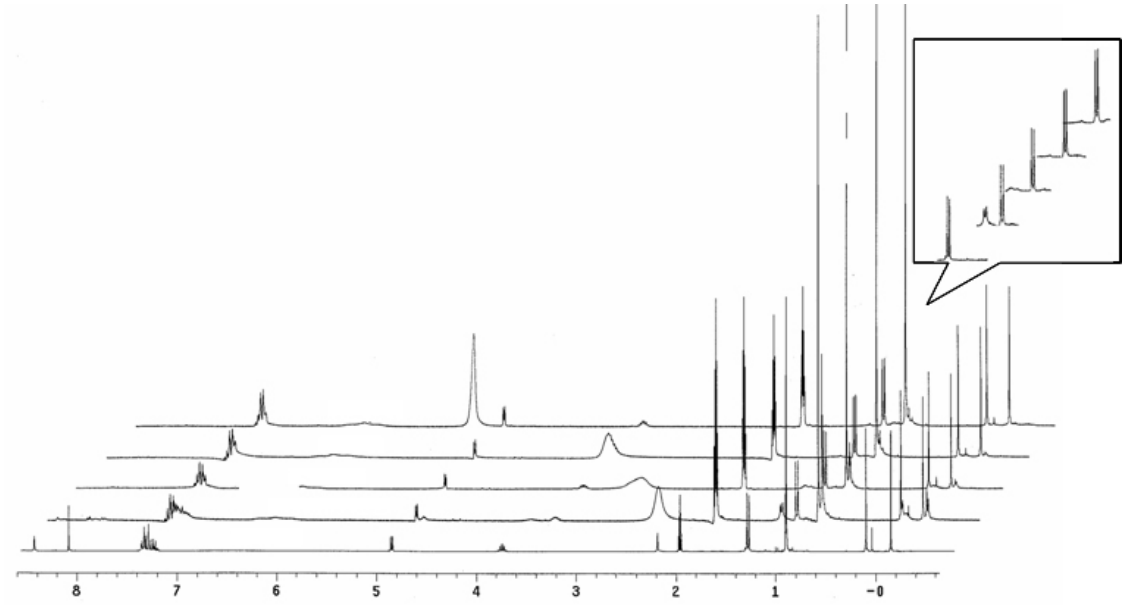

Figure 55. NMR spectra of **66** in the presence of increasing amount of Y^{3+}.

4.3 Coordination chemistry of the ligands derived from 3,6-bis(hydroxymethyl)-pyridazine

4.3.1 NMR studies

Synthesis of a dinuclear aluminum complex was achieved by slow addition of a solution of **44** in pentane to an excess of trimethylaluminum in pentane followed by cooling to -40ºC resulted in the formation of a white precipitate. Analysis of this precipitate by ^{1}H NMR in pyridine-d_5 confirmed the formation of a dinuclear aluminum complex (**82**, figure 56, figure 57).

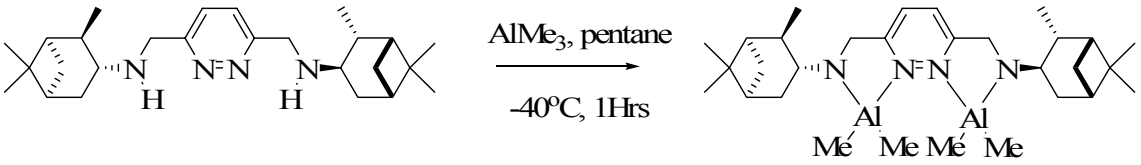

82

Figure 56. Coordination reaction of **44** with $AlMe_3$.

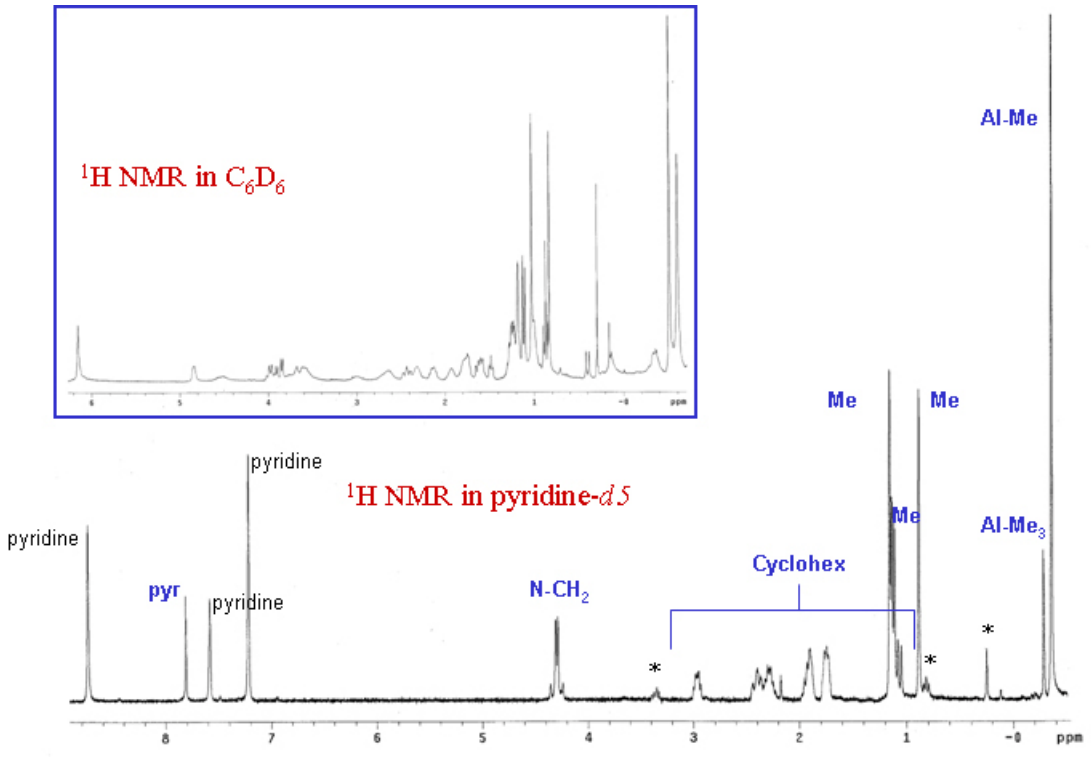

Figure 57. NMR resolution of **82** from C_6D_6 to pyridine-d_5.

Just like for the coordination studies of the Schiff bases, a NMR titration experiment of **46** was carried out with Y^{3+} and Sc^{3+} triflates as coordination metal center. Portions of 0.5 mol-equivalent of Y^{3+} and Sc^{3+} triflate salts were added to a CD_3CN solution of the dinucleating ligand **46** (figure 59). It appears that the resonances of the free ligand progressively shift until 1 equivalent of the metal cation has been added. Further addition of the metal cation does not lead to further changes in the chemical

shifts of the proton of the ligand. These observations suggest the formation of 2:2 complexes **83** (figure 58) whose structure is fluxional in the presence of excess ligand. Just like in the case of complexes **80** and **81**, the signal of the aromatic protons also indicates that the C_2 symmetry of the ligand is retained in the 2/2 complexes.

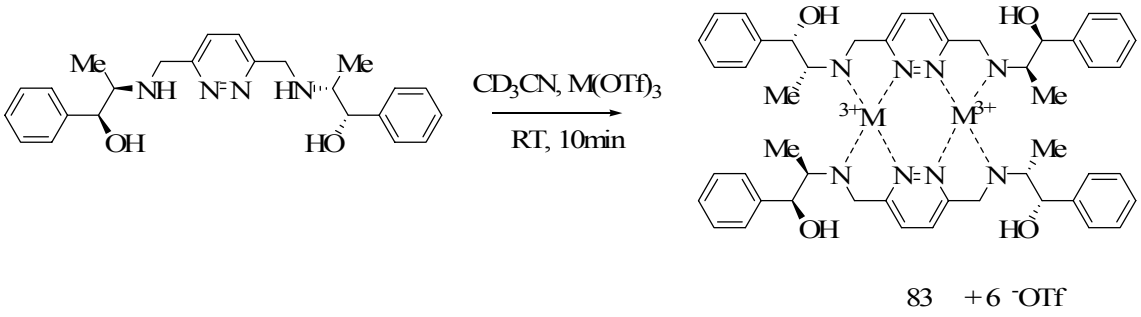

Figure 58. Coordination reaction of **46** with Y and Sc triflate.

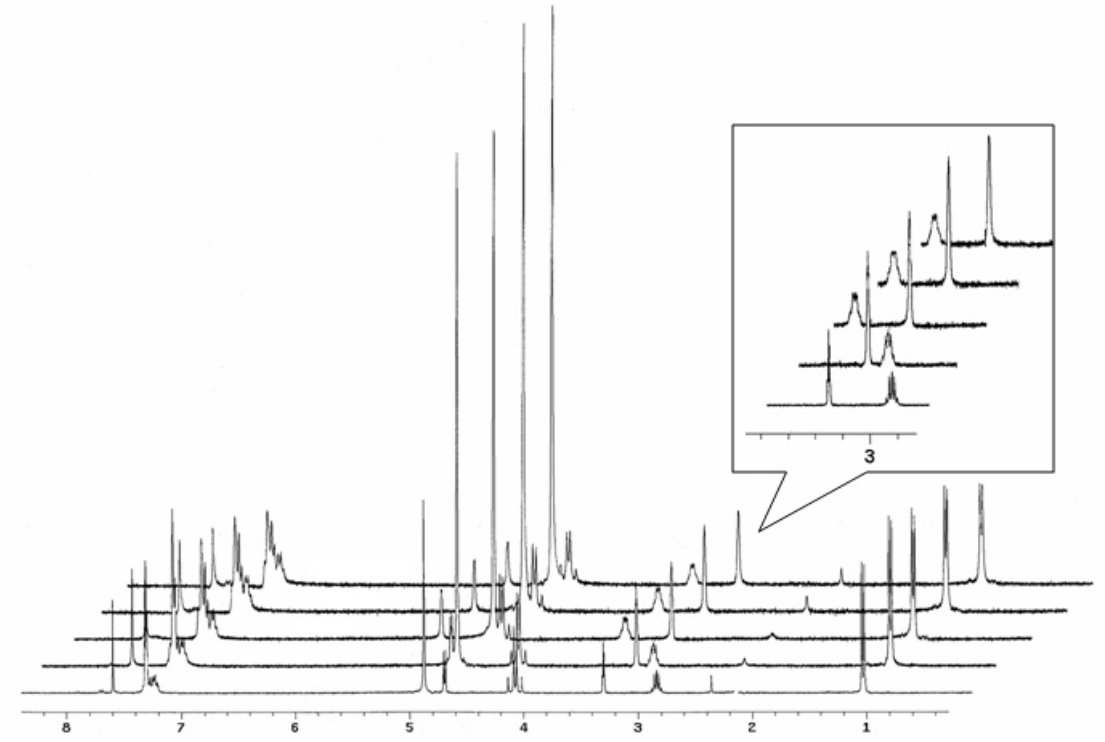

Figure 59. NMR spectra of **46** in the presence of increasing amount of Sc^{3+}.

4.3.2 Synthesis of dinuclear copper complexes

Because of the ubiquity of copper in metalloenzymes and artificial catalyst, it was decided to use this metal in order to probe the ligating properties of the **46** and **48**. Thus, in order to evaluate the stoichiometry of the metal complexes, spectrometric titration experiment were undertaken. Incremental addition of Cu^{2+} in ethanol to a solution of **46** or **48** resulted in the appearance of a band at 365 nm (Figure 60, 61).

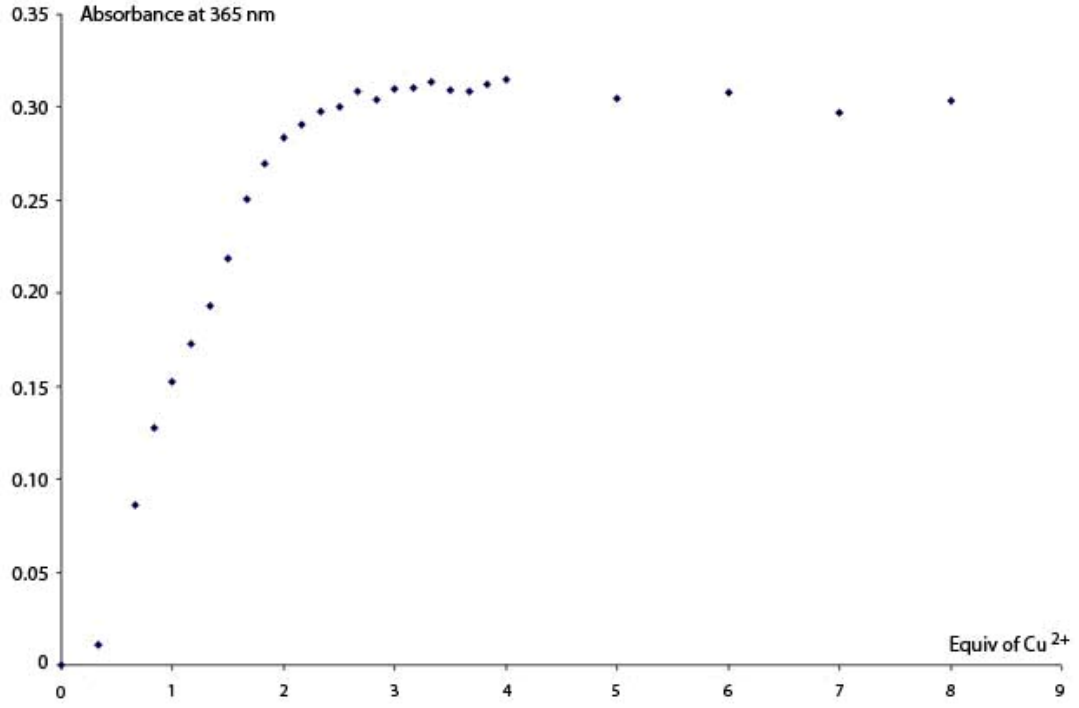

Figure 60. Spectrometric titration of **46** (10^{-4} M) with $CuCl_2$ in EtOH. Absorbance variation at 365 nm as a function of the number of equivalents of $CuCl_2$ added.

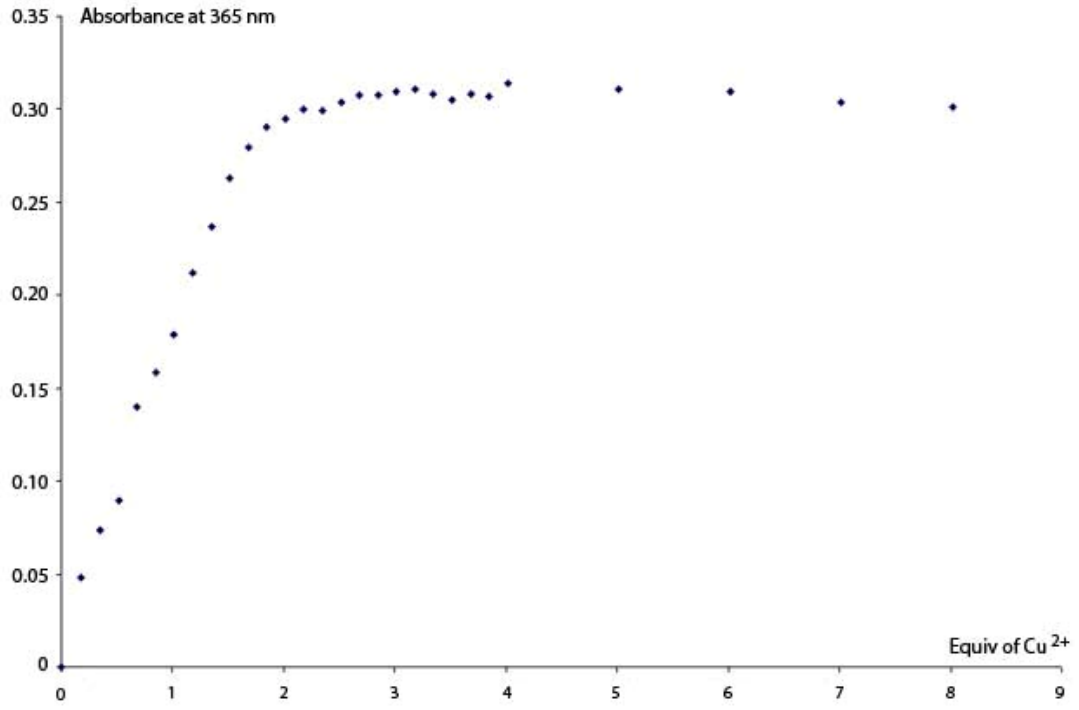

Figure 61. Spectrometric titration of **48** (10^{-4} M) with $CuCl_2$ in EtOH. Absorbance variation at 365 nm as a function of the number of equivalents of $CuCl_2$ added.

In both cases, absorption correction was undertaken by removing the constant UV signal related to the addition of Cu (II) in solution. Depicted in figure 60 and 61, the absorption at 365 nm increased steadily until exactly two equivalents of metals had been added. With further addition of Cu^{2+}, the absorbance at that wavelength remained constant. This experiment undoubtedly revealed the formation of dimeric species with

high thermodynamic stability (**84**, **85**, figure 62, and 63 respectively), thus indicating the nearly quantitative formation of the dinuclear complexes.

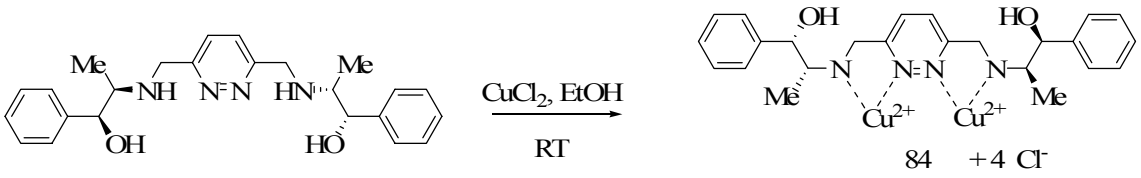

Figure 62. Coordination reaction of **46** and with Cu^{2+}.

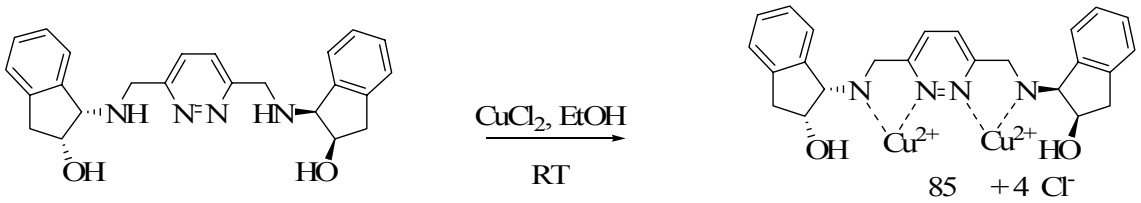

Figure 63. Coordination reaction of **48** and with Cu^{2+}.

In the case of **48**, the existence of dinuclear complexes could also be confirmed by ESI mass spectrometry of methanol solutions containing **48** and two equivalents of $Cu(OTf)_2$. The base peak, observed at 675 amu, results from the loss of two molecule of HOTf and one OTf^- anion from the parent complex **48**·$(CuOTf_2)_2$ (figure 64). Loss of an additional HOTf molecule results in a peak observed at 525 amu.

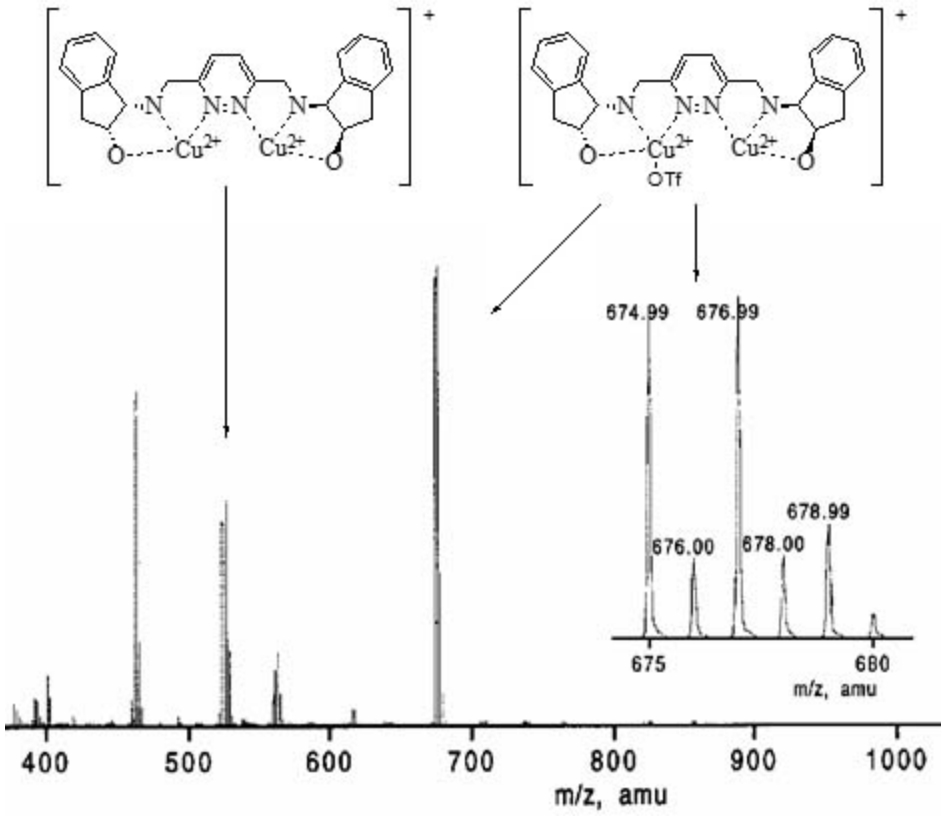

Figure 64. ESI mass spectrometry of **48** and with Cu^{2+}.

In order to compare the activity of the dinuclear catalysts to that of mononuclear analogs, mononucleating ligands such as **86** and **87** were also prepared. These ligands, which are designed to simulate a half of ligands **84** and **85**, were prepared following the published procedures. [90,91] Just like we did for compound **84** and **85**, the spectrometric titration using $CuCl_2$ was carried out. Incremental addition of Cu^{2+} in ethanol to a solution of **86** or **87** resulted in the appearance of a band at 700 nm (Figure 65, 67) whose intensity increased until almost exactly one equivalent of copper cation had been added.

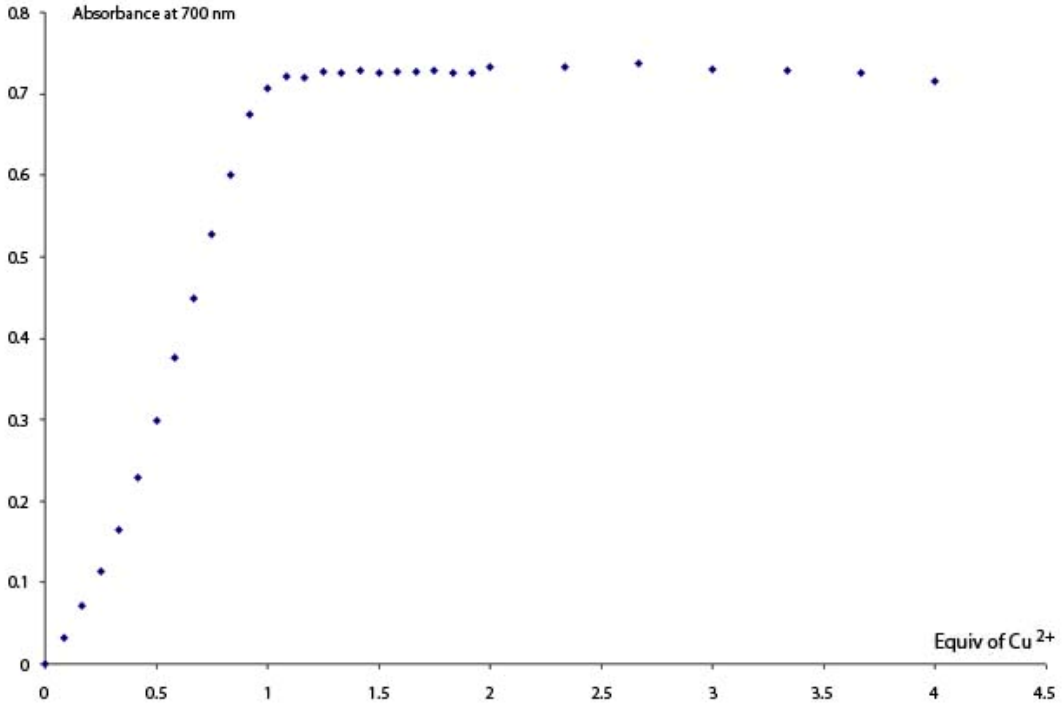

Figure 65. Spectrometric titration of **86** (10^{-2} M) with $CuCl_2$ in EtOH. Absorbance variation at 700 nm as a function of the number of equivalents of $CuCl_2$ added.

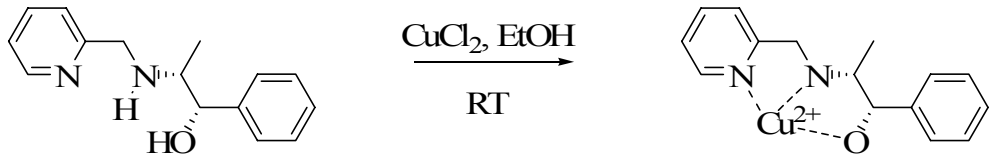

86 88

Figure 66. Coordination reaction of **86** and with Cu^{2+}.

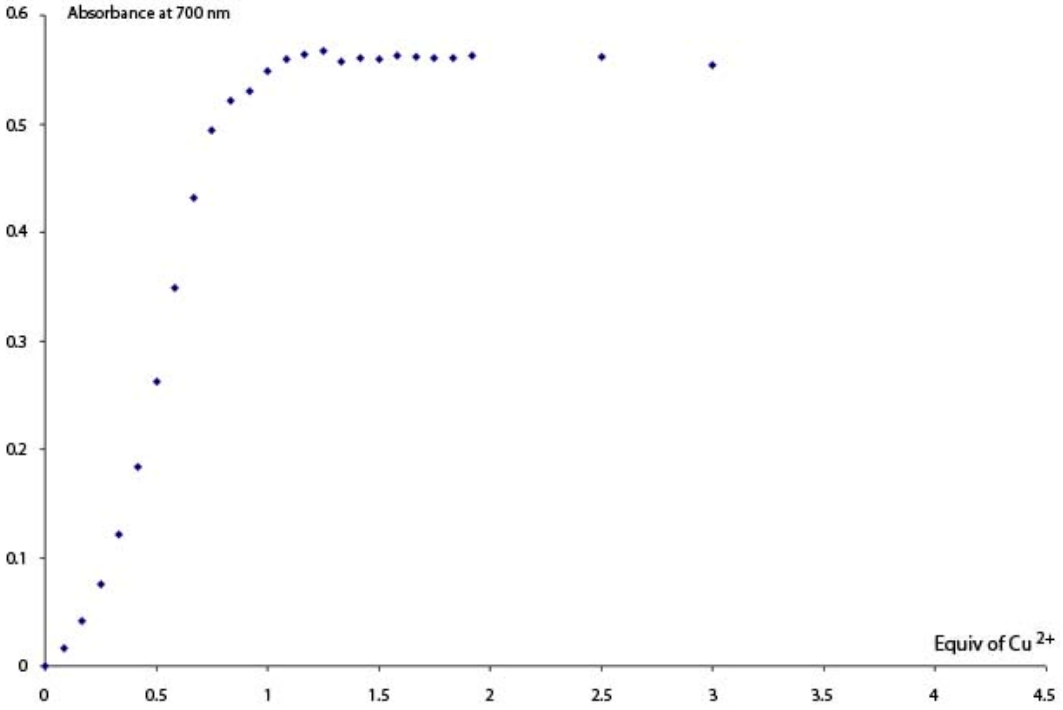

Figure 67. Spectrometric titration of **87** ($8x10^{-3}$ M) with $CuCl_2$ in EtOH. Absorbance variation at 700 nm as a function of the number of equivalents of $CuCl_2$ added.

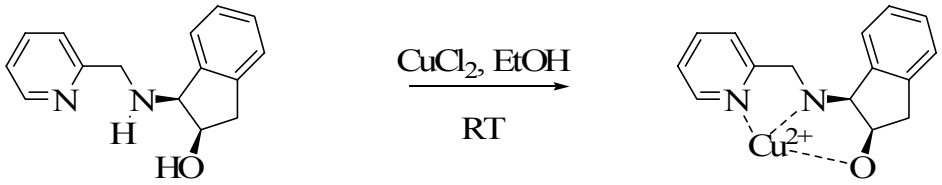

87 89

Figure 68. Coordination reaction of **87** and with Cu^{2+}.

In both cases, absorption at that wavelength increased steadily until almost one equivalent of metal had been added thus indicating the formation of 1:1 complexes (**88**, **89**, figure 66, and 68 respectively).

4.4 Summary

In conclusion, with the use of simple techniques such as ^{1}H NMR and UV titration we report the coordination chemistry of our chiral dinucleating ligands with *C*2 symmetry in which two metal centers can be embedded.

4.5 Experimental

UV-Vis spectra were recorded on a Hewlett Packard 8453. Typical UV experiment consists on the preparation of 2 sets of solutions. Solutions of **46** (10^{-4} M), **48** (10^{-4} M), were prepared in ethanol. 3 mL of these solutions were placed in a quartz UV cell, and 5 μL portions of $CuCl_2$ (10^{-2} M) solution in ethanol were added. Typical ^1H NMR titrations were recorded at room temperature on a Bruker VXR 300 MHz. Chemical shifts are quoted to higher frequency of $SiMe_4$ as internal standard and are given in ppm, with coupling constant *j* in Hz. First a 25 μ-mol solution of the ligand in CD_3CN is prepared. 6 x 0.5 equivalents (6 x 12.5 μ-mol) of the metal studied are weighted and stored in 6 different vials. After completion of the first ^1H NMR, the solution is added to a first vial increasing the concentration of metal present by increment of 0.5 equivalents.

CHAPTER V

ORTHOMETALATED PD (II) COMPLEXES

5.1 Introduction

As stated in the introductory chapter of this thesis, organophosphorus esters that inhibit the acetylcholine esterase enzyme are used as nerve agents.[1] Because of the toxic natures of these chemicals,[92,93] much attention has been devoted to the development of methods that allow for their neutralization.[94] In this regard, hydrolysis reactions that produce non-toxic phosphate or phosphonate anions have been investigated. In the case of parathion (*O,O*-diethyl *O*-*p*-nitrophenyl thiophosphate), a pesticide whose environmental presence is generating growing concerns,[95] the hydrolysis reaction produces *p*-nitrophenol and the corresponding thiophosphate diester which is non-toxic. This hydrolysis is slow and takes up to several months at neutral pH.[86] In the presence of Lewis acidic transition metal catalysts, the rate of this reaction is increased. While coordination complexes typically display a marginal activity,[44,46,88] recent reports presented in the first chapter of this thesis suggest that organometallic catalysts can be remarkably active.[96] In particular, the group of Ryabov has investigated several cyclometallated palladium and platinum aryl oxime complexes ([MCl{*C,N*-($C_6H_4C(CH_3)$=NOH)-2}(L)], M = Pd or Pt, L = DMSO or pyridine) that greatly accelerate the hydrolysis of parathion.[55] Although no reaction intermediates have been isolated, it has been proposed that the activity of such catalysts results from the

coordination of parathion at the metal center followed by an intramolecular nucleophilic attack by the neighboring oximate (figure 69). Regeneration of the catalysts is proposed to occur by hydrolysis of the phosphorylated oximate.

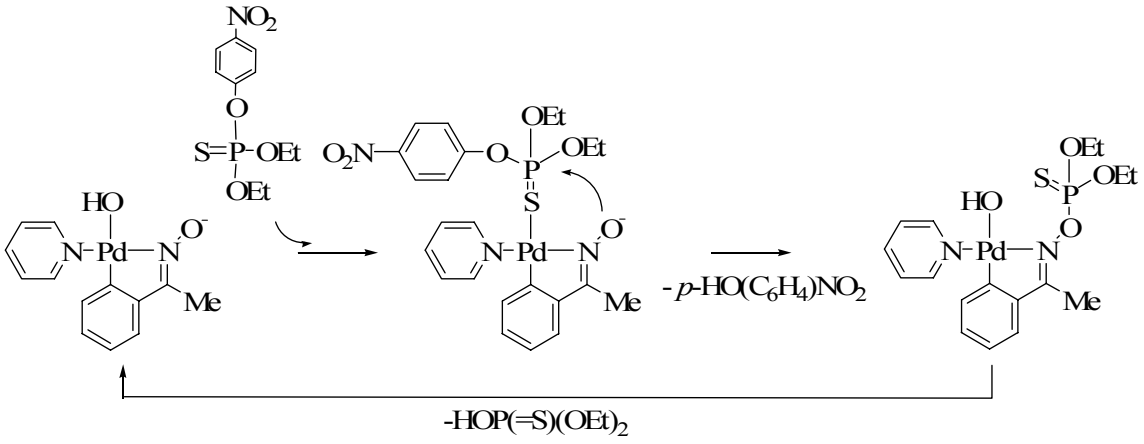

Figure 69. Ryabov's cyclopalladated Complex, catalytic process.

In order to assess the importance of the oximate functionality in the catalytic cycle proposed by Ryabov, we decided to investigate simple *o*-metallated palladacycle such as [2-(2-pyridyl)-phenyl-*C,N*]palladium(II) derivative that do not feature an oximate functionality. In the context of these studies, it was also decided to study palladium complexes that contain two proximal metal centers in the hope of discovering catalysts

whose efficiency is increased by cooperative effects occuring at neighboring metal centers. Such cooperative effects have been proposed for the hydrolysis of organophosphorus esters at the dinuclear active site of the phosphotriesterase metalloenzyme (PTE).

5.2 Mononuclear palladium (II) complexes

The reaction of methylparathion (**20**, Figure 70) with of [2-(2-pyridyl)-phenyl-*C,N*]palladium(II) acetate (**90**, figure 70) leads to the isolation of the corresponding *o*-palladated complex di-μ-(dimethylthiophosphate-*S,*S)-bis[2-(2-pyridyl)phenyl-*C,N*]dipalladium(II) (**91**, figure 70).

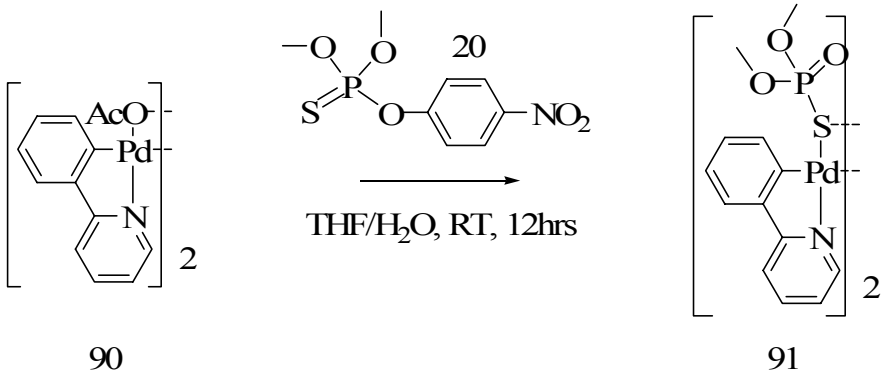

Figure 70. Coordination reaction of [2-(2-pyridyl)-phenyl-*C,N*]palladium(II) with methylparathion.

This reaction was first monitored in THF by ^{31}P $\{^{1}H\}$NMR spectroscopy (figure 70). While **20** is stable for several weeks in this aqueous solvent mixture, addition of **90** results in hydrolysis of the phosphorus ester and the rapid production of *p*-nitrophenol. This reaction is also accompanied by the appearance of the monomeric, phosphorous containing, compound **92** whose ^{31}P NMR resonance appears at 50.5 ppm. This signal is upfield from the ^{31}P resonance of **20** which appears at 66 ppm and do not correspond to the thiosphosphoric acid $HSP(=O)(OMe)_2$ derivative which gives rise to a resonance at 59.7 ppm (Figure 71).

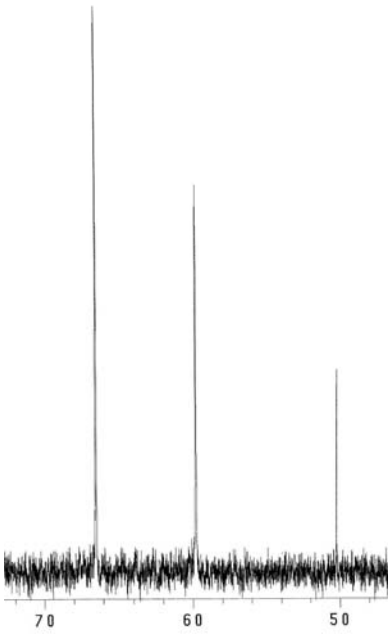

Figure 71. ^{31}P $\{^{1}H\}$ NMR spectra of a solution of methylparathion (5 mg) in the presence of **90** (1 mg) in THF.

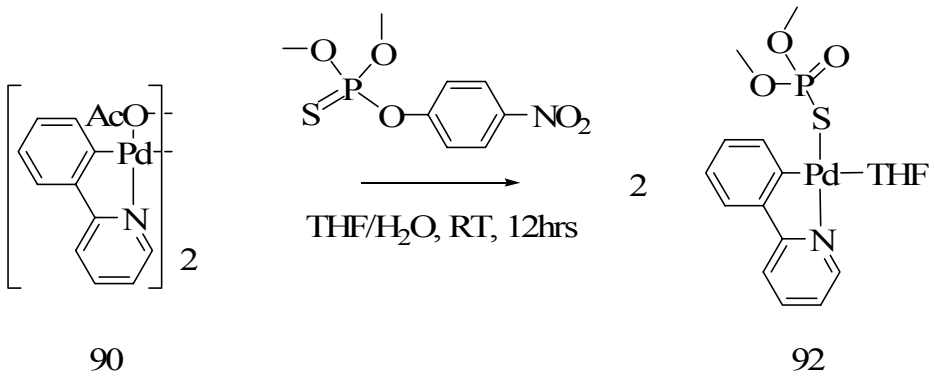

90 92

Figure 72. Proposed structure of **92**.

This reaction could be conveniently followed by monitoring the release of *p*-nitrophenol which features an absorption band at 400 nm ($10300 < \varepsilon < 18600$ cm^{-1} M^{-1} from pH 7 to pH 9). In the presence of 5% of **90** as a catalyst in water at pH 9 (CHES buffer), methylparathion (**20,** 5.7×10^{-3} M) was quickly and completely hydrolyzed indicating that the reaction is catalytic. The hydrolysis reaction was 50% complete after 2.6 minutes yielding a turnover frequency of 1.6×10^{-2} s^{-1}. After 14 min the reaction was 95% complete.

In order to ascertain the nature of the palladium complex formed in this catalytic reaction, an excess of water was added to a 2×10^{-3} M solution of both **90** and methylparathion in THF (5 ml). The solution was stirred overnight at 65° C (Figure 70).

After evaporation of the solvents, colorless needles of **91** were isolated by slow evaporation in DMF at room temperature (Figure 73).

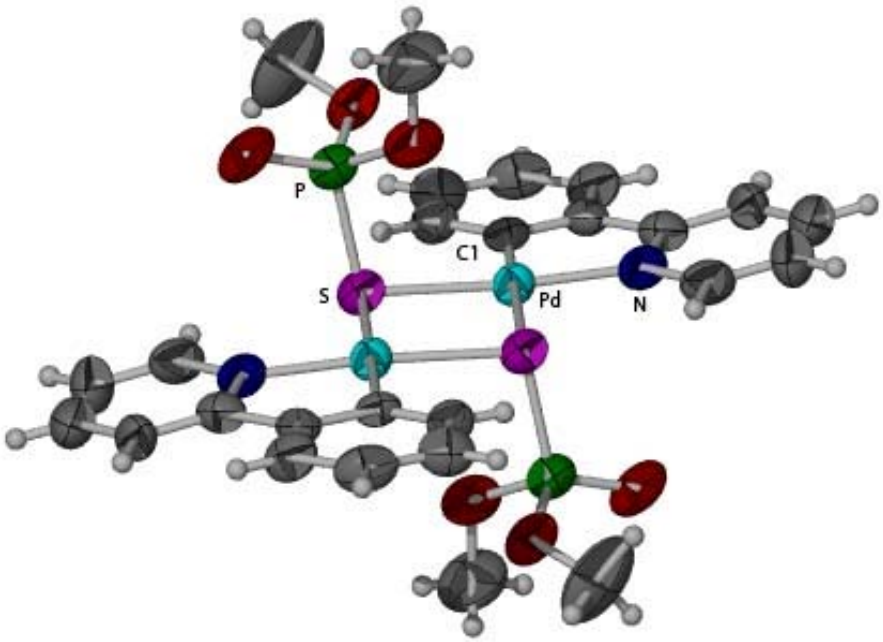

Figure 73. Structure of complex **91** in the crystal (50% ellipsoid). Selected bond lengths [Å] and angles [deg]. Pd-C(1) 2.049(11), Pd-N 2.060(11), Pd-S 2.418(3), Pd-S#1 2.467(3), S-P 2.089(5), S-Pd#1 2.467(3), P-O(1) 1.478(10), P-O(3) 1.594(10), P-O(2) 1.621(9). C(1)-Pd-N 80.9(5), C(1)-Pd-S 96.7(3), N-Pd-S 175.5(3), C(1)-Pd-S#1 177.3(3), N-Pd-S#1 98.6(3), S-Pd-S#1 83.98(11), P-S-Pd 101.75(17), P-S-Pd#1 97.72(16), Pd-S-Pd#1 96.02(11), C(7)-N-Pd 115.7(8), C(11)-N-Pd 125.2(10), C(2)-C(1)-Pd 127.1(10), C(6)-C(1)-Pd 114.9(8).

Complex **91** crystallizes in the triclinic space group *P*-1 (Table on page 114). In this complex, the two square planar palladium moieties (sum of angle of Pd = 360.2(2)˚) are linked by the sulfur atoms of the bridging dimethylthiophosphate ligands. The Pd-S distances of 2.418(3) and Pd-S 2.467(3) Å are comparable to those observed in related complexes such as (*R,S*)-di-μ-(dimethylthiophosphate-*S,S*)-bis{2-[2-(4-carbomethoxy)oxazolinyl]-phenyl-*C,N*}dipalladium(II) (av. Pd-S = 2.40 Å)[12] which also features bridging thiophosphate groups. The remaining coordination sites of the palladium center are occupied by the phenylpyridine carbon and nitrogen donor atoms. The resulting Pd-C(1) (2.049(11) Å) and Pd-N (2.060(11) Å) bonds are comparable to those observed for [2-(2-pyridyl)phenyl]palladium(II) chloride [LPd(μ–Cl)$_2$PdL]. [97]

Interestingly, the solid state $^{31}P\{^1H\}$ NMR of **91** revealed two different sets of data (figure 74). The first set corresponds to the "eclipsed" regio-isomer **93** (figure 75), where the two phosphorus nucleus have a different environment (29.3 ppm and 35.9 ppm). The second set correspond to the staggered regio-isomer **94** (figure 75), where a unique peak is observed (32.9 ppm). Indeed in such conformation, the two phosphorus nuclei have an identical environment.

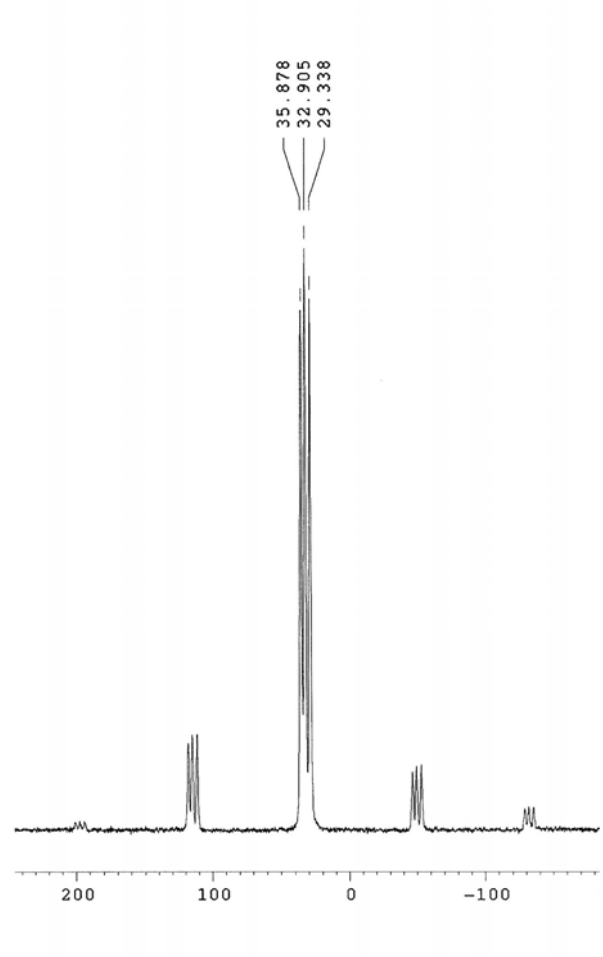

Figure 74. Solid state $^{31}P\{^{1}H\}$ NMR spectra of **91**.

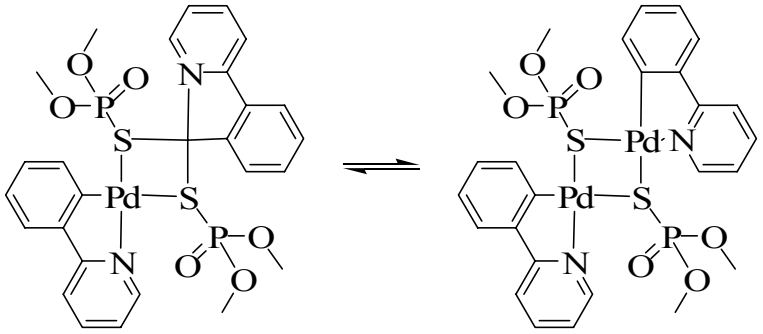

93 94

Figure 75. Regio-isomers **93-94** equilibrium.

Compound **91** can also react with triphenylphosphine in THF overnight at room temperature forming the 1:1 adduct (dimethylthiophosphate-*S,S*)-[2-(2-pyridyl)phenyl-*C,N*]palladium(II) trimethylphosphine (**95**, figure 76). The formation of **95** was first proven by ^{31}P NMR in THF. The addition of 1 equivalent of triphenylphosphine to **91** resulting to the rapid formation of 2 peaks at 43.1 ppm (Pd-SPO(OCH_3)$_2$), and 44.5 ppm (Pd-PPh_3) corresponding to **95**.

Figure 76. Coordination reaction of di-μ-(dimethylthiophosphate-*S,*S)-bis[2-(2-pyridyl)phenyl-*C,N*]dipalladium(II) with triphenylphosphine.

Crystals of **95** were isolated and studied by X-ray analysis (Figure 77). Complex **95** crystallizes in the triclinic space group *P*-1 (Table on page 114). In this complex, we can observe the typical square planar palladium environment (sum of angle of Pd = 360.36(52)˚), with the sulfur bound thiophosphate and triphenylphosphine ligands in a forced cis-arrangement. The resulting Pd-P (2.261(15) Å) and Pd-S (2.414(14) Å) distances fall within the expected range. [98] The remaining coordination sites of the palladium center are occupied by the phenylpyridine carbon and nitrogen donor atoms. The Pd-N distances of 2.089(4) Å and Pd-C 2.024(5) Å are comparable to those observed in **91**.

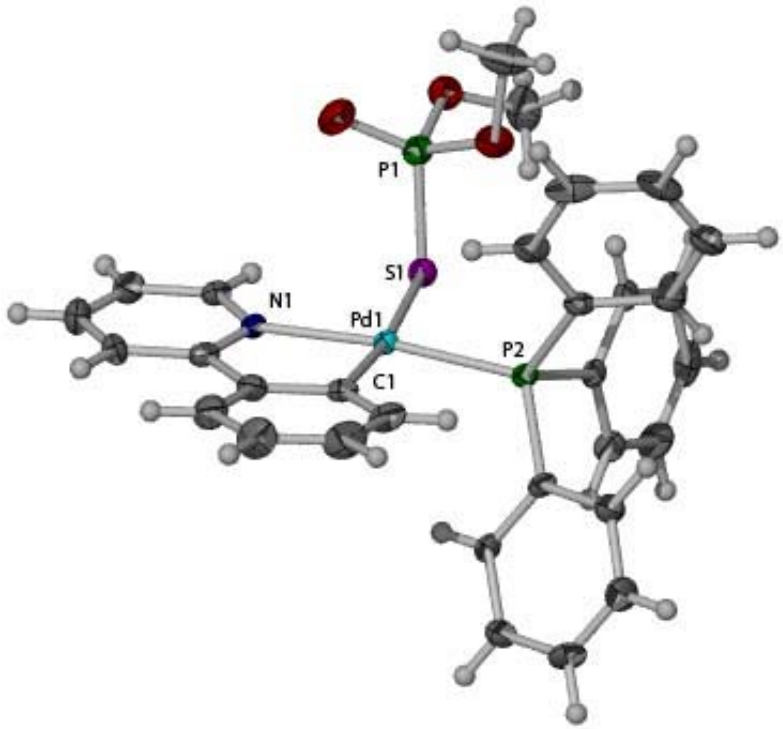

Figure 77. Structure of complex **95** in the crystal (50% ellipsoid). Selected bond lengths [Å] and angles [deg]. Pd(1)-C(1) 2.024(5), Pd(1)-N(1) 2.089(4), Pd(1)-P(2) 2.2612(15), Pd(1)-S(1) 2.4139(14), Pd(2)-C(32) 2.026(5), Pd(2)-N(2) 2.080(4), Pd(2)-P(4) 2.2548(15), Pd(2)-S(2) 2.4427(15). C(1)-Pd(1)-N(1) 80.56(18), C(1)-Pd(1)-P(2) 95.79(14), N(1)-Pd(1)-P(2) 173.68(11), C(1)-Pd(1)-S(1) 172.67(13), N(1)-Pd(1)-S(1) 93.51(12), P(2)-Pd(1)-S(1) 90.50(6), C(32)-Pd(2)-N(2) 81.14(17), C(32)-Pd(2)-P(4) 92.83(14), N(2)-Pd(2)-P(4) 173.97(11), C(32)-Pd(2)-S(2) 172.95(14), N(2)-Pd(2)-S(2) 91.81(11), P(4)-Pd(2)-S(2) 94.21(5), P(1)-S(1)-Pd(1) 99.20(7), C(14)-P(2)-Pd(1) 114.13(16), C(20)-P(2)-Pd(1) 113.99(16), C(26)-P(2)-Pd(1) 115.55(15), C(45)-P(4)-Pd(2) 117.88(16), C(57)-P(4)-Pd(2) 112.49(16), C(51)-P(4)-Pd(2) 113.96(17), P(3)-S(2)-Pd(2) 95.93(7), C(7)-N(1)-Pd(1) 114.9(3), C(38)-N(2)-Pd(2) 115.1(3), C(42)-N(2)-Pd(2) 126.7(3), C(2)-C(1)-Pd(1) 130.2(4), C(6)-C(1)-Pd(1) 113.2(4), C(33)-C(32)-Pd(2) 131.3(4), C(37)-C(32)-Pd(2) 112.1(3).

5.3 Dinuclear palladium (II) complexes

1,2-Orthopalladation of ligands **69**, **71**, **73**, and **74** have been carried out following two general procedures.[42,99] Most of the original experimental work centered on the metallation of ligand **71**. At first, this ligand was palladated with Pd (II) acetate in acetic acid. Only different methodological pathways were employed (temperature, time, work-up). From each experiment, we were able to observe the formation of the desired product **96** (figure 78) through ^{1}H NMR and Mass spectroscopy. A series of recrystallizations were attempted but no clean product could be isolated.

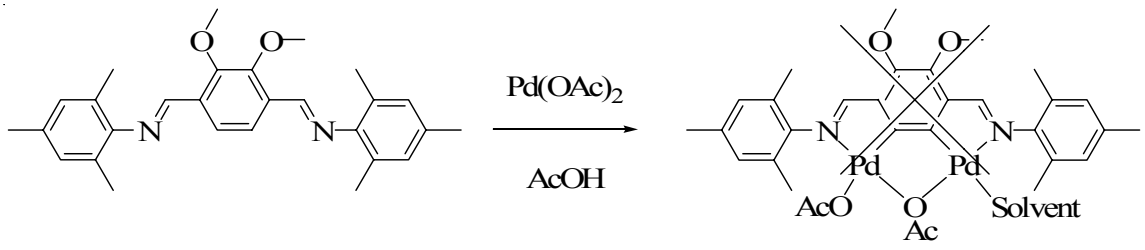

96

Figure 78: Reaction of **71** with $Pd(OAc)_2$.

In the same way, the reaction of **71** with Na_2PdCl_4 in CH_2Cl_2 leads to formation of the palladium chloride complex which presumably adopts a polymeric structure. Although we have not been able to thoroughly characterize this product. The ^1H NMR in DMSO shows poorly resolved peaks corresponding to the mesityl (CH_3, 25ppm; CH_{ar} 6.9 ppm), the methoxy (CH_3, 3.81 ppm), as well as the pyridazine (CH=N, 8.39 ppm; CH_{ar}, 6.9 ppm) H atoms. However, elemental analysis data confirms the proposed formulation and indicate the absence of any additional ligands. In order to obtain a more tractable dinuclear palladium complex, the chlorinated intermediate was allowed to react with TlACAC. This reaction was carried out on the crude chloride complex produced by the reaction of **63** with Na_2PdCl_4. The crude product was treated with 3 equivalents of TlACAC which resulted in the precipitation of TlCl. The product was extracted in pentane and recrystallized from hexane at room temperature which afforded red crystals of **97** (figure 79) in a 26% yield. This derivative has been fully characterized by EA, ^1H NMR, ^{13}C NMR and ES mass spectrometry.

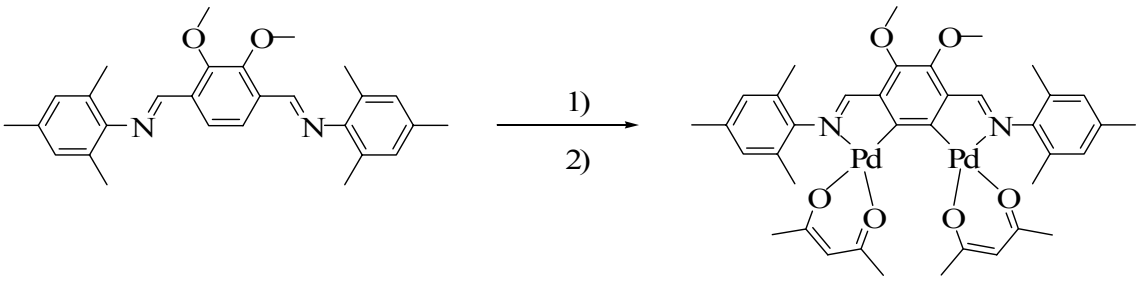

97

1) 3 Na_2PdCl_4, 3 NaOAc, CH_2Cl_2, EtOH, RT, 20h, b) Tl(acac), CH_2CL_2, RT, 1h

Figure 79: Reaction of **71** with Na_2PdCl_4.

This compound was also subjected to X-ray analysis. **97** crystallizes in the monoclinic space group *C*2/c (table on page 115) with one molecule per unit cell (figure 80). After examination of the structure, there are no unusual bond lengths and angles in each moiety that flank each side of the palladium centers. The X-ray structure revealed the typical square planar palladium (sum of angle of Pd = 361.61(43)˚) with the two ACAC oxygen atoms bound to the Pd center in a cis-arrangement. The resulting Pd-O (2.073(15) Å, and 2.073(14) Å) distances fall within the expected range.[99] The remaining coordination sites of the palladium center are occupied by the phenylpyridine carbon and nitrogen donor atoms. The Pd-N distances of 2.0008(4) Å and Pd-C 1.964(5) Å are comparable to those observed in **91**.

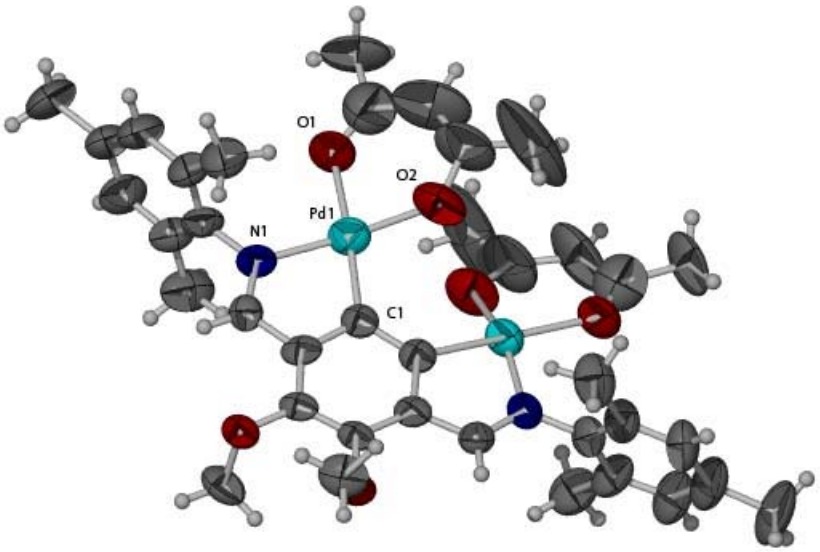

Figure 80. ORTEP view of **97** in the crystal (50% ellipsoids). Selected bond lengths [Å] and angles [deg]. N-Pd 2.008(10), Pd-C(1) 1.964(11), Pd-O(1) 2.073(10), Pd-O(2) 2.073(11). C(5)-N-Pd 115.5(8), C(6)-N-Pd 124.5(8), C(1)-Pd-N 80.6(4), C(1)-Pd-O(1) 173.8(5), N-Pd-O(1) 95.9(4), C(1)-Pd-O(2) 93.8(5), N-Pd-O(2) 158.0(4), O(1)-Pd-O(2) 91.3(4), C(16)-O(1)-Pd 128.2(14), C(18)-O(2)-Pd 124.9(14), C(2)-C(1)-Pd 114.4(8), C(1)#1-C(1)-Pd 128.6(4).

Following the same experimental procedure, ligands **69** and **73** were doubly palladated with Na_2PdCl_4 in EtOH. These reactions also produced the polymeric chloride complexes which upon treatment with TlACAC produced complex (**98**, figure 81) and (**99**, figure 82) in a 46% and 55 % yield respectively. Both of these compounds

have been fully characterized. Compound **98** is a yellow powder while **99** is red. Like **97**, both of these compounds dissolve in unpolar solvents such as pentane or hexane. Despite repeated attempts, no single crystals could be isolated for X-ray analysis.

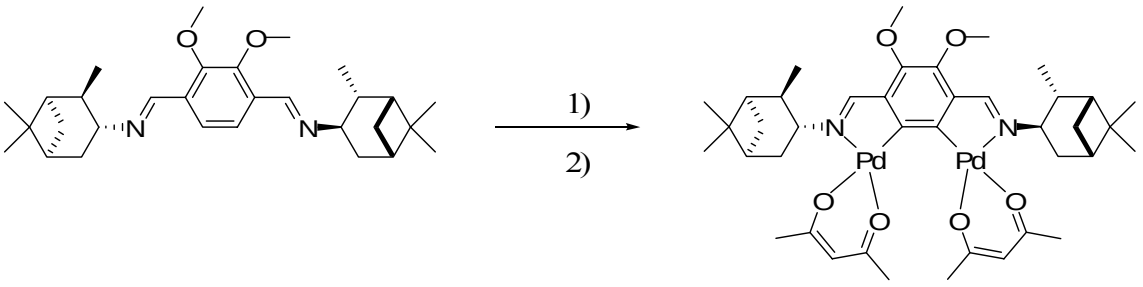

98

1) 3 Na_2PdCl_4, 3 NaOAc, CH_2Cl_2, EtOH, RT, 20h, b) Tl(acac), CH_2CL_2, RT, 1h

Figure 81: Reaction of **69** with Na_2PdCl_4.

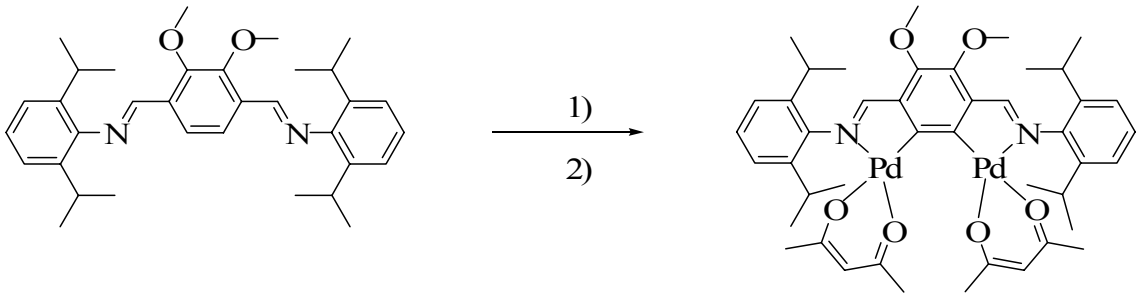

99

1) 3 Na_2PdCl_4, 3 NaOAc, CH_2Cl_2, EtOH, RT, 20h, b) Tl(acac), CH_2CL_2, RT, 1h

Figure 82: Reaction of **73** with Na_2PdCl_4.

5.4 Summary

Reaction of methylparathion with [2-(2-pyridyl)-phenyl-*C,N*]palladium(II) acetate leads to the formation of the corresponding dimethylthiophosphate complex **83** which has been isolated in a 74% yield. Complex **83** has been characterized by NMR, and elemental analysis. As indicated by X-ray analysis, this complex assumes a dinuclear structure with the two palladium phenylpyridine moieties linked by two S-bridging dimethylthiophosphate. Compound **83** also reacts with triphenylphosphine leading to the formation of the 1:1 adduct **86** which can be isolated and crystallized with high yield (85%). Orthopalladation of ligands **61**, **63**, **65** can be achieved by reacting a 3 equivalents excess of Na_2PdCl_4, in a 1:1 CH_2Cl_2/ethanol mixture. The isolation of the desired product was successfully achieved by displacing the chlorines with thallium ACAC.

5.5 Experimental

General considerations:

Methylparathion is highly toxic and should be handled in a well-ventilated fume hood. All glassware exposed to methylparathion should be decontaminated with bleach. Solvents were dried by standard method. All ^{31}P NMR studies were carried out on an

Inova 300 NMR spectrometer (121.4 MHz for ^{31}P). 85% H_3PO_4 was used as an external standard for the solution ^{31}P NMR spectra.

Synthesis of di-μ-(dimethylthiophosphate-*S,*S)-bis[2-(2-pyridyl)phenyl*C,N*] dipalladium(II) (**91**): A solution of **90** (320 mg, 0.5 mmol) in THF (10 ml) was added to a solution of Methylparathion (145 mg, 0.55 mmol) in THF (20 ml). Following addition of water (0.5 ml), the resulting yellow solution was stirred overnight at 65^o C. Upon evaporation of the Solvents, the resulting precipitate was washed with ether and dichloromethane and extracted with THF. Slow evaporation in DMF at room temperature led to the formation of colorless needles which were suitable for further X-ray analysis. Yield (297 mg, 74%). Mp 281˚C. ^1H NMR DMSO (500 Mhz): δ 3.65 (d, $^3J_{HP}$ = 9.3 Hz, 12H), 6.99 (m, 2H), (m, 2H), 7.41 (m, 2H), 7.52 (m, 2H), 7.65 (m, 2H), 8.07 (m, 6H CH ar), 8.46 (m, 3H, CH ar). ^{13}C NMR $CDCl_3$, (500 Mhz): δ 53.0, 119.2, 123.1, 124.3, 124.5, 129.0, 137.7, 140.1, 145.7, 147.7, 149.7, 163.3 (C ar). ^{31}P NMR DMSO/D_2O (300 Mhz): δ 50.5. Solid state $^{31}P\{^1H\}$ NMR: δ 35.9, 32.9, 29.3. Elemental analysis calc. (%) for $C_{26}H_{28}N_2O_6P_2Pd_2S_2$: C 38.87, H 3.51, N 3.49. Found: C 39.25, H 3.60, N 3.51.

Synthesis of (dimethylthiophosphate-*S,S*)-[2-(2-pyridyl)phenyl-*C,N*]palladium (II) trimethylphosphine (**95**): To a solution of complex **91** (40 mg, 50 μmol) in THF (10 ml) was added a solution of triphenylphosphine (13 mg, 50 μmol) in THF (10 ml). After 20 hours at room temperature, the colorless solution was evaporated under vacuum. Slow

recrystallization of the white residue in acetone led to the formation of colorless needles which were suitable for further X-ray analysis. Yield (45 mg, 85%). Mp. 281˚C. ^{1}H NMR $CDCl_3$ (300 Mhz): δ 3.32 (d, $^{3}J_{HP}$ = 7.2 Hz, 6H), 6.47 (m, 1H), 6.57 (m, 1H), 6.94 (m, 1H), 7.28 (m, 2H), 7.37 (m, 6H), 7.43 (m, 3H), 7.55 (m, 1H), 7.78 (m, 1H), 7.83 (m, 7H). ^{13}C NMR $CDCl_3$ (300 Mhz): δ 53.0 119.2, 123.1, 124.3, 124.5, 129.0, 137.6, 140.1, 145.7, 147.7, 149.6, 163,2 (Cq non detected). ^{31}P NMR THF (300 Mhz): δ 43.1, 44.5. Elemental analysis calc. (%) for $C_{31}H_{29}NO_3P_2SPd$: C 56.07, H 4.40, N 2.11. Found C 55.89, H 4.33, N 2.25.

Synthesis of 3,6-(2,4,6-trimethylphenyliminomethyl)-1,2-dimethoxy-1,2-phenylenedipalladium-(II)-bis(2,4-pentanedionate) (**97**): A solution of Na_2PdCl_4 (1.54 g, 5.25 mmol) and NaOAc (0.43 g, 5.25 mmol) was prepared in 10 ml ethanol and added to a solution of **71** (0.75g, 1.75 mmol). The reaction mixture was stirred at room temperature for 20 hours before being filtered under vacuum and washed 3 times with pentane. The resulting red crude material was thoroughly dried and use for the next step without further purifications. The red powder was then dissolved in 10 ml of CH_2Cl_2 and 3 equivalent of TlACAC (1.59 g, 5.25 mmol) was directly added. The rapid precipitation of $TlCl_2$ was observed and the reaction vessel was stirred for 1 hour at room temperature. Typical workup was followed with filtration of the precipitate, and evaporation of solvent under vacuum. The red crude product was then dissolved in pentane, filtered, and dried. After recrystallization in hexane at room temperature, red crystals of **97** (0.38g, 26%) were isolated. Mp 241-243˚C. $[M\text{-}Cl]^+$ 673. ^{1}H NMR C_6D_6

(300 MHz): δ 1.65 (s, 6H), 2.13 (s, 12H), 2.39, (m, 12H), 3.49 (s, 6H), 5.14 (s, 2H), 6.76 (s, 4H), 8.02 (s, 2H). ^{13}C NMR $CDCl_3$ (500 MHz): δ 18.9, 18.7, 21.2, 27.8, 27.5, 62.2, 99.2, 128.7, 131.0, 136.2, 140.3, 144.3, 148.7, 157.6, 172.1, 187.5. Elemental analysis calc. (%) for $C_{38}H_{44}N_2O_6Pd_2$: C 54.49, H 5.29, N 3.34. Found C 54.37, H 5.23, N 3.47.

Synthesis of 3,6-(1R,2R,3R,5S)-(-)isopinocampheylaminomethyl-4,5-dimethoxy-1,2-phenylenedipalladium-(II)-bis(2,4-pentanedionate) (**98**): A solution of Na_2PdCl_4 (1.54 g, 5.25 mmol) and NaOAc (0.43 g, 5.25 mmol) was prepared in 10 ml ethanol and added to a solution of **69** (0.81g, 1.75 mmol). The reaction mixture was stirred at room temperature for 20 hours before being filtered under vacuum and washed 3 times with pentane. The resulting red crude material was thoroughly dried and use for the next step without further purifications. The yellow powder was then dissolved in 10 ml of CH_2Cl_2 and 3 equivalent of TlACAC (1.59 g, 5.25 mmol) was directly added. The rapid precipitation of $TlCl_2$ was observed and the reaction vessel was stirred for 1 hour at room temperature. Typical workup was followed with filtration of the precipitate, and evaporation of solvent under vacuum. The yellow crude product was then dissolved in CH_2Cl_2 and purified by flash chromatography (rf = 0.8). A yellow powder of **98** was isolated (0.70 g, 46%). Mp 194-197°C. $[M\text{-}Cl]^+$ 709. ^{1}H NMR C_6D_6 (300 MHz): δ 1.12 (d, $^3J_{HH}$ = 7.5 Hz, 6H), 1.15 (s, 6H), 1.30 (s, 6H), 1.92 (m, 4H), 1.98 (s, 6H), 2.08 (m, 6H), 2.11 (s, 6H), 2.42 (m, 2H), 2.55 (m, 2H), 4.00 (s, 6H), 4.45 (m, 2H), 5.39 (s, 2H), 8.57 (s, 2H). ^{13}C NMR $CDCl_3$ (500 MHz): δ 20.4, 23.4, 25.4, 27.5, 27.6, 28.6, 34.6, 36.2, 39.8, 41.9, 42.7, 48.2, 62.4, 100.5, 124.7, 130.3, 150.9, 168.9, 186.7, 190.3.

Elemental analysis calc. (%) for $C_{40}H_{56}N_2O_6Pd_2$: C 54.99, H 6.46, N 3.21. Found C 55.11, H 6.23, N 2.84.

Synthesis of 3,6-(2,6-diisopropylphenyliminomethyl)-4,5-dimethoxy-1,2-phenylene-dipalladium-(II)-bis(2,4-pentanedionate) (**99**): A solution of Na_2PdCl_4 (1.54 g, 5.25 mmol) and NaOAc (0.43 g, 5.25 mmol) was prepared in 10 ml ethanol and added to a solution of **73** (0.90 g, 1.75 mmol). The reaction mixture was stirred at room temperature for 20 hours before being filtered under vacuum and washed 3 times with pentane. The resulting red crude material was thoroughly dried and use for the next step without further purifications. The red powder was then dissolved in 10 ml of CH_2Cl_2 and 3 equivalent of TlACAC (1.59 g, 5.25 mmol) was directly added. The rapid precipitation of $TlCl_2$ was observed and the reaction vessel was stirred for 1 hour at room temperature. Typical workup was followed with filtration of the precipitate, and evaporation of solvent under vacuum. The red crude product was then dissolved in pentane, filtered, and dried. After several attempts to recrystallize **99** (0.89 g, 55%) no crystals suitable for X-ray analysis were isolated. $[M\text{-}Cl]^+$ 757. ^1H NMR C_6D_6 (300 MHz): δ 1.14 (d, $^3J_{HH}$ = 2.1 Hz, 6H), 1.16 (d, $^3J_{HH}$ = 3.6 Hz, 6H) 1.23 (d, $^3J_{HH}$ = 6.9 Hz, 6H), 1.32 (d, $^3J_{HH}$ = 6.6 Hz, 6H), 1.54 (s, 6H), 1.92 (s, 6H), 3.43 (m, 2H), 3.62 (m, 2H), 3.84 (s, 6H), 5.09 (s, 2H), 7.17 (m, 4H), 7.28 (m, 2H), 8.18 (s, 2H). ^{13}C NMR $CDCl_3$ (500 MHz): δ 23.5, 24.1, 25.0, 26.8, 27.5, 28.1, 62.4, 99.2, 123.2, 123.3, 127.4, 140.5, 142.0, 142.4, 144.0, 148.9, 157.9, 171.7, 185.4, 186.7. Elemental analysis calc. (%) for $C_{44}H_{56}N_2O_6Pd_2$: C 57.33, H 6.12, N 3.04. Found C 57.40, H 6.04, N 2.82.

Table 6: Crystal data for complexes **91** and **95**.

Crystal data	**91**	**95**
Formula	C26 H28 N2 O6 P2 Pd2 S2	C62 H58 N2 O6 P4 Pd2 S2
M_r	803.36	1327.90
Crystal size (mm^3)	0.32x0.35x0.42	0.15x0.32x0.20
Crystal system	Orthorhombic	Triclinic
Space group	Pbca	*P-1*
a (Å)	*7.8374(16)*	9.0616(18)
b (Å)	19.451(4)	17.793(4)
c (Å)	19.600(4)	19.315(4)
α (°)	90	112.91(3)`
β (°)	90	96.39(3)
γ (°)	90	94.58(3)
V ($Å^3$)	2987.9(10)	2824.9(10)
Z	4	2
ρ_{calc} (Mg/m^3)	1.786	1.561
μ(Mo $K\alpha$)(mm^{-1})	1.493	0.878
F(000) (e)	1600	1352
Data Collection		
T/K	273(2)	273(2)
Scan mode	ω	ω
hkl range	-8<=h<=8	-11<=h<=5
	-22<=k<=14	-22<=k<=23
	-20<=l<=22	-23<=l<=25
Measured refl.	12111	17862
Unique refl., [R_{int}]	2281 [R(int) = 0.0780]	12514 [R(int) = 0.0368]
Refl. used for refinement	2281	12514
Absorption correction	none	none
T_{min}/T_{max}	none	none
Refinement		
Refined parameters	181	707
R1, wR2 [I>2σ(I)]	R1 = 0.0767, wR2 = 0.1510	R1 = 0.0548, wR2 = 0.1035
ρ_{fin} (max/min) ($eÅ^{-3}$)	2.129 and -0.690	0.942 and -0.886

[a] R1 = $(F_o - F_c)/F_o$. [b] wR2 = $\{[w(F_o^2 - F_c^2)^2]/[w(F_o^2)^2]\}^{1/2}$; $w = 1/[\square^2(F_o^2) + (ap)^2 + bp]$; $p = (F_o^2 + 2F_c^2)/3$ with: a = 0.02 and b = 50 for **91**; a = 0.0407 and b = 3.2958 for **95.**

Table 7: Crystal data for complex **97**.

Crystal data	**97**
Formula	C38 H44 N2 O6 Pd2
M_r	837.55
Crystal size (mm^3)	0.24x0.20x0.18
Crystal system	Monoclinic
Space group	C2/c
a (Å)	*22.043(10)*
b (Å)	16.271(7)
c (Å)	10.094(5)
α (°)	90
β (°)	98.834(9)
γ (°)	90
V ($Å^3$)	3578(3)
Z	4
ρ_{calc} (Mg/m^3)	1.555
μ(Mo $K\alpha$)(mm^{-1})	1.053
F(000) (e)	1704
Data Collection	
T/K	273(2)
Scan mode	ω
hkl range	-23<=h<=25 -14<=k<=18 -11<=l<=11
Measured refl.	8296
Unique refl., [R_{int}]	2812 [R(int) = 0.0777]
Refl. used for refinement	2812
Absorption correction	Empirical
T_{min}/T_{max}	0.4749 and 0.4066
Refinement	
Refined parameters	217
R1, wR2 [I>2σ(I)]	R1 = 0.0878, wR2 = 0.1946
ρ_{fin} (max/min) ($eÅ^{-3}$)	1.292 and -0.904

[a] R1 = $(F_o - F_c)/F_o$. [b] wR2 = $\{[w(F_o^2 - F_c^2)^2]/[w(F_o^2)^2]\}^{1/2}$; $w = 1/[\square^2(F_o^2) + (ap)^2 + bp]$; $p = (F_o^2 + 2F_c^2)/3$ with: a = 0.1308 and b = 0.

CHAPTER VI

METAL CATALYSED ORGANOPHOSPHATE ESTER HYDROLYSIS

6.1. Introduction

As mentioned in the introductory paragraph of this dissertation, the organophosphorus hydrolase (OPH), from *Pseudomonas diminuta*, is very active in the hydrolysis of various organophosphorus esters including organothiphosphates. The X-ray structure of this enzyme indicates the presence of a dinuclear active site containing two Zn^{2+} cations bridged by a hydroxide.[100] The proposed mechanism suggests that a water molecule is activated and oriented at the more buried metal center while the organophosphate coordinates at the more accessible metal site. It has been suggested that hydrolysis occurs by a S_N2 mechanism in which a water molecule attacks the phosphoryl center and displaces the leaving group. A number of studies have recently focused on optimizing the rate of hydrolysis observed with the native enzyme but it is important to note that so far, no dinuclear complexes that mimic the function of OPH have been reported or investigated. [101]

In the context of this thesis, it was decided to determine whether or not some of the dinuclear complexes presented in the preceding chapters could serve to mimic the activity of OPH in the hydrolysis of methylparathion. As part of these studies, a number of metal ions and complexes have been tested.

6.2. Dinuclear Cu(II) complexes catalysis

The dinuclear complexes **85** as well as its monofunctional analog **89** were first investigated. None of these complexes showed any activity in the hydrolysis of paraoxon in the 7-10 pH range. Elevation of the temperature did not appear to have any effects. Since organothiophosphotriester are known to be more reactive toward synthetic catalysts,[88] we decided to focus on the hydrolysis of methyl parathion (**20**, figure 83).

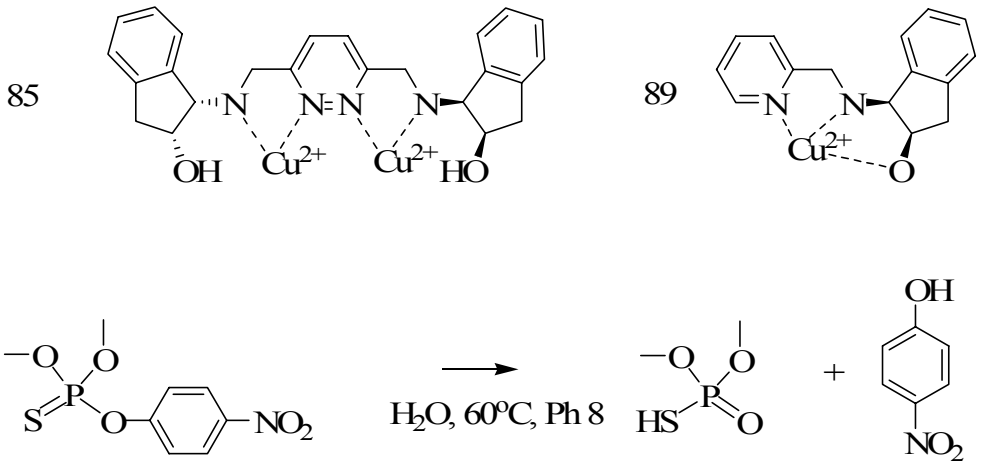

Figure 83: Hydrolysis of methylparathion, primary tests.

These experiments were monitored by following the addition of KOH in aqueous media by pH-Stat without additional buffer. This experiment was done at 60°C with 2 x 10^{-4} M of **20** and 2 x 10^{-4} M of the selected metal complex in an aqueous solution (20% methanol, 0.1 M KCl). The pH of the solution was set at pH 8 prior to addition of the catalyst, and was kept constant by slow addition of a 5 x 10^{-2} M KOH solution (figure 84). As the pH is remained constant, the number of moles of hydrolysed product is directly proportional to the amount of KOH added to the solution.

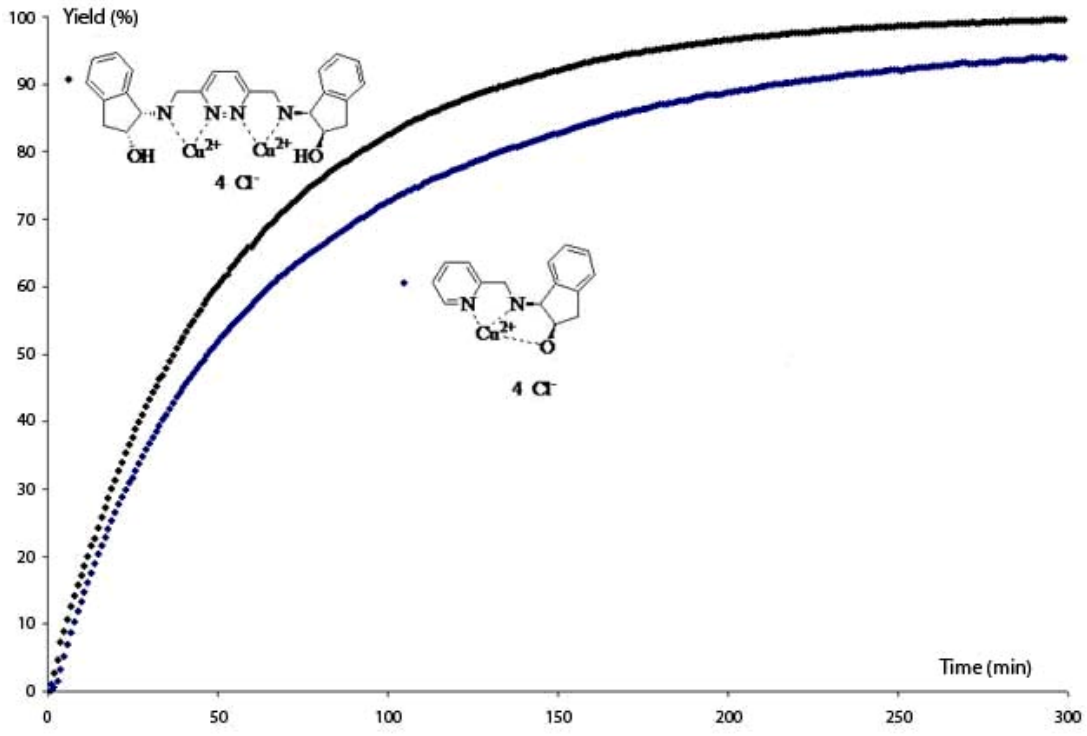

Figure 84. Hydrolysis of methylparathion by **85**, and **89** at 60°C and pH 8.

As shown above, the catalytic activity is definitely present but very weak. The hydrolysis reaction with 1 equivalent of Cu (II) and 0.5 equivalent of dinucleating ligand was 50% completed after 40 minutes yielding a turnover frequency of 2.1 x 10^{-4} s^{-1}. After 3 hours the reaction was 95% complete. It is also interesting to note that no cooperative effects between the 2 Cu (II) metal centers was observed as the catalytic activity of the monofunctional analogues **89** is comparable to that of the dinuclear systems **85**.

6.3. Metal ion screening

At this point, alternative systems had to be considered. In order to better design a new type of catalyst, we decided to test the activity of a series of metal ions such as Pd (II), Pt (II), Cu (II), Zn (II), and Ni (II) Co (II), and Mn (II) in the hydrolysis of **20**. This experiment was done also by pH-Stat with 2 x 10^{-4} M of **20** and 2 x 10^{-4} M of the selected ions in aqueous solution (20% methanol, 0.1 M KCl. This catalysis was also observed at pH 8 and at a temperature of 60^{o}C (figure 85).

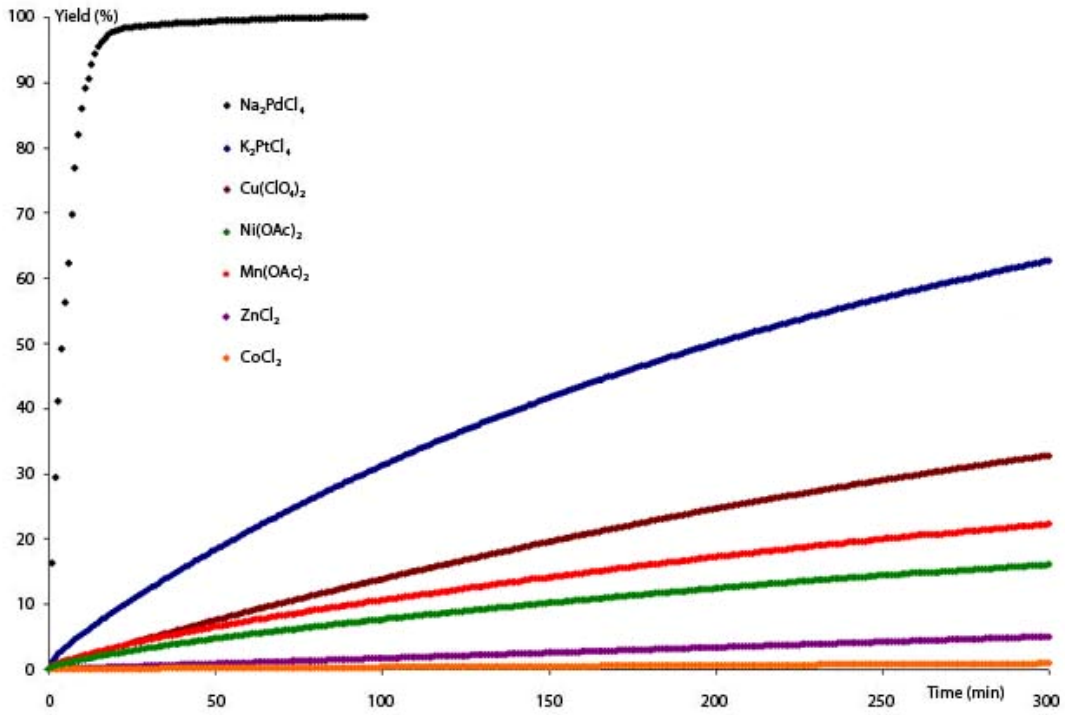

Figure 85. Hydrolysis of methylparathion by metal ions at 60°C and pH 8.

Our first surprise came from the low catalytic activity of Zn^{2+}, Cu^{2+}, Ni^{2+}, Co^{2+}, and Mn^{2+} cations. However, the catalytic activity of platinum and more importantly palladium looked very promising. The hydrolysis reaction with 1 equivalent of Pd^{2+} was 50% completed after 5 minutes yielding a turnover frequency of 1.66×10^{-3} s^{-1}. After 12 min the reaction was 98% complete.

6.4. Dinuclear Pd(II) complexes catalysis

Based on the above observations, we decided to investigate the use of the dinuclear palladium complexes **97**, **98**, and **99** as catalysts for the hydrolysis of paraoxon (**19**), and parathion (**20**). For our first experiments, catalyst **97** was chosen and tested. The reactions were followed by monitoring the absorbance of the *p*-nitrophenol released after addition of the palladium catalyst to a buffered solution of the organophosphotriester. Just like for the Cu (II) complexes **85** and **89**, no catalytic activity was observed from pH 7 to pH 10 for the hydrolysis reaction of paraoxon. However, when the same experiment was carried out with the more reactive substrate parathion, catalysis was readily observed. These experiments were monitored by following the release of *p*-nitrophenol in aqueous media by UV at 400 nm. This experiment was done at room temperature with 3.5×10^{-5} M of **20** and 1.75×10^{-6} M of catalyst (10% Pd) in a 5.7×10^{-3} CHESS solution (pH 9). We rapidly noticed that even with the use of only 0.1 equivalents on catalyst, the hydrolysis of **20** was observed at a high rate (figure 79). The hydrolysis reaction by **97** was 50% completed after 29 minutes yielding a turnover frequency of 2.87×10^{-3} s^{-1}. After 2.6 hours the reaction was 90% complete. The exact same experimental procedure was followed for catalysts **98** and **99**. It appears that catalyst **98** yielded the most promising results yet (figure 86). The hydrolysis reaction by **98** was 50% completed after 10 minutes yielding a turnover frequency of 8.33×10^{-3} s^{-1}. After 34 min the reaction was 95% complete. As for the last catalyst **99**, only a turnover frequency of 2.66×10^{-4} s^{-1} was observed (figure 86).

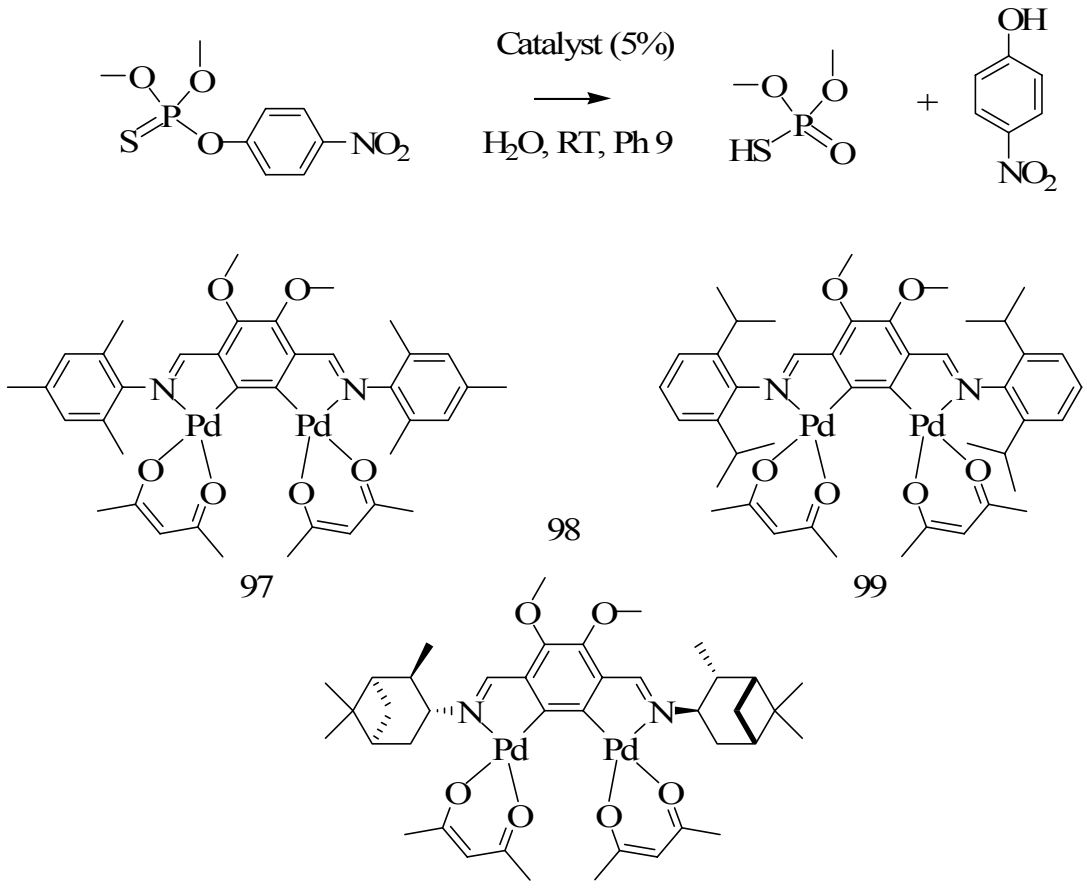

Figure 86. Hydrolysis of methylparathion by **97**, **98**, and **99** at RT at pH 9.

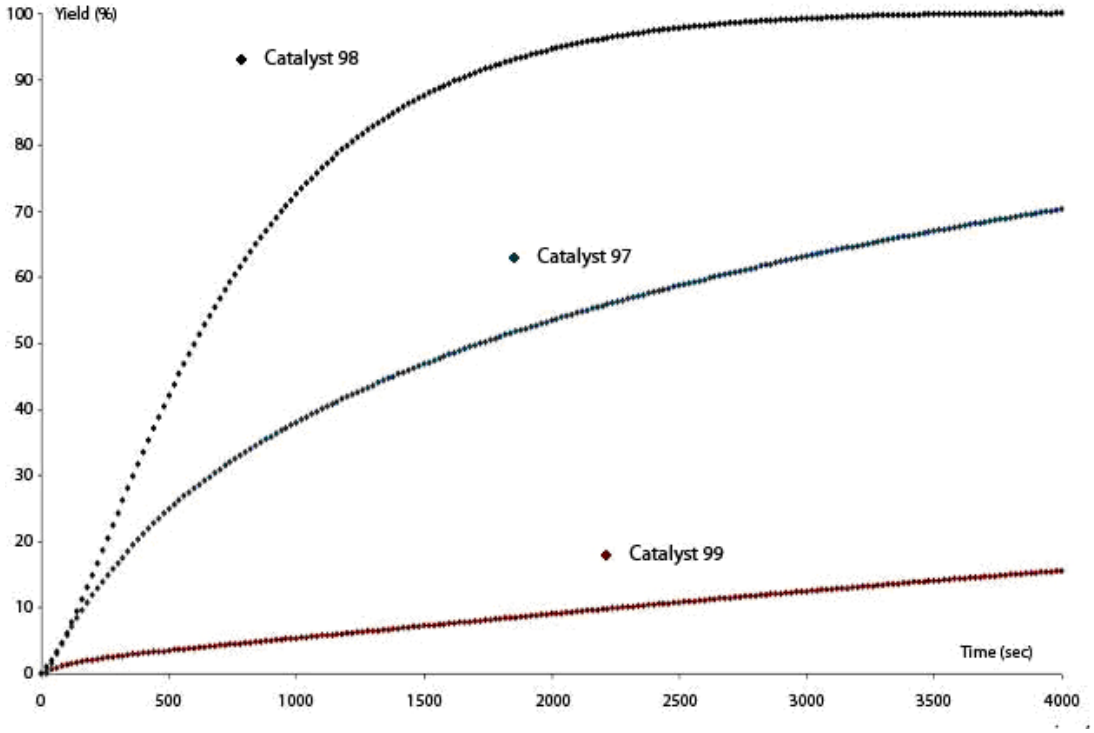

Figure 86. Hydrolysis of methylparathion by **97**, **98**, and **99** at RT at pH 9.

In order to obtain a more detailed insight in the kinetics involved in this reaction, catalytic experiments were carried out at various substrate and catalyst (**97**) concentrations at pH 9 (CHES, at 5.7 mM), and were analyzed using the initial slope methods. As indicated by this kinetic analysis, the reaction rate follows a second order kinetics with a first order dependence on substrate (figure 87) and palladium (figure 88) ($v = k_2[Pd][parathion]$). The k_2 value of 190 $M^{-1}s^{-1}$ obtained from these measurements is

comparable to earlier work on *ortho*-palladated phenyloxazoline derivatives that have been investigated in our laboratory. [42,117]

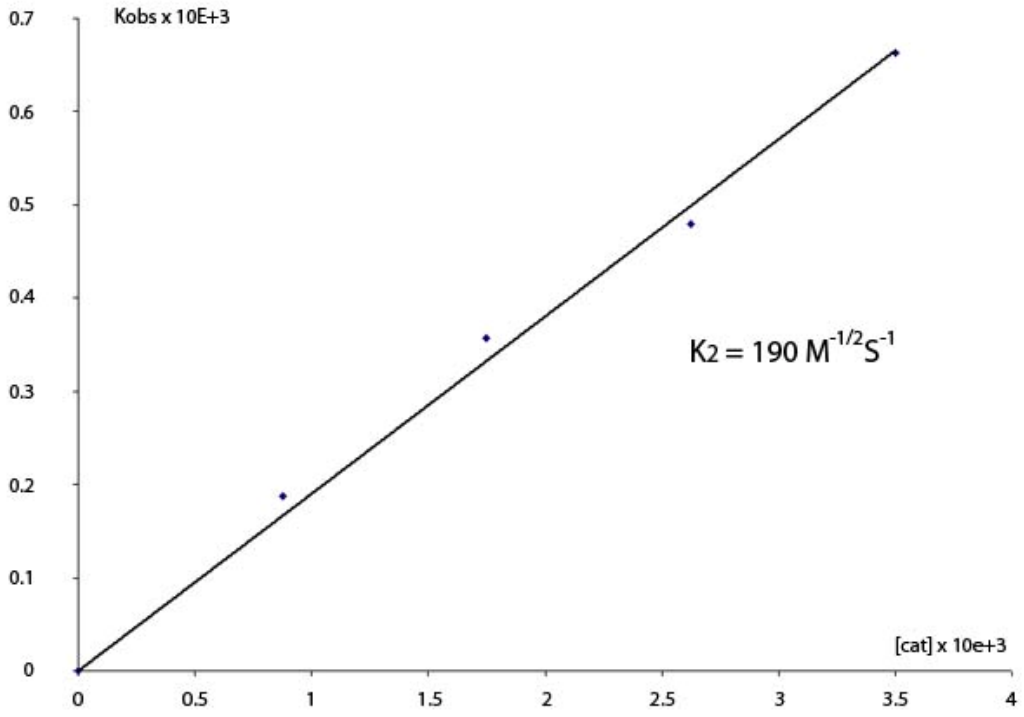

Figure 87. Pseudo first order kinetic resolution of the hydrolysis of **20** ($3.5\ 10^{-5}$ M) by **97** at pH 9.

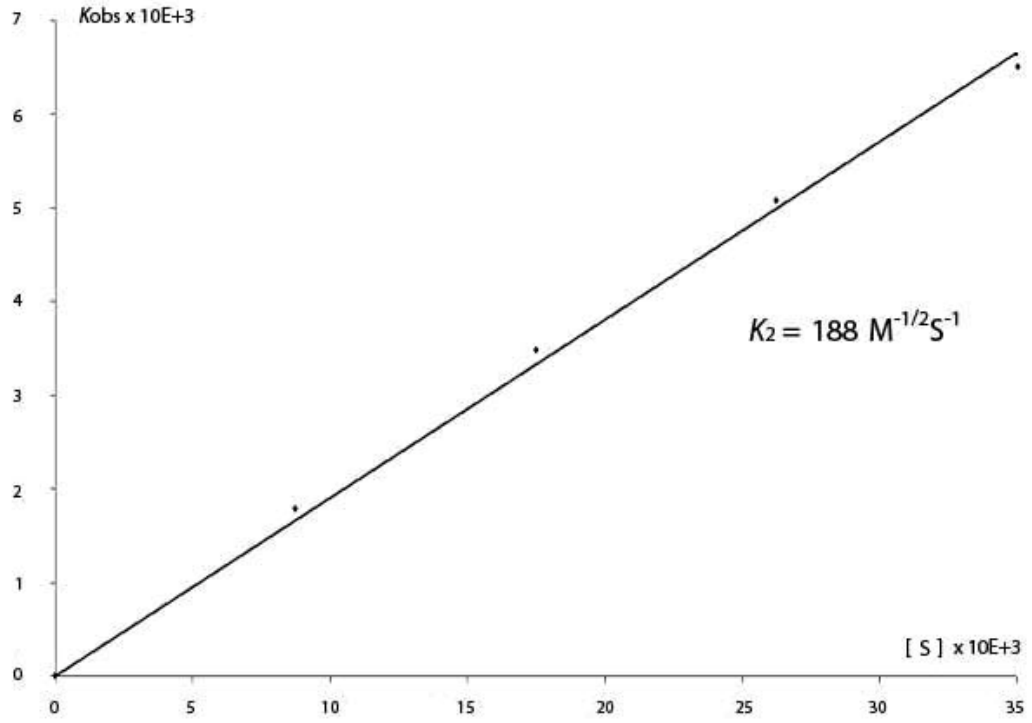

Figure 88. Pseudo first order kinetic resolution of the hydrolysis of **20** by **97** ($1.75\ 10^{-6}$ M) at pH 9.

6.5. Mononuclear Pd(II) complexes catalysis

In order to compare the activity of the dinculear catalysts **97**, **98**, and **99** to that of a mononuclear derivative, the monofunctional palladium complex **91** was investigated. (figure 89). The catalysis experiments were carried out also at various methylparathion

and catalyst concentrations in the 6 - 10 pH range (Buffer: HEPES, EPPS, CHES, at 5.7 mM). The data were analyzed using the initial slope methods.

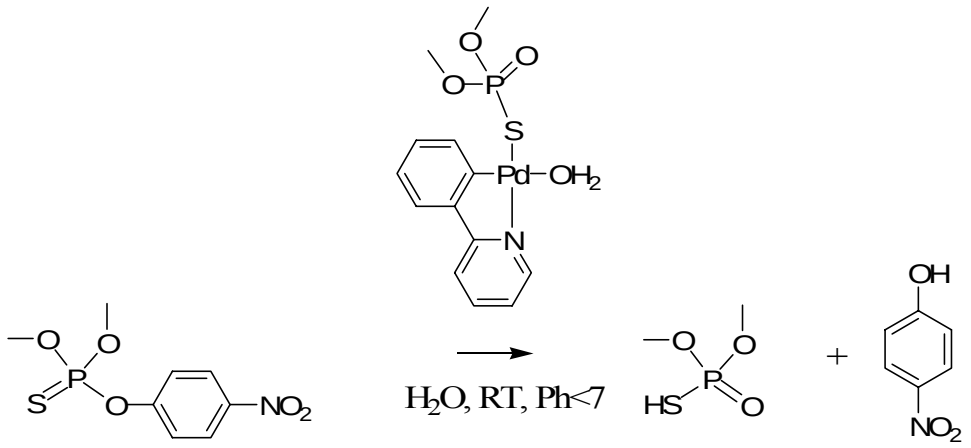

Figure 89. Hydrolysis reaction of methylparathion by **91** at RT.

As indicated by this kinetic analysis at pH7, the reaction rate follows a second order kinetics with a first order dependence both in substrate and palladium catalyst ($v = k_2[Pd][parathion]$). The k_2 value of 147(2) $M^{-1}s^{-1}$ obtained from these measurements is the highest ever recorded for a synthetic catalyst at neutral pH (figure 90, 91).

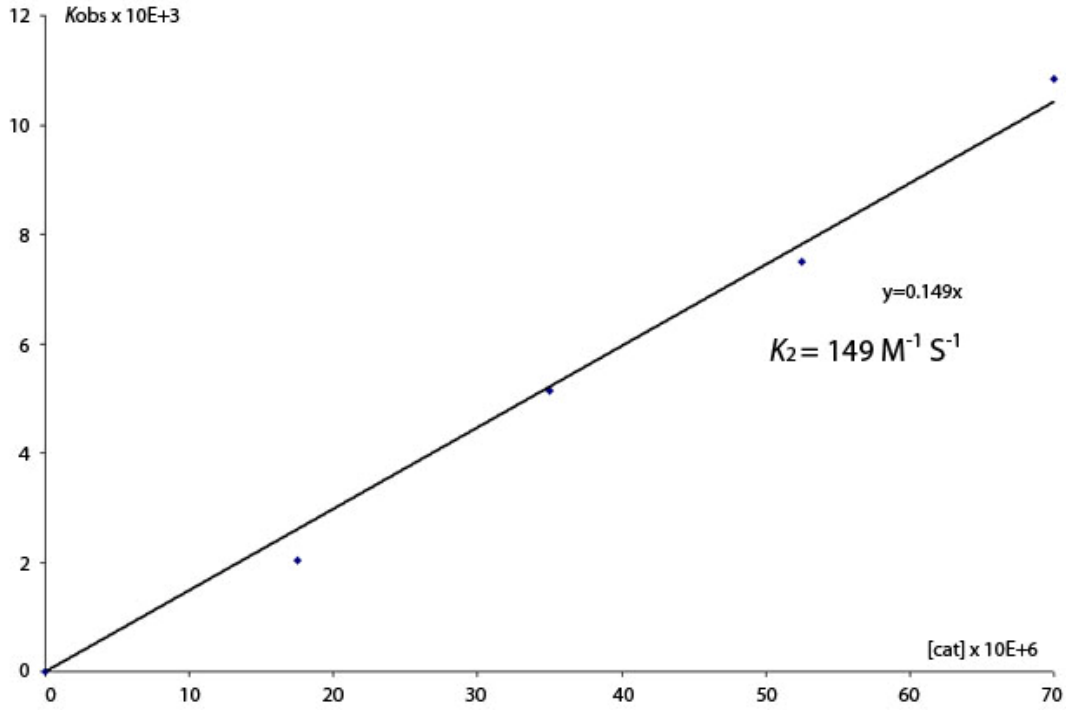

Figure 90. Pseudo first order kinetic resolution of the hydrolysis of methylparathion ($3.5\ 10^{-5}$ M) by **91** at pH 7.

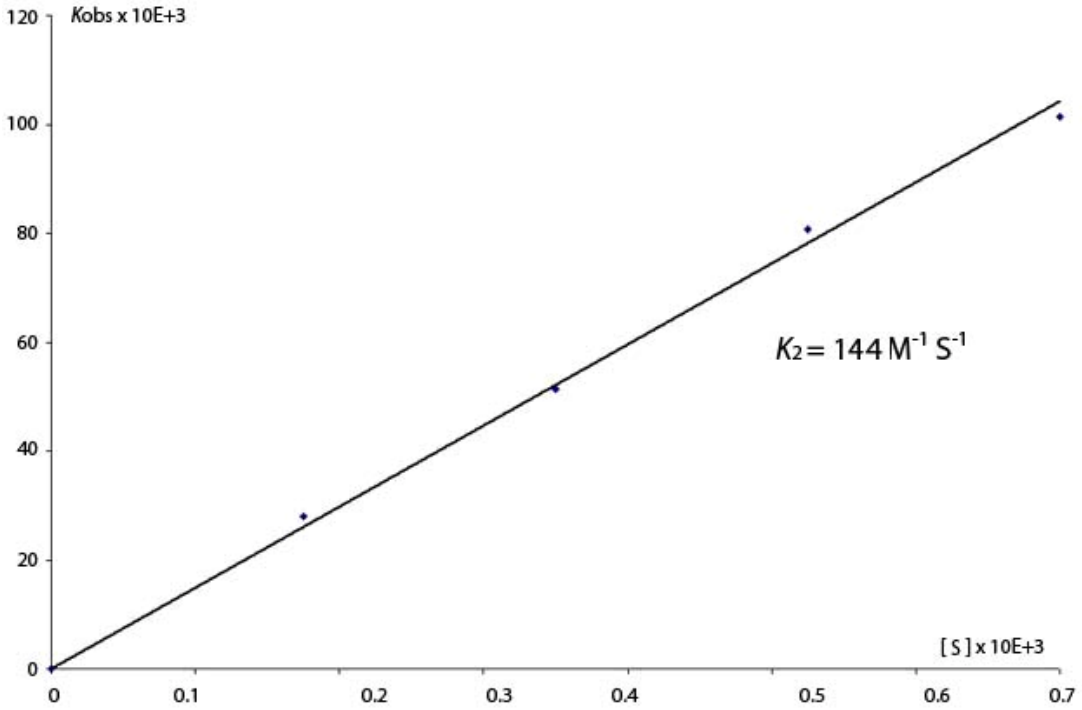

Figure 91. Pseudo first order kinetic resolution of the hydrolysis of methylparathion by **91** (1.75 10^{-6} M) at pH 7.

In fact, the k_2 value reported herein at neutral pH is comparable to those reported by Ryabov for organoplatinum and palladium complexes in the 8.5 – 9.5 pH range. Since **91** is the only species observed in solution, it is logical to assume that the catalyst is a mononuclear palladium species. In an effort to understand the structure of **91** in solution, a number of physical measurements have been carried out. Pulse field gradient spin-echo (PGSE) has emerged as a valid method for the determination of diffusion

coefficients and hydrodynamic radii of organometallic compounds.[102] When the PGSE experiment of complex **91** in DMSO-d_6 was carried out (figure **92**), the dimethylthiophosphate and phenylpyridine moity were found to diffuse at the same rate indicating that dimethylthiophosphate anion is still ligated to the palladium center. This result suggests that, in solution, dimethylthiophosphate is still bound to the palladium center during the catalytic process (figure 93).

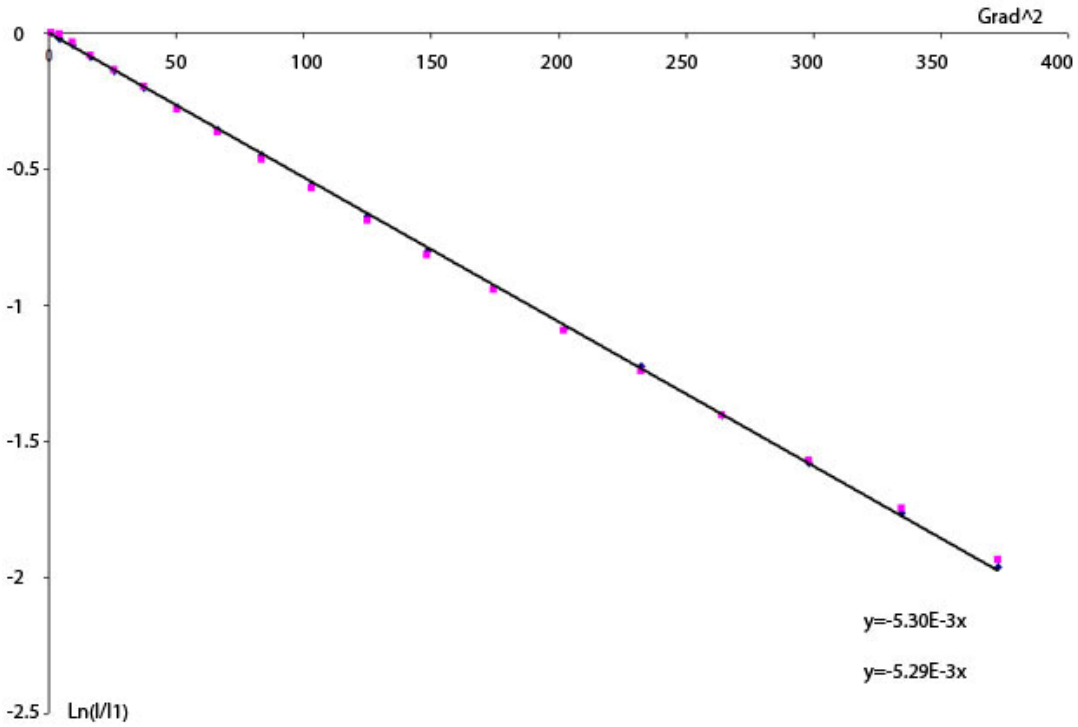

Figure 92. ^{1}H PGSE analysis of **91** (1 mg) in DMSO-d_6.

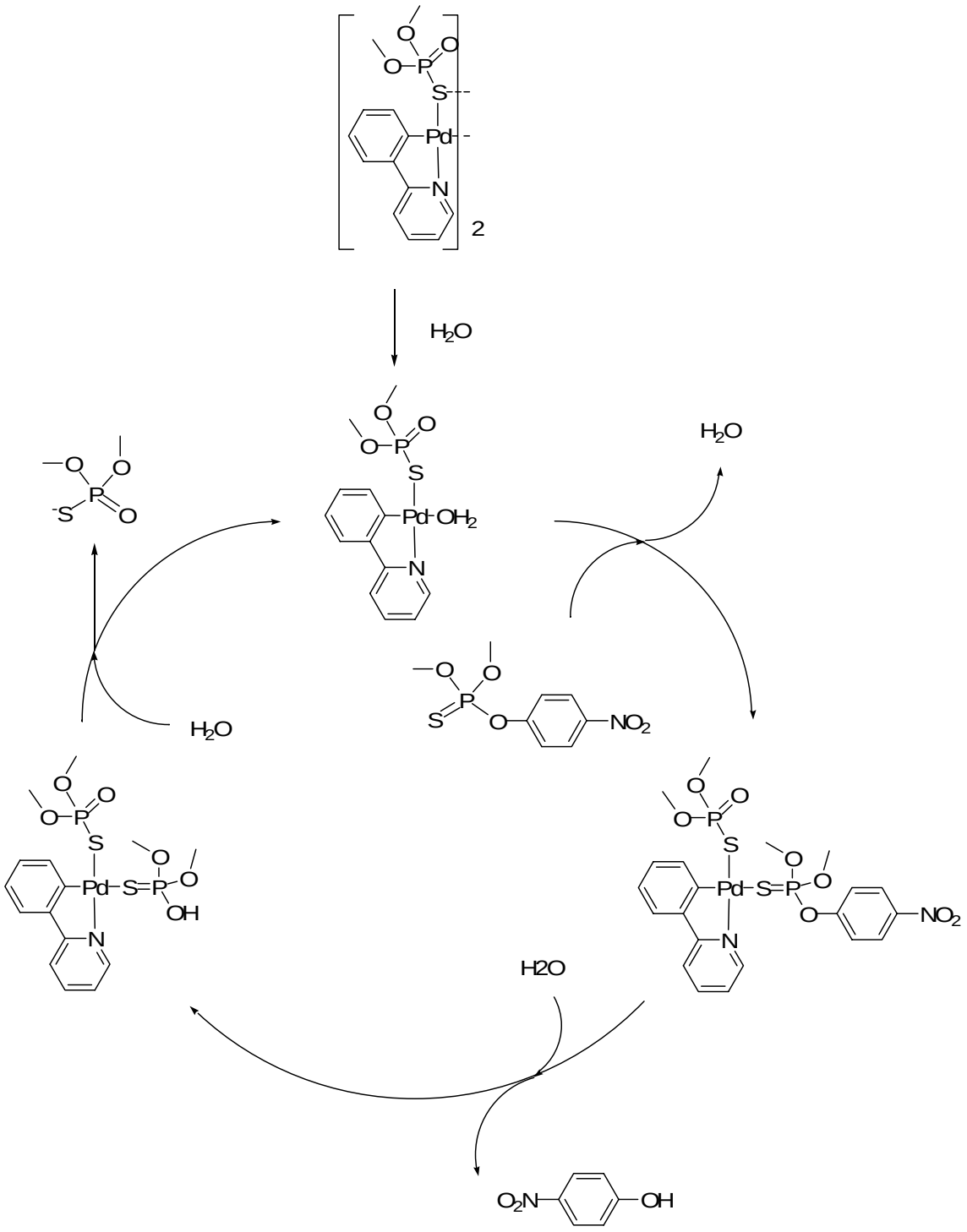

Figure 93. Proposed mechanism for the hydrolysis of **20** by **91** at neutral pH.

At pH9, the reaction rate follows another kinetic pathway with the same first order dependence in substrate (figure 94) but a half order dependence in palladium catalyst (figure 95). The catalytic activity of compound **91** has a turnover frequency of 1.6×10^{-2} s^{-1}. The data can be fit to an expression for the hydrolysis of methylparathion by compound **91** as in the following equation: $k_2K_{eq}^{1/2} = 3.02(1)\ M^{-1/2}s^{-1}$ ($v = k_2K_{eq}^{1/2}[Pd]^{1/2}[parathion]$; $K_{eq} = [monomer]^2 /[Dimer]$). These observations can be reconciled on the basis of a mechanism in which the active form of the catalyst is a monomer whose concentration is controlled by an equilibrium with a dimer (figure 96).

In order to further investigate such drastic increase in the catalytic activity of the system from neutral to alkaline media, the pH of the catalytic hydrolysis of **20** by compound **91** was studied between pH 7 and 9. This profile reveals the existence of 2 pH independent plateaus connected by an intermediate regime where the rate of hydrolysis depends on the pH (figure 97). Furthermore, the UV spectrum of **91** depending on the pH was investigated (figure 98). The corresponding plot showed the decrease of a UV band at 258 nm establishing that a new species was forming in solution: Complex **91** at neutral pH, and the hydroxo derivative **100** at higher pH (figure 99).

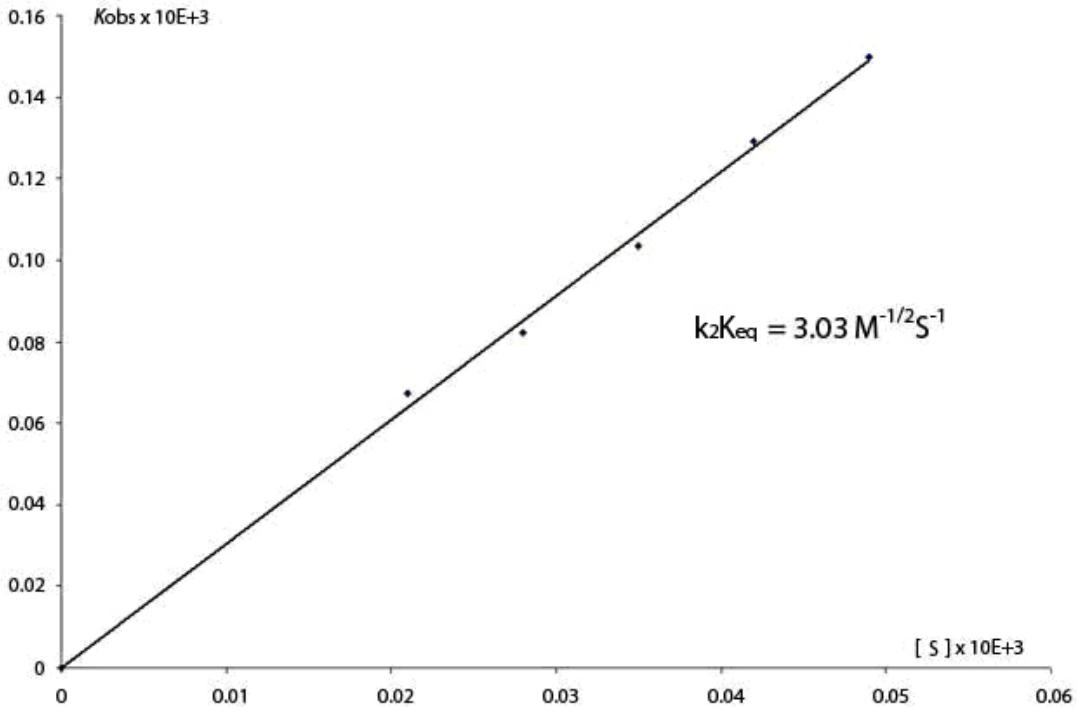

Figure 94. Pseudo first order kinetic resolution of the hydrolysis of methylparathion by **91** ($1.75\ 10^{-6}$ M) at pH 9.

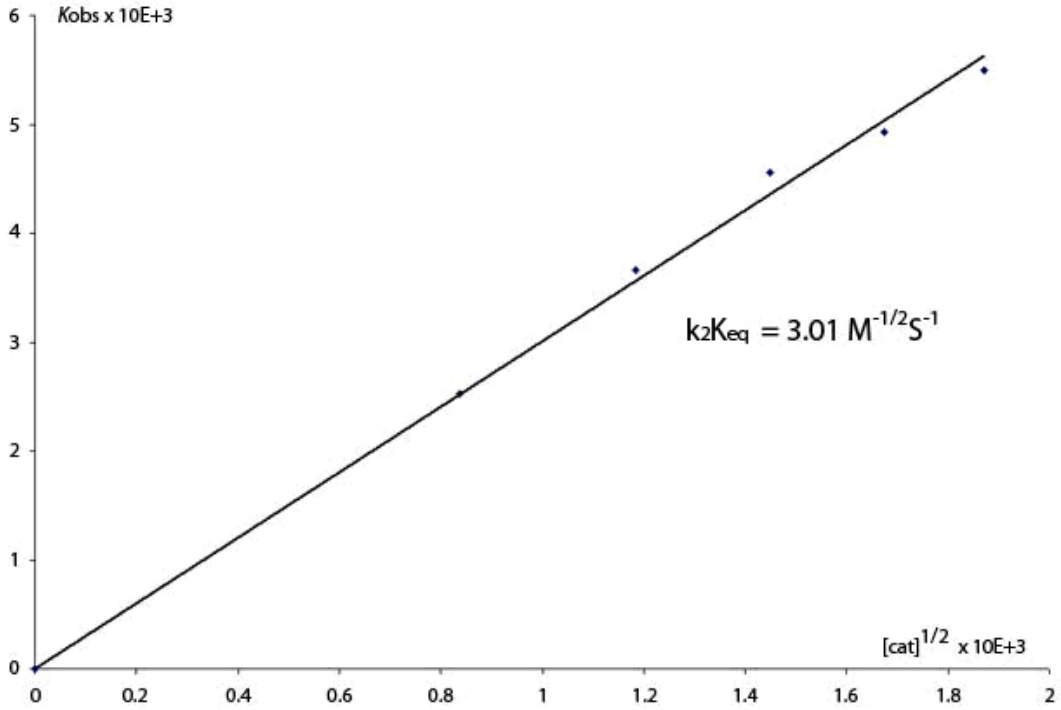

Figure 95. Pseudo half order kinetic resolution of the hydrolysis of **20** ($3.5\ 10^{-5}$ M) by **91** at pH 9.

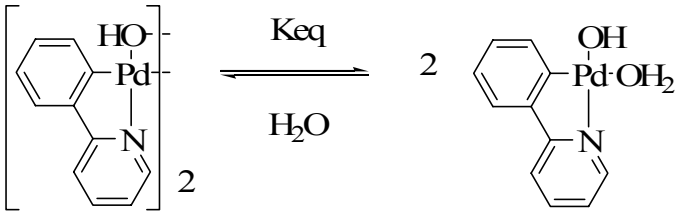

Figure 96. Equilibrium constant K_{eq} = [monomer]^2 /[Dimer]).

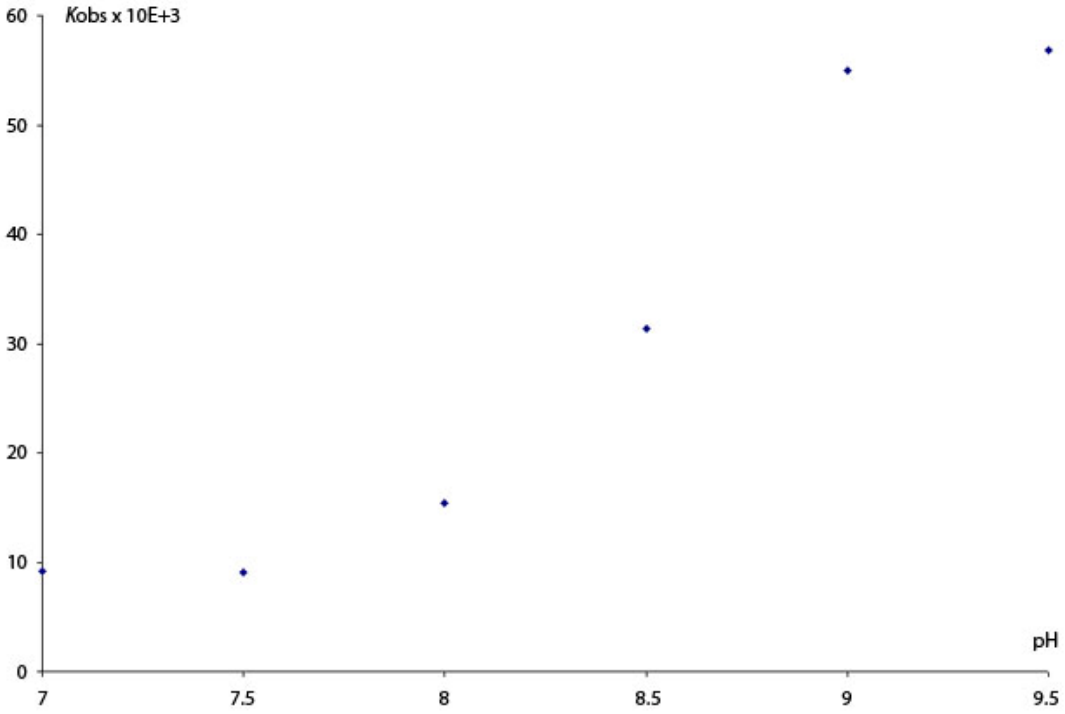

Figure 97. Expression of the Kobs vs pH for the hydrolysis of methylparathion by **91** ([methylparathion] = 3.5 10^{-5} M; [**91**] = 1.75 10^{-6} M).

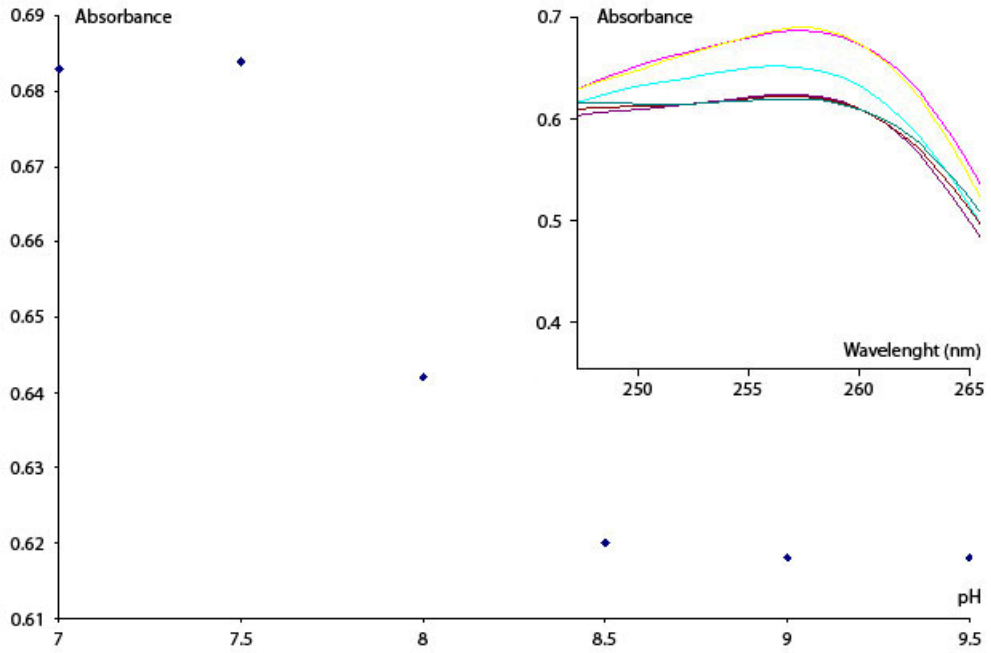

Figure 98. UV recording of **91** (35 μmol) in aqueous buffer with 16% dioxane from pH 7 to pH 9.5.

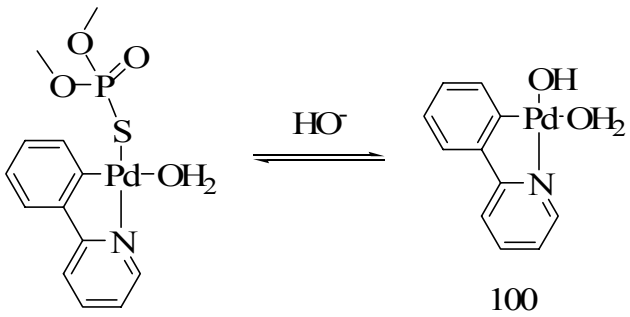

100

Figure 99: Complex **91** equilibrium between neutral and basic pH.

Furthermore, to corroborate the existence of **100**, PGSE analysis of **91** in a 50% mixture of DMSO-d_6 and a pH 12 D_2O solution was investigated. It appeared that the hydrodynamic radius derived from the diffusion of the dimethylthiophosphate ligand and the phenylpyridine moiety greatly differed. Dimethylthiophosphate was found to diffuse at the faster rate than the phenylpyridine moiety. These results suggest that, in basic solution, dimethylthiophosphate was no longer bound to the palladium center leading to the same proposed structure (figure 100).

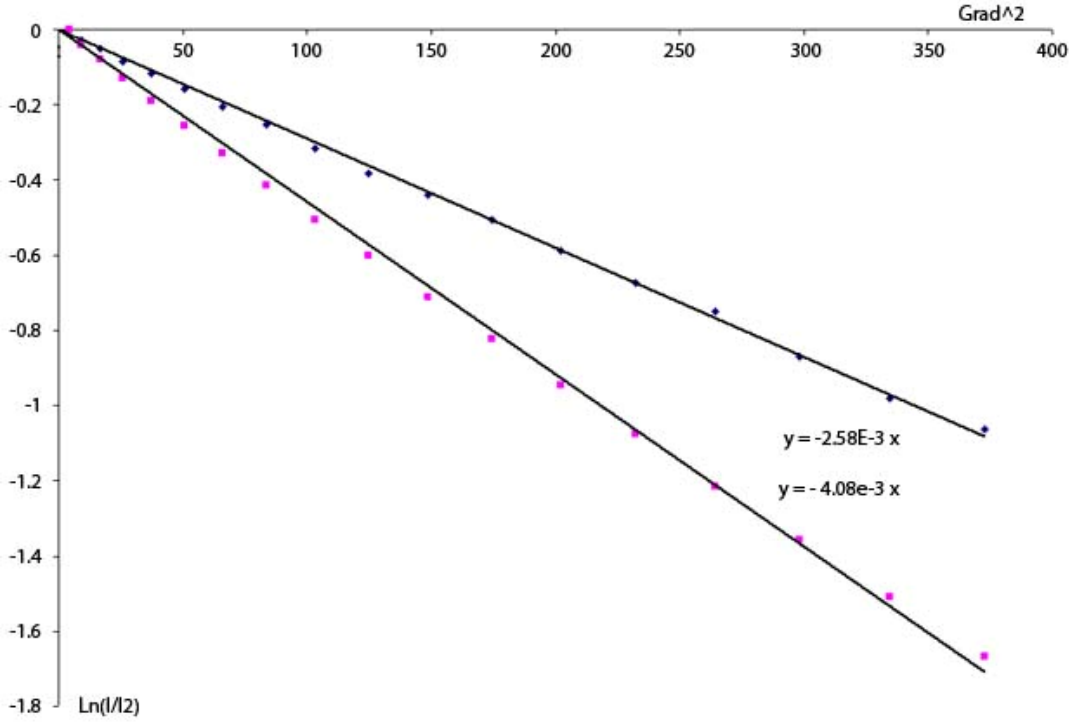

Figure 100. ^{1}H PGSE analysis of **91** (1 mg) in a 50% DMSO/D2O mixture.

In a PGSE experiment, the slope of the line observed in the Ln(I/Io) vs G^2 plot (I = intensity of the signal when a gradient G is applied; when G = 0, I = Io) is directly proportional to the diffusion coefficient of the molecule and therefore inversely proportional to the molecular hydrodynamic radius. In the present experiment, both the dimethylthiophosphate ligand and the phenylpyridine moiety were found to diffuse at different rate. The ratio of the slopes observed in the Ln(I/Io) vs G^2 plot of each of these species suggest that the hydrodynamic radius of the molecule containing the phenylpyridine moiety is larger than that of the molecule containing the dimethylthiophosphate ligand (PGSE anaylis: [(phenylpyridine)Pd(OH)] $_2$ V = 520 Å^3, R = 4.97 Å, dimethylthiophosphate anion V = 127 Å^3 and R = 3.17 Å). This ratio correspond almost exactly to that which can be calculated for the dimeric complex [(phenylpyridine)Pd(OH)]$_2$ (the volume of this molecule should be very similar to that of the known complex [(phenylpyridine)Pd(Cl)]$_2$,[103] V = 498 Å^3, R = 4.92 Å and free dimethylthiophosphate anion (V = 127 Å^3 and R = 3.17 Å). Assuming that ion paring in our highly polar system isn't likely to occur,[104] these data therefore suggest that, under basic condition, dimethylthiophosphate ligand of complex **91** is displaced to yield a dimeric hydroxide bridged complex (figure 101).

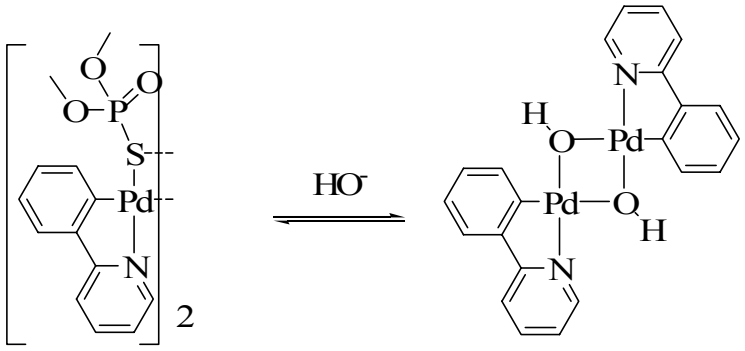

Figure 101. Formation of the dimeric hydroxide bridged complex

This proposal is in agreement with the ^{31}P $\{^{1}H\}$NMR spectrum of **91** in a 50% mixture of DMSO-d_6 and a pH 12 D_2O/DO^- solution. Indeed, this spectrum reveals the presence of a resonance at 59.7 ppm which correspond to the chemical shift of the free $^-SP(=O)(OMe)_2$ derivative.

From the latest analytical and kinetic studies the following mechanism for the hydrolysis of methylparathion has been proposed (figure 102). In a first step, compound **91** monomerize to the active species hydroxy-bis[2-(2-pyridyl)phenyl-*C,N*]dipalladium(II), hydrate is complexed by the methylparathion followed by rapid hydrolysis and release of the nontoxic thiophosphate.

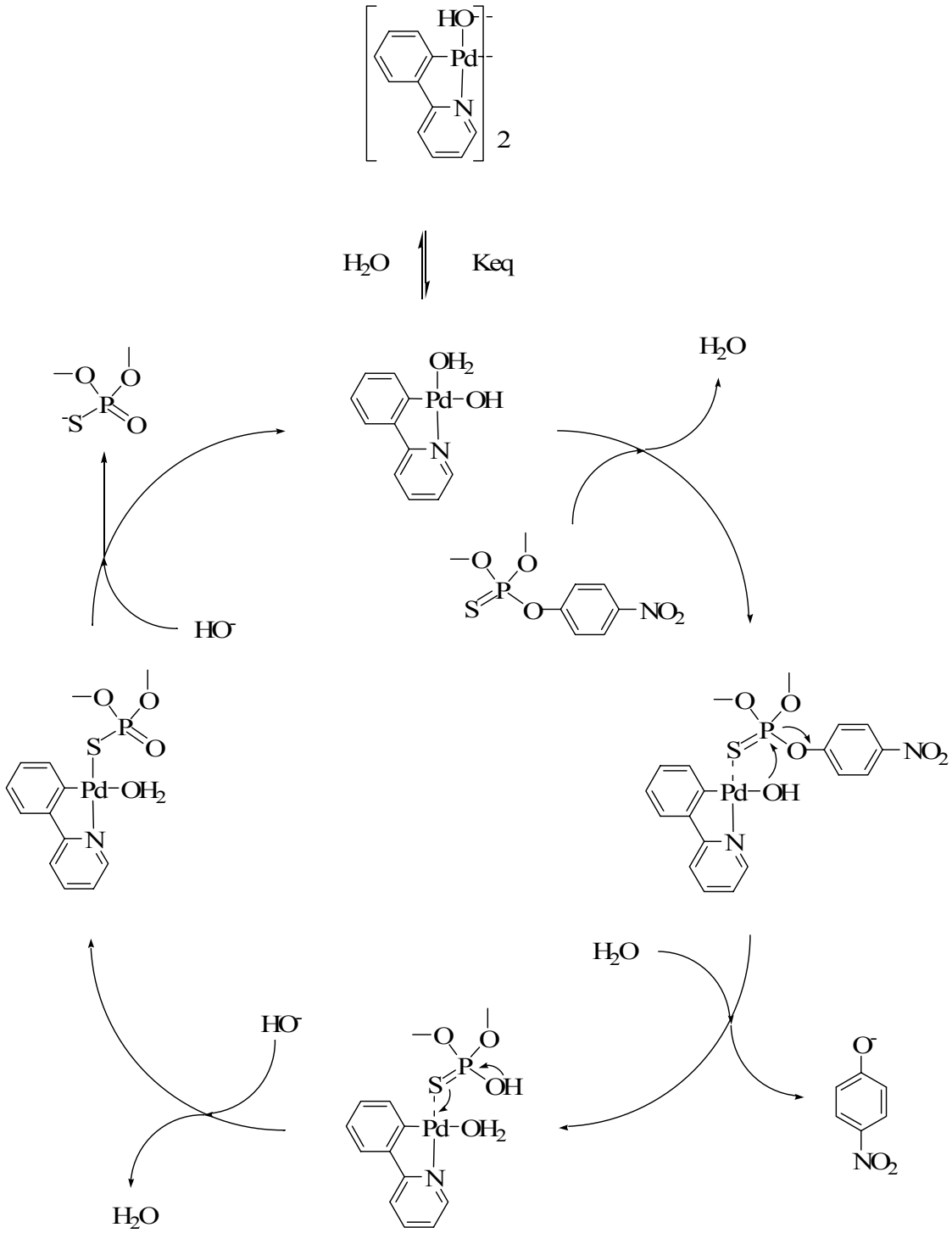

Figure 102. Proposed mechanism for the hydrolysis of **20** by **91** at basic pH.

6.6. Summary

The results presented in this chapter indicate that both mononuclear and dinuclear organopalladium catalysts are competent in the hydrolysis of parathion and by far outperform copper (II) coordination complexes. Another important aspect of the work described in this chapter concerns the fact that dinuclear palladium complexes do not appear more active than mononuclear palladium complexes. In fact, the mononuclear palladium catalyst **91** is very potent and features the highest activity ever recorded for an artificial parathion hydrolysis catalyst. Remarkably, this catalyst is active at slightly acidic and neutral pH where the reaction follows a second order rate law with a first order dependence in palladium catalyst and parathion ($v_{(pH=9)} = k_{2(pH=9)}$[parathion][cat] with $k_{2(pH=9)} = 147\ M^{-1}s^{-1}$). It becomes even more active at pH 9 where the rate law displays a half order dependence in catalyst and a first order dependence in parathion ($v_{(pH=9)} = k_{2(pH=9)}K_{eq}^{1/2}$[cat]$^{1/2}$[parathion] with $k_{2(pH=9)}K_{eq}^{1/2} = 3.02\ M^{-1/2}s^{-1}$). While the change in the kinetic rate law does not allow for a direct comparison of the activity, the initial rate of the catalytic reaction at pH 9 is faster than that of pH 7 by an acceleration factor A given by:

$$A = v_{(pH=9)} / v_{(pH=7)} = k_{2(pH=9)}K_{eq}^{1/2} / (k_{2(pH=7)} \times [cat]^{1/2})$$

With a palladium catalyst concentration of $1.75\ 10^{-5}$ M, the acceleration factor A is equal to 4.78. In fact, initial rate of the catalytic reaction at pH 9 is comparable to that

observed by Ryabov with more expensive platinum catalysts (k_2 = 200-900 $M^{-1}s^{-1}$). Because of the half order dependence in palladium catalysts observed in the case of **91**, the acceleration factor A observed at lower palladium concentration would be even greater so that **91** would outperform the platinum catalysts reported by Ryabov at micromolar catalyst concentrations. For example, at pH 9 and with a catalyst concentration of 3.5 10^{-6} M, the initial rate of the reaction with **91** as a catalyst is faster than that employing the platinum catalyst **32** (figure 13, k_2 = 914 $M^{-1}s^{-1}$) by an acceleration factor A given by:

$$A = v_{(cat=\mathbf{91})} / v_{(cat=\mathbf{32})} = k_{2(cat=\mathbf{91})} K_{eq}^{1/2} / (k_{2(cat=\mathbf{32})} \times [cat]^{1/2}) = 1.76$$

6.7. Experimental

Catalytic hydrolysis of methylparathion by complex **82**: In a typical experiment, the cell was filled with 2.0 mL of a buffer solution (HEPES, 6 < pH < 7; EPPS, 7.5 < pH <8.5; CHES, 9 < pH < 10 ; 10 mM) and 0.278 mL of a stock solution of catalyst in dioxane ([Pd] = 2 × [**82**] = 4.4 × 10^{-5} M). Following addition of 0.278 mL of a stock solution of methylparathion ([methylparathion] = 4.4 × 10^{-4} M in dioxane), the total volume of the solution was adjusted to 3.5 mL by addition of water and the reaction was followed by monitoring the release of *p*-nitrophenol which features an absorption band at 400 nm (ε = 18600 M^{-1} cm^{-1} at pH 9). The dependence of the reaction rate on methylparathion was established by varying the methylparathion concentration at

constant catalyst concentration (([Pd] = 3.5 x 10^{-6} M). The dependence of the reaction rate on catalyst was established by varying the catalyst concentration at constant methylparathion concentration (3.5 x 10^{-5} M).

CHAPTER VII

GENERAL CONCLUSIONS

The family of organophosphorus hydrolase exhibits striking structural diversity and molecular complexity. The supply of such complex catalyst for extensive investigations towards their mode of action is sometimes limited to its availability. Hence a few numbers of scientists have decided to study their mode of action toward organophosphorus hydrolysis leading to the development of new synthetic methodologies. Indeed, we have achieved this goal by the synthesis of active Palladium (II) mononuclear and binuclear complexes. In a first step, using the condensation reaction of primary, secondary amines, as well as amino-alcohols to 3,6-Di(hydroxymethyl)Pyridazine di-*p*-tosylate, 2,3-dimethoxy-benzene-1,4-dicarbaldehyde, and 3,6-pyridazinedi-carboxaldehyde, we developed a large series of new symmetrical and asymmetrical dinucleating ligands.

Scheme 1: Dinucleating ligand design.

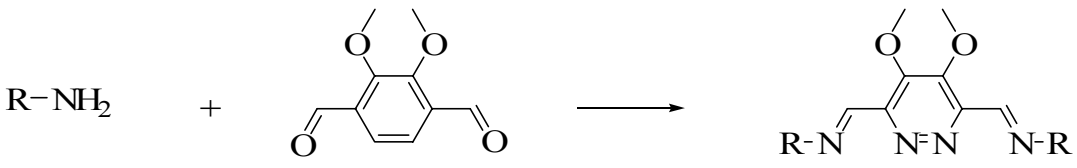

Scheme 1: Continued.

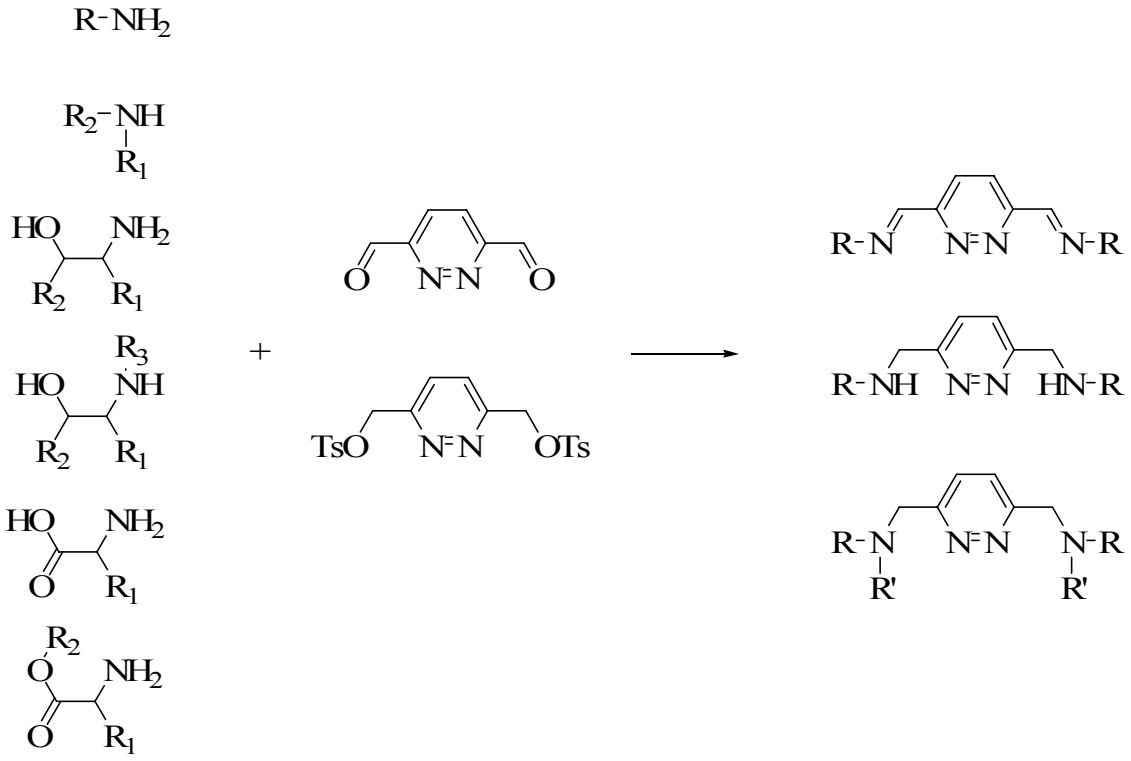

With the use of simple techniques such as ^{1}H NMR and UV titration, these dinucleating ligands revealed interesting coordination chemistry properties chelating 2 metal centers such as Cu (II) while preserving the *C*2 symmetry of the complexes. The orthopalladation reaction of our latest ligands was also a success. By reacting ligands **61**, **63**, **65** with 3 equivalent of Na_2PdCl_4 in a 1:1 CH_2Cl_2/ethanol mixture followed by the displacement of the chlorines with Thallium Acetonylacetonate, the isolations of the desired products were successfully achieved. Reaction of methylparathion and with [2-

(2-pyridyl)-phenyl-*C,N*]palladium(II) acetate leads also to the formation of the corresponding dimethylthiophosphate complex **83**. The later can further react with 1 equivalent of triphenylphosphine leading to the formation of the 1:1 adduct **86**.

Scheme 2: Dinuclear organometallic design.

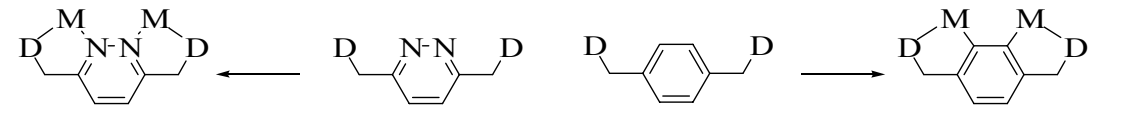

After testing our different catalysts, it is interesting to note that both mononuclear and dinuclear organopalladium catalysts are competent in the hydrolysis of parathion and by far outperform copper (II) coordination complexes. Furthermore, dinuclear palladium complexes, who catalyze the reaction with a second order rate law and a first order dependence in catalyst and parathion ($v = k_2[\text{parathion}][\text{cat}]$ with $k_2 = 190\ M^{-1}s^{-1}$ at pH 9), do not appear to be more active than the mononuclear complex di-μ-(dimethylthiophosphate-*S,*S)-bis[2-(2-pyridyl)phenyl-*C,N*]dipalladium(II) toward the hydrolysis reaction. The latest revealed to be reactive at neutral pH with a second order

rate law and a first order dependence in catalyst and parathion ($v = k_2[\text{parathion}][\text{cat}]$ with $k_2 = 150\ M^{-1}s^{-1}$). It becomes even more active at pH 9 where the rate law displays a half order dependence in catalyst and a first order dependence in parathion ($v = k_2K_{eq}^{1/2}[\text{cat}]^{1/2}[\text{parathion}]$ with $k_2K_{eq}^{1/2} = 3.02\ M^{-1/2}s^{-1}$). Remarkably, this mononuclear catalyst is very potent and features the highest activity ever recorded for a synthetic parathion hydrolysis catalyst.

REFERENCES

[1] (a) *A Guide to Organophosphorus Chemistry* Quin, L. D. Wiley, New York, **2000**. (b) *Pesticides Remediation in Soils and Water* Roberts, T.; Keaney, P. C. Wiley, New York, **1998**.

[2] Algeria, H. A.; Shaw, T, J, *Environ. Sci. Technol.* **1999,** *33,* 850.

[3] Gilliom, R. J.; Barbash, J. E.; Kolpin, D. W. Larson, S. J. *Environ. Sci. Technol.* **1999,** *33,* 164 A.

[4] Squillace, P. J.; Scott, J. C.; Moran, M. J.; Nolan, B. T.; Kolpin, D. W. *Environ. Sci. Technol.* **2002,** *36,* 1923.

[5] *Water Resources Assessment* Matzner, R.; Waldman, E. U.S. Environmental Protection Agency, Washington DC, **1999**.

[6] *Military Chemical and Biological Agents, Chemical and Toxicological Properties* Compton, J. A. The Telford Press, Caldwell, NJ, **1987**.

[7] *Chemical Warfare Agents: Toxicology and Treatments* Marrs, T. C.; Maynard, R. L. Sidell, F. R. Wiley, New York, **1996**, p1-26.

[8] Benschop, H. P.; de Jong, L. P. A. *Acc. Chem. Res.* **1988,** *21,* 368.

[9] *Chemical Warfare Agents* Somani, S. M. Academic Press, New York, **1992**, Chapter IV.

[10] Sultatos, L. G. *J. Toxicol. Environ. Health* **1994,** *43,* 271.

[11] (a) Ember, L. S. *Chem. Eng. News* **1997,** *75*(11), 22. (b) Yang, Y. C. *Acc. Chem. Res.* **1999,** *32,* 109.

[12] (a) Gustafson, R. L.; Martell, A. E. *J. Am. Chem. Soc.* **1962,** *84,* 2309. (b) Ward, J. R.; Yang, Y. C.; Wilson, R. B. Jr.; Burrows, W. D.; Ackman, L. L. *Bioorg. Chem.* **1988,** *16,* 12. (c) Epstein, J.; Bauer, V. E.; Saxe, M.; Demek, M. M. *J. Am. Chem. Soc.* **1956,** *78,* 4068.

[13] *Development of Decontamination Solution DS2* Jackson, J. B. CWLR, 2368, April, **1960**.

[14] *Reactions of Chemical Warfare Agents with DS2* Beaudry, W. T.; Szafraniec, L. L.; Leslie, D. R. CRDEC-TR-364, June, **1992**.

[15] (a) Verma, K. K.; Gupta, A. K. *Talanta* **1982,** *102,* 18. (b) De Munari, S.; Frigerio, M.; Santagostino, M. *J. Org. Chem.* **1996,** *61,* 9272. (c) Nicolaou, K. C.; Baran, P. S.; Zhong, Y. L. *J. Am. Chem. Soc.* **2001,** *123,* 3183. (d) Wirth, T. *Angew. Chem., Int. Ed.* **2001,** *40,* 2812.

[16] (a) Moss, R. A.; Alwis, K. W.; Bizzigotti, G. O. *J. Am. Chem. Soc.* **1983,** *105,* 681. (b) Moss, R. A.; Alwis, K. W.; Shin, J. S. *J. Am. Chem. Soc.* **1984,** *106,* 2651.

[17] (a) Segues, B.; Rico-Lattes, I *Bull. Soc. Chim. Fr.* **1996,** *133,.*925. (b) Stang, P. J.; Zhdankin, V. V. *Chem. Rev.* **1996,** *96,* 1123.

[18] (a) *The Chemistry of Halides, Pseudo Halides and Azides* Koser, G. F. Wiley, New York, **1995**. (b) Katritzky, A. R.; Savage, G. P; Palenik, G. J.; Qian, K.; Zhang, Z. *J.*

Chem. Soc. Perkin Trans. 2 **1990,** 1657. (c) Moss, R. A.; Bracken, K.; Emge, T. J. *J. Org. Chem.* **1995,** *60,* 7739.

[19] Moss, R. A.; Zhang, H.; Chatterjee, S.; Krogh-Jespersen, K. *Tetrahedron. Lett.* **1993,** *34,* 1729.

[20] *Surfactants and Polymers in Aqueous Solutions* Jönsson, B.; Lindman, B.; Holmberg, K.; Krongberg, B. Wiley, New York, **1998**.

[21] Moss, R. A.; Morales-Rojas, H. *Langmuir* **2000,** *16,* 6485.

[22] (a) Panetta, C. A.; Garlick, S. M.; Durst, H. D.; Longo, F. R.; Ward, J. R. *J. Org. Chem.* **1990,** *55,* 5202. (b) Moss, R. A.; Fujiyama, R.; Zhang, H.; Chung, Y. C.; McSorley, K. *Langmuir,* **1993,** *9,* 2902.

[23] (a) Bunton, C. A.; Ihara, Y. *J. Org. Chem.* **1977,** *42,* 2865. (b) Bunton, C. A.; Nelson, S. E.; Quan, C. *J. Org. Chem.* **1982,** *47,* 1157.

[24] Terrier, F.; MacCormack, P.; Kizilian, E.; Halle, J. C.; Demersemen, P.; Guir, F.; Lion, C. J. *J. Chem. Soc. Perkin trans. 2* **1991,** 153.

[25] Biresaw, G.; Bunton, C. A. *J. Phys. Chem.* **1986,** *90,* 5849.

[26] Bunton, C. A.; Mhala, M. M.; Moffatt, J. R.; *J. Phys. Org. Chem.* **1990,** *9,* 2832.

[27] Yang, Y. C.; Berg, F. J.; Szafraniec, L. L.; Beaudry, W. T.; Bunton, C. A.; Kumar, A. *J. Chem. Soc. Perkin Trans. 2* **1997,** 607.

[28] (a) Lion, C.; Hedayatullah, M.; Bauer, J. P.; Charvy, C.; Delmas, G.; Despangne, B.; Sentenac-Roumanou, H. *Bull. Soc. Chem. Belg.* **1991,** *100,* 555. (b) Bhattacharya, S.; Snehalatha, K. *J. Org. Chem.* **1997,** *62,* 2198.

[29] DeBruin, K. E.; Tang, C. I. W.; Johnson, D. M.; Wilde, R. L. *J. Am. Chem. Soc.* **4989,** *111,* 5871.

[30] Oumar-Mahamat, H.; Slebocka-Tilk, H.; Brown, R. S. *Can. J. Chem.* **1999,** *77,* 1577.

[31] *Review of Pesticide Disposal Research* Munnecke, D. M.; Day, R.; Trask, H. W. U.S. Environmental Protection Agency, Washington DC, **1976**.

[32] Vilanova, E.; Sogorb, M. A. *Crit. Rev. Toxicol.* **1999,** *29,* 21.

[33] Raushel, F. M.; Holden, H. M *Advances in Enzymology and Related Areas of Molecular Biology* **2000,** *74,* 51.

[34] (a) Dumas, D. P.; Caldwell, S. R.; Wild, J. R.; Raushel, F. M. *J. Biol. Chem.* **1989,** *264,* 19659. (b) Dumas, D. P.; Durst, H. D.; Landis, W. G.; Raushel, F. M.; Wild, J. R. *Arch. Biochem. Biophys.* **1990,** *277,* 155.

[35] Benning, M. M.; Kuo, J. M.; Raushel, F. M.;. Holden, H. M. *Biochemistry* **1994,** *33,* 15001.

[36] Omburo, G. A.; Kuo, J. M.; Mullins, L. S.; Raushel, F. M. *J. Biol. Chem.* **1992,** *267,* 13278.

[37] Vanhooke, J. L.; Benning, M. M.; Raushel, F. M.; Holden, H. M. *Biochemistry* **1996,** *35,* 6020.

[38] Chae, M. Y.; Postula, J. F.; Raushel, F. M. *Bioorg. Med. Chem. Lett.* **1994,** *4,* 1473.

[39] Lewis, V. E.; Donarksi, W. J.; Wild, J. R.; Raushel, F. M. *Biochemistry* **1988,** *27,* 1591.

[40] Lai, K.; Dave, K. I.; Wild, J. R. *J. Biol. Chem.* **1994,** *269,* 16579.

[41] Kursheva, L. I.; Il'in, A. M.; Batyeva, E. S.; Kataeva, O. N.; Gubaidullin, A. T. *Russ. J. Gen. Chem.* **2001,** *71,* 484.

[42] Kim, M.; Gabbai, F.P *J. Chem. Soc., Dalton Trans.* **2004**, articles ASAP.

[43] Shi, Q.; Cao, R.; Hong, M. C.; Wang, Y. Y.; Shi, Q. Z. *Trans. Met. Chem.* **2001,** *26,* 657.

[44] (a) Wadsworth, W. S. *J. Org. Chem.* **1981,** *46,* 4080. (b) Hendry, P.; Sargeson, A. M. *Aust. J. Chem.* **1986,** *39,* 1177. (c) Morrow, J. R.; Trogler, W. C. *Inorg, Chem.* **1989,** *28,* 2330. (d) Chin, J. *Acc. Chem. Res.* **1991,** *24,* 145.

[45] Wagner-jauregg, T.; Hackley, B. E.; Lies, T. A.; Owen, O. O.; Proper, R. J. *J. Am. Chem. Soc.* **1955,** *77,* 922.

[46] (a) Zeinali, M.; Torrents, A. *Environ. Sci. Technol.* **1998,** *32,* 2338. (b) Smolen, J. M.; Stone, A. L. *Environ. Sci. Technol.* **1997,** *31,* 1664.

[47] Hay, R. W.; Govan, N. *Chem. Comm.* **1990,** 714.

[48] Oh, S. J.; Yoon, C. W.; Park, J. W. *J. Chem. Soc. Perkin Trans. 2* **1996,** 329.

[49] Courtney, R. C.; Gustafson, R. L.; Westerback, S. J.; Hyytiainen, H.; Chabarek, S. C.; Martell, A. E. *J. Am. Chem. Soc.* **1957,** *79,* 3030.

[50] Gellman, S. H.; Petter, R.; Breslow, R. *J. Am. Chem. Soc.* **1986,** *108,* 2388.

[51] (a) Bunton, C. A.; Scrimin, P.; Tecilla, P. *J. Chem. Soc. Perkin Trans. 2* **1996,** 419. (b) Scrimin, P.; Tecilla, P.; Tonellato, U. *J. Org. Chem.* **1991,** *56,* 161.

[52] Scrimin, P.; Ghirlanda, G.; Tecilla, P.; Moss, R. A. *Langmuir* **1996,** *12,* 6235.

[53] Kuo, L. Y.; Perera, N. M. *Inorg. Chem.* **2000,** *39,* 3117.

[54] Kazankov, G. M; Sergeeva, V. S.; Efremenko, E. N.; Alexandrova, L.; Varfolomeev, S. D.; Ryabov, A. D. *Angew. Chem., Int. Ed.* **2000,** *39,* 3117.

[55] Carlsson, H.; Haukka, M.; Nordlander, E. *Inorg. Chem.* **2004,** *20(5),* 5681-5687.

[56] Gutierrez, M. A.; Newkome, G. R.; Selbin J. *J. Organometallic Chem.* **1980,** *202,* 341-350.

[57] (a) Sträter, N.; Lipscomb, W. N.; Klabunde, T.; Krebs, B. *Angew. Chem.,* Int. *Ed. Engl.* **1996**, *35*, 2024. (b) Wilcox, D. E. *Chem. Rev.* **1996**, *96*, 2435.

[58] (a) Williams, N. H.; Takasaki, B.; Wall, M.; Chin, *J. Acc. Chem. Res.* **1999**, *32(6),* 485-493. (b) Van Den Beuken, E. K.; Feringa, B. L. *Tetrahedron* **1998**, *54(43),* 12985-13011. (c) Corey, E. J.; Bakshi, R. K.; Shibata, S.; Chen, C. P.; Singh, V. K. *J. Am. Chem. Soc.* **1987**, *109(25),* 7925-6. (d) Corey, E. J.; Bakshi, R. K.; Shibata, S. *J. Am. Chem. Soc.* **1987**, *109(18),* 5551-3. (e) Noyori, R.; Kitamura, M. *Angew. Chem., Int. Ed. Engl.* **1991**, *30(1)*, 34-48.

[59] (a) Ooi, T.; Takahashi M.; Maruoka, K. *J. Am. Chem. Soc.* **1996**, *118*, 11307-11308. (b) Ooi, T.; Kii, S.; Hanawa, H.; Maruoka, K. *Tetrahedron Lett.* **1998**, *39*, 3729-3732. (c) Ooi, T.; Saito, A.; Maruoka, K. *Tetrahedron Lett.* **1998**, *39*, 3745-3748. (d) Ooi, T.; Asao, N.; Maruoka, K. *J. Syn. Org. Chem. Jpn.* **1998**, *56*, 377-385. (e) Maruoka, K.. *Catal. Today* **2001**, *66*, 33-45.

[60] (a) Wuest, J. D. *Acc. Chem. Res.* **1999**, *32*, 81-89. (b) Wuest, J. D.; Zacharie, B. *J. Am. Chem. Soc.* **1985**, *107*, 6121-6123

[61] Lee, H.; Diaz, M.; Hawthorne, M. F *Tetrahedron Lett.* **1999**, *40*, 7651-7655.

[62] (a) Jacobsen, E. N. *Acc. Chem. Res.* **2000**, *33*, 421-431. (b) Annis, D. A.; Jacobsen, E. N. *J. Am. Chem. Soc.* **1999**, *121*, 4147-4154. (c) Konsler, R. G.; Karl, J.; Jacobsen, E. N. *J. Am. Chem. Soc.* **1998**, *120*, 10780-10781. (d) Fields, L. B.; Jacobsen, E. N. *Tetrahedron: Asymmetry* **1993**, *4*, 2229-40.

[63] (a) Matsunaga, S.; Das, J.; Roels, J.; Vogl, E. M.; Yamamoto, N.; Iida, T.; Yamaguchi, K.; Shibasaki, M. *J. Am. Chem. Soc.* **2000**, *122*, 2252-2260. (b) Shibasaki, M.; Groger, H. *Top. Organomet. Chem.* **1999**, *2*, 199-232. (c) Shibasaki, M. *Enantiomer* **1999**, *4*, 513-527. (d) Yamada, K.-I.; Harwood, S. J.; Groger, H.; Shibasaki, M. *Angew. Chem., Int. Ed.* **1999**, *38*, 3504-3506. (e) Yamasaki, S.; Iida, T.; Shibasaki, M. *Tetrahedron* **1999**, *55*, 8857-8867. (f) Shibasaki, M.; Sasai, H. *Adv. Asymmetric Synth.* **1998**, *3*, 191-233. (g) Shibasaki, M.; Sasai, H.; Arai, T.; Iida, T. *Pure Appl. Chem.* **1998**, *70*, 1027-1034. (h) Shibasaki, M.; Sasai, H.; Arai, T. *Angew. Chem., Int. Ed. Engl.* **1997**, *36*, 1237-1256.

[64] Kii, S.; Maruoka, K. *Tetrahedron Lett.* **2001**, *42*, 1935-1939.

[65] For a recent example of a chiral dinucleating ligand see: Trost, B. M.; Ito, H.; Silcoff, E. R. *J. Am. Chem. Soc.* **2001**, *123,* 3367-3368.

[66] Oxidation, MMO, Oxygen transport, transesterification.

[67] (a) Koike, T.; Inoue, M.; Kimura, E.; Shiro, M. *J. Am. Chem. Soc.* **1996***, 118*, 3091. (b) Young M. J.; Wahnon D.; Hynes R. C.; Chin J. *J. Am. Chem. Soc.* **1995**, *117*, 9441. (c)Takasi, B. T.; Chin, J. *J. Am. Chem. Soc.* **1995**, *117*, 8582. (d) Oh, S. J.; Song, K. H.; Whang, D.; Kim, K.; Yoon, T. H.; Moon, H.; Park, J. W. *Inorg. Chem.* **1996**, *35*, 3780.

(e) Hettich, R.; Schneider, H.-J. *J. Am. Chem. Soc.* **1997**, *119*, 5638. (f) Ott, R.; Krämer, R. *Angew. Chem., Int. Ed.* **1998**, *37*, 1957. (g) Bracken, K.; Moss, R. A.; Ragunathan, K. G. *J. Am. Chem. Soc.* **1997**, *119*, 9323. (h) Kim, A. D.; Burstyn, J. N. *Inorg. Chem.* **1996**, *35*, 2792. (i) Molenveld, P.; Engbersen, J. F. J.; Kooijman, H.; Spek, A. L.; Reinhoudt, D. N. *J. Am. Chem. Soc.* **1998**, *120*, 6726. (j) Gajda, T.; Duepre, Y.; Toeroek, I.; Harmer, J.; Schweiger, A.; Sander, J.; Kuppert, D.; Hegetschweiler, K. *Inorg. Chem*. **2001**, *40(19),* 4918-4927. (k) Kövári, E.; Krämer, R. *J. Am. Chem. Soc.* **1996**, *118*, 12704. (l) Liu, S.; Hamilton, A. D. *Chem. Commun.* **1999**, 587.

[68] (a) Maruoka, K. *Catal. Today* **2001**, *66(1),* 33-45. (b) Hanawa, H.; Kii, S.; Asao, N.; Maruoka, K. *Tetrahedron Lett.* **2000**, *41(29),* 5543-5546. (c) Asao, N.; Kii, S.; Hanawa, H.; Maruoka, K. *Tetrahedron Lett.* **1998**, *39(22),* 3729-3732.

[69] Ooi, T.; Takahashi, M.; Maruoka, K. *J. Am. Chem. Soc.* **1996**, *118(45),* 11307-11308.

[70] (a) Shibasaki, M.; Sasai, H.; Arai, T. *Angew. Chem., Int. Ed. Engl.* **1997**, *36(12),* 1237-1256. (b) Yoshikawa, N.; Kumagai, N.; Matsunaga, S.; Moll, G.; Ohshima, T.; Suzuki, T.; Shibasaki, M. *J. Am. Chem. Soc.* **2001**, *123(16),* 3856. (c) Kumagai, N.; Matsunaga, S.; Yoshikawa, N.; Ohshima, T.; Shibasaki, M. *Org. Lett.* **2001**, *3(10),* 1539-1542.

[71] (a) Noyori, R.; Kitamura, M.; Nakamura, A. *Angew. Chem. Int. Ed. Engl.,* **1991,** *30,* 49. (b) Kitamura, M.; Suga, S.; Niwa, M.; Noyori, R. *J. Am. Chem. Soc.,* **1995,** *117,* 4832-4842.

[72] Trost, B. M.; Silcoff, E. R.; Ito, H. *Org. Lett.* **2001**, *3(16),* 2497-2500.

[73] Jacobsen, E. N. *Acc. Chem. Res.* **2000**, *33(6),* 421-431.

[74] (a) Barrios, A. M.; Lippard, S. J. *Inorg. Chem.* **2001**, *40*, 1060-1064. (b) Manzur, J.; Garcia, A. M.; Gomez, B.; Spodine, E. *Polyhedron* **2000**, *19*, 2367-2372. (c) Robichaud, P.; Thompson, L. K. *Inorg. Chim. Acta* **1984**, *85*, 137-142. (d) Thompson, L. K.; Mandal, S. K.; Rosenberg, L.; Lee, F. L.; Gabe, E. J. *Inorg. Chim. Acta* **1987**, *133*, 81-91. (e) Sullivan, D. A.; Palenik, G. J. *Inorg. Chem.* **1977**, *16*, 1127-1133. (f) Thompson, L. K.; Chako, V. T.; Elvidge, J. A.; Lever, A. B. P.; Parish, R. V. *Can. J. Chem.* **1969**, *47*, 4141-4152.

[75] (a) Fahrni, C. J.; Pfaltz, A. *Helv. Chim. Acta* **1998**, *81(3),* 491-506. (b) Fahrni, C. J.; Pfaltz, A.; Neuburger, M.; Zehnder, Ma. *Helv. Chim. Acta* **1998**, *81(3),* 507-524.

[76].Brooker, S.; Kelly, R. J. *J. Chem. Soc., Dalton Trans.* **1996**, *10*, 2117-2122.

[77] Sueur, S.; Lagrenee, M.; Abraham, F.; *J. Heterocyclic Chem.*, **1987**, 24, 1285-1289.

[78] Abraham, F.; Mernari, B.; Lagrenee, M.; Sueur, S. *Acta Crystallogr.,Sect.C* **1988**, *44*, 1267.

[79] Wiley, R. H. *J. Macromol. Sci., Chem.* **1987**, *A24(10),* 1183-90.

[80] Fulop, F.; Dahlqvist, M.; Pihlaja, K. *Acta Chem. Scand.* **1991**, *45(3),* 273-5.

[81] Hu, X. E.; Cassady, J. M. *Synth. Commun.* **1995**, *25(6),* 907-13.

[82] Cabezon, B.; Cao, J.; Raymo, F. M.; Stoddart, J. F.; White, A. J. P.; Williams, D. J. *Chem. Eur. J.* **2000**, *6(12),* 2262-2273.

[83] Metz, B.; Moras, D.; Weiss, R. *J. Am. Chem. Soc.* **1971,** *93,* 1808-1809.

[84] (a) Fukuda, Y.; Seto, S.; Furuta, H.; Ebisu, H.; Oomori, Y.; Terashima, S. *J.Med.Chem*. **2001,** *44,* 1396-1406. (b) Weitl, F. L.; Raymond, K. N.; Durbin, P. W. *J. Med. Chem.* **1981,** *24,* 203.

[85] Lartiges, S. B.; Garrigues, P. P. Environ. Sci. Technol. **1995,** 29, 1246-1254.

[86] (a) Donarski, W. J.; Dumas, D. P.; Heitmeyer, D. P.; Lewis, V. E.; Raushel, F. M. *Biochemistry* **1989,** *28*, 4650-4655. (b) Caldwell, S. R.; Newcomb, J. R.; Schlecht, K. A; Raushel, F. M. *Biochemistry* **1991,** *30*, 7438-7444.

[87] (a) Morales-Rojas, H.; Moss, R. A. *Chem. Rev.* **2002,** *102*, 2497-2522. (b) Ketellaar, J. A. A.; Gersmann, H. R.; Beck, M. *Nature* **1956**, *177*, 392-393. (c) Wan, H. B.; Wong, M. K.; Mok, C. Y. *Pestic. Sci.* **1994,** *42*, 93-99. (d) Hartshorn, C. M.; Singh, A.; Chang, E. L. *J. Mater. Chem.* **2002,** *12*, 602-605. (e) Menger, F. M.; Gan, L. H.; Johnson, E.; Durst, D. H. *J. Am. Chem. Soc.* **1987,** *109*, 2800-2803. (f) Moss, R. A.; Gong, P. K.; Morales-Rojas, H. *Org. Lett.* **2002,** *4*, 1835-1838. (g) Hay, R. W.; Clifford, T.; Richens, D. T.; Lightfoot, P. *Polyhedron* **2000,** *19*, 1485-1492.

[88] Diemer, R.; Dittes, U.; Nuber, B.; Seifried, V.; Opferkuch, W.; Keppler, B. K. *Metal-Based Drugs* **1995,** *2(5),* 271-92.

[89] Kuncheria, B.; Devi, G. S.; Indrasenan, P. *Inorganica Chimica Acta* **1989,** *155(2),* 255-8.

[90] Hong, Y.; Gao, Y.; Nie, X.; Zepp, C. M. *Tet. Lett.* **1994,** *35,* 6631-6634.

[91] Klosa, J. *J.Prakt.Chem.* **1967,** *36,* 1-4.

[92] Alegria H. A.; Shaw, T. J. *Environ. Sci. Technol.* **1999,** *33,* 850-856.

[93] Gilliom, R. J.; Barbash, J. E.; Kolpin, D. W.; Larson, S. J. *Environ. Sci. Technol. A.* **1999,** *33,* 164 A-169 A.

[94] (a) Morales-Rojas, H.; Moss, R. A. Chem. Rev. **2002,** *102,* 2497-2521. (b) Yang, Y. C.; Baker, J. A.; Ward, J. R. *Chem. Rev,* **1992**, *92,* 1729-1743.

[95] Reichman, R.; Mahrer, Y.; Wallach, R. *Environ. Sci. Technol.* **2000,** *34,* 1321-1330.

[96] Kuo, L. Y.; Perera, N. M. *Inorg. Chem.* **2000,** *39,* 2103-2106.

[97] Constable, E. C.; Thompson, A. M. W. C.; Leese, T. A.; Reese, D. G. F.; Tocher, D. A. *Inorganica Chimica Acta* **1991,** *182(1),* 93-100.

[98] Qin, Y.; Selvaratnam, S.; Vittal, J. J.; Leung, P. *Organometallics* **2002,** *21(24),* 5301-5306.

[99] Kim, M.; Liu, Q.; Gabbai, F. P. *Organometallics* **2004,** articles ASAP.

[100] (a) Hong, H.-B.; Raushel, F. M. *Biochemistry* **1996**, *35*, 10904. (b) Shim, H.; Hong, S.-B.; Raushel, F. M. *J. Biol. Chem.* **1998**, *273*, 17445.

[101] Carlsson, H.; Haukka, M.; Nordlander, E. *Inorg. Chem.* **2004,** *43(18),* 5681-5687.

[102] (a) Valentini, M.; Pregosin, P. S.; Ruegger, H. *Organometallics* **2000**, *19*, 2551-2555. (b) Valentini, M.; Pregosin, P. S.; Ruegger, H. *Dalton Trans.* **2000**, *24*, 4507-4510. (c) Sandstrøm, J. *Dynamic NMR Spectroscopy*; Academic Press: New York, **1982,** 77-92. (d) Kaplan, J. I. Fraenkel, G. *NMR of Chemically Exchanging Systems*; Academic Press: New York, **1980,** 71-128.

[103] Klement, U. Zeitschrift fuer Kristallographie **1993,** *208(2),* 299-301.

[104] Martínez-Viviente, E.; Rüegger, E.; Pregosin, P. S.; López-Serrano, J. *Organometallics*, **2002,** *21,* 5841-5846.

APPENDIX

Pulsed Field Gradient Spin-Echo NMR.

All measurements were performed on a Varian Inova 500 MHz spectrometer using Varian's diffusion software package. Samples were recorded in d_6-DMSO/D_2O at 293 K without spinning.

In a typical PGSE experiment, the following spin echo sequence is applied:

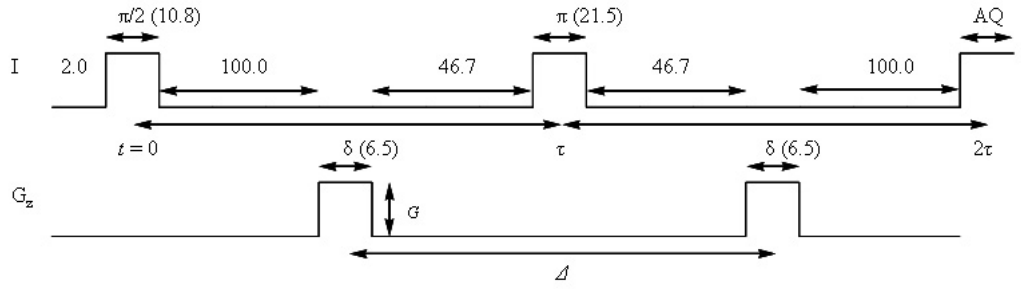

As depicted above, a π/2 pulse magnetization is first created and followed by an intermediate π pulse at t = τ. The latest generates a simple echo at t = 2τ which would result to a standard NMR spectrum after acquisition if no further modifications were

applied. In a PGSE experiment, a first pulsed-linear-field gradient *G* (length: δ = 6.5 ms) is generated at $\tau/2$ which provokes a linear one-dimensional dephasing of the spins, the magnitude of which varies along the direction of the applied field gradient. After a time $\Delta = \tau$ and after application of the π pulse, the same pulsed-linear-field gradient is applied which linearly rephase the spins before the acquisition. Simply put, if spins move out of their starting position between the 2 pulsed gradients, their acquisitions are lost as their rephasing does not occur so that they do not contribute to the intensity of the spins ultimately detected.

During a typical experiment, all factors are kept constant while the gradient strength (G) is arrayed between 0 and 14 G/cm and calibrated using d_5-DMSO. Following data collection, the spectra are carefully integrated and the resulting data points (Ln(I/Io) vs G^2) are subjected to a least-squares fit which produces a regression line whose slope is proportional to the diffusion coefficient and inversely proportional to the molecular hydrodynamic radius r_H ($D = (kT)/(6\pi\eta r_H)$

VITA

PERSONAL:

Alexandre Picot
Born: July 21, 1975, Toulouse, France

c/o Dr. F. P. Gabbaï
Department of Chemistry
Texas A&M University
College Station, TX 77843-3255

EDUCATION:

1999-2004 Texas A&M University, Texas, Ph.D., Chemistry
1998-1999 Université Paul Sabatier at Toulouse, France, M.S. Chemistry
1994-1998 Université Paul Sabatier at Toulouse, France, B.S. Chemistry

PUBLICATIONS:

"Bismuth(III) bis(trifluoromethanesulfonyl)amide" Picot, Alexandre; Repichet, Sigrid; Le Roux, Christophe; Dubac, Jacques; Roques, Nicolas. *Journal of Fluorine Chemistry* **2002,** *116(2)*, 129-134.

"Composition and compound based on salts of metals and acids having a sulfonyl group borne by a perhalogenated carbon and their use as Lewis acid catalysts" Roques, Nicolas; Dubac, Jacques; Le Roux, Christophe; Repichet, Sigrid; Bernard, Jean-Marie; Maestro, Jean-Pierre; Vidal, Thierry; Peyronneau, Magali; Picot, Alexandre; Mazieres, Stephane. *PCT Int. Appl.* **2002,** WO 0205954.

"C2-chiral dinucleating ligands with a 3,6-disubstituted pyridazine core" Picot, Alexandre; Gabbaï, Francois P. *Tetrahedron Letters* **2001,** *43(1),* 11-13.

"Interaction of the Bifunctional Lewis Acid 1,2-Bis(chloromercurio)-tetrafluorobenzene with Aldehydes, Nitriles, and Epoxides" Beckwith, Julie D.; Tschinkl, Martin; Picot, Alexandre; Tsunoda, Mitsukimi; Bachman, Robert; Gabbaï, Francois P. *Organometallics* **2001,** *20(14),* 3169-3174.

"Dinucleating ligands derived from 3,6-bis(hydroxymethyl)pyridazine" Picot, Alexandre; Gabbaï, Francois P. *To be submitted.*

"Synthesis of cyclometalated binuclear palladium complexes" Picot, Alexandre; Gabbaï, Francois P. *To be submitted.*

"di-μ-(dimethylthiophosphate-*S,*S)-bis[2-(2-pyridyl)phenyl-*C,N*]dipalladium(II), a remarkably active precatalyst for the hydrolysis of methylparathion" Picot, Alexandre; Gabbaï, Francois P. *To be submitted.*